

# Edwards Statistical Mechanics for Jammed Granular Matter

Adrian Baule<sup>1</sup>, Flaviano Morone<sup>2</sup>, Hans J. Herrmann<sup>3</sup>, and Hernán A. Makse<sup>2</sup>

<sup>1</sup>*School of Mathematical Sciences,  
Queen Mary University of London,  
London E1 4NS, UK*

<sup>2</sup>*Levich Institute and Physics Department,  
City College of New York,  
New York, New York 10031, USA*

<sup>3</sup>*ETH Zürich, Computational Physics for Engineering Materials,  
Institute for Building Materials,  
Wolfgang-Pauli-Str. 27,  
HIT, CH-8093 Zürich,  
Switzerland*

(Dated: March 4, 2024)

In 1989, Sir Sam Edwards made the visionary proposition to treat jammed granular materials using a volume ensemble of equiprobable jammed states in analogy to thermal equilibrium statistical mechanics, despite their inherent athermal features. Since then, the statistical mechanics approach for jammed matter – one of the very few generalizations of Gibbs-Boltzmann statistical mechanics to out of equilibrium matter – has garnered an extraordinary amount of attention by both theorists and experimentalists. Its importance stems from the fact that jammed states of matter are ubiquitous in nature appearing in a broad range of granular and soft materials such as colloids, emulsions, glasses, and biomatter. Indeed, despite being one of the simplest states of matter – primarily governed by the steric interactions between the constitutive particles – a theoretical understanding based on first principles has proved exceedingly challenging. Here, we review a systematic approach to jammed matter based on the Edwards statistical mechanical ensemble. We discuss the construction of microcanonical and canonical ensembles based on the volume function, which replaces the Hamiltonian in jammed systems. The importance of approximation schemes at various levels is emphasized leading to quantitative predictions for ensemble averaged quantities such as packing fractions and contact force distributions. An overview of the phenomenology of jammed states and experiments, simulations, and theoretical models scrutinizing the strong assumptions underlying Edwards' approach is given including recent results suggesting the validity of Edwards ergodic hypothesis for jammed states. A theoretical framework for packings whose constitutive particles range from spherical to non-spherical shapes like dimers, polymers, ellipsoids, spherocylinders or tetrahedra, hard and soft, frictional, frictionless and adhesive, monodisperse and polydisperse particles in any dimensions is discussed providing insight into an unifying phase diagram for all jammed matter. Furthermore, the connection between the Edwards' ensemble of metastable jammed states and metastability in spin-glasses is established. This highlights that the packing problem can be understood as a constraint satisfaction problem for excluded volume and force and torque balance leading to a unifying framework between the Edwards ensemble of equiprobable jammed states and out-of-equilibrium spin-glasses.

## CONTENTS

I. Introduction	2	Edwards ensemble	15
II. Statistical Mechanics for jammed granular matter	4	A. Jamming in soft and hard sphere systems	15
A. Definition of jammed states	5	1. Isostaticity in jammed packings	15
B. Metastability of jammed states	5	2. Packing of soft spheres	16
C. Edwards statistical ensemble for granular matter	7	3. Packing of hard spheres	18
D. Volume ensemble	10	4. The nature of random close packing	20
1. Conventions for space tessellation	11	5. Force statistics	23
2. Statistical mechanics of planar assemblies using quadrants	13	B. Test of ergodicity and the uniform measure in the Edwards ensemble	24
3. $\Gamma$ -distribution of volume cells	13	IV. Edwards volume ensemble	27
E. Stress and force ensemble	13	A. Mean-field calculation of the microscopic volume function	27
1. Force tilings	13	B. Packing of jammed spheres	30
2. Force network ensemble	14	C. Packing of high-dimensional spheres	33
3. Stress ensemble	14	D. Packing of disks	34
III. Phenomenology of jammed states and scrutinization of the		E. Packing of bidisperse spheres	36
		F. Packing of attractive colloids	38
		G. Packing of non-spherical particles	39

1. Coarse-grained Voronoi volume of non-spherical shapes	41
2. Parametrization of non-spherical shapes	43
3. Dependence of coordination number on particle shape	43
H. Towards an Edwards phase diagram for all jammed matter	44
V. Jamming Satisfaction Problem, JSP	47
A. Cavity approach to JSP	47
B. Edwards uniform measure hypothesis in the Edwards-Anderson spin-glass model	49
C. Opening Pandora's box: Test of Edwards uniform measure in the Sherrington-Kirkpatrick spin-glass model	51
1. Penultimate test of Edwards in the SK model	52
VI. Conclusions and outlook	54
Acknowledgments	56
A. Bounds on the average coordination number	56
B. Density of states $g(z)$	56
C. Algorithm to calculate Voronoi boundaries analytically	57
References	57

## I. INTRODUCTION

Materials composed of macroscopic grains such as sand, sugar, and ball bearings are ubiquitous in our everyday experience. Nevertheless, a fundamental description of both static and dynamic properties of granular matter has proven exceedingly challenging. Take for example the pouring of sand into a sandpile, Fig. 1a. This process can be considered as a simple example of a fluid-to-solid phase transition of a multi-particle system. However, it is not clear whether this transition is governed by a variational principle of an associated thermodynamic quantity like the free energy in equilibrium systems. Granular materials do not explore different configurations in the absence of external driving because thermal fluctuations induce negligible particle motion at room temperature and inter-grain dissipation and friction quickly drain the kinetic energy from the system. On the other hand, the *jammed* state of granular matter bears a remarkable resemblance with an amorphous solid in thermal equilibrium: both are able to sustain a non-zero shear stress; the phase transition from liquid to solid states and the analogous *jamming transition* in grains are both governed by one or a few macroscopic control parameters; and, when using certain packing-generation protocols, macroscopic observables, such as the packing fraction, are largely reproducible.

Jamming transitions not only occur in granular media, but also in soft materials such as colloidal suspensions which may asymptotically reach jamming under centrifugation, compressed emulsions, foams, glasses and spin-glasses below their glass transition temperature and bio-

logical materials such as cells, DNA and protein packing. Even more broadly, the jamming transition pertains to a larger family of computational problems named Constraint Satisfaction Problems (CSP) (Krzakala and Kurchan, 2007). These problems involve finding the values of a set of variables satisfying simultaneously all the constraints imposed on those variables and maximizing (or minimizing) an objective function. For example, in the problem of sphere packings, the goal is to minimize the volume occupied by the packing subject to the geometrical constraint of non-overlapping particles and the mechanical constraints of force and torque balance at mechanical equilibrium. In general, packing problems play a central role in various fields of science in addition to physics, such as discrete mathematics, number theory and information theory. An example of practical interest is the problem of efficient data transmission through error-correcting codes, which is deeply related to the optimal packing of (Hamming) spheres in a high-dimensional space (Conway and Sloane, 1999). The common feature of all packing problems is the existence of a phase transition, the jamming transition, separating the phase where the constraints are satisfiable from a phase where they are unsatisfiable.

The existence of constraints in physical systems causes, in general, a significant metastability. Metastability is the phenomenon by which the system remains confined for a relatively long time in suboptimal regions of the phase space. It is related to the rough energy (or free energy) landscape characterized by the presence of many non-trivially related minima as a function of the microscopic configurations (or the macroscopic states). Metastability is, indeed, the *leitmotiv* in most complex physical systems, whatever its origin. For example, in granular materials metastability arises from geometrical and mechanical constraints, but it is found also in spin glasses, which are magnetic systems with competing ferromagnetic and antiferromagnetic exchange interactions. In spin glasses, the emergence of metastability is due to frustration, which is the inability of the system to satisfy simultaneously all local ordering requirements. Notwithstanding their differences, these two physical systems, jammed grains and spin-glasses, exhibit a remarkably similar organization of their metastable states, a fact that stimulates our search for further analogies within these systems and common explanations. It is, indeed, this analogue approach, as best exemplified by the encompassing vision of Sir Sam Edwards (Goldbart *et al.*, 2005), that may shed new light on the solution to jamming problems otherwise doomed to remain obscure.

Due to their substantial metastability, these systems are fundamentally out-of-equilibrium even in a macroscopically quiescent state. Nevertheless, the commonalities with equilibrium many body systems suggest that ideas from equilibrium statistical mechanics might be useful. In this review, we consider theories for jammed

matter based on generalizations of equilibrium ensembles. These statistical mechanics-based approaches were pioneered by Sir Sam F. Edwards in the late 1980s (Fig. 1b).

Investigations of the structural properties of jammed packings are much older. In fact, the related problem of identifying the densest packing of objects has an illustrious history in the mathematical literature (Kepler, 1611; Weaire and Aste, 2008). Exact mathematical proofs of the densest packings are extremely challenging even for spherical particles. The Kepler conjecture of 1611 stating that the densest arrangement of spheres in three spatial dimensions (3d) is a face-centered-cubic (FCC) crystal with a packing volume fraction  $\phi_{\text{fcc}} = \pi/(3\sqrt{2}) \approx 0.74048\dots$  remained an unsolved mathematical problem for almost four centuries (Hales, 2005; Kepler, 1611). Systematic experiments on disordered hard-sphere packings began in the 1960s with the work by Bernal (Bernal, 1964; Bernal and Mason, 1960). These experiments are conceptually simple, yet give fundamental insight into the structure of dense liquids, glasses, and jammed systems. Equally sized spherical particles were placed into a container and compactified by shaking or tapping the system until no further volume reduction was detected. These experiments typically yielded configurations with packing fraction  $\phi_{\text{rcp}} \approx 0.64$ , which is historically referred to as random close packing (RCP).

In order to apply a statistical mechanical framework to these jammed systems, it is first necessary to identify the variables characterizing the state of the system macroscopically. Clearly, the system energy is not suitable, since it may either not be conserved (for frictional dissipative particles) or not be relevant (for frictionless hard particles). On the other hand, an obvious state variable is the system volume. In fact, unlike in equilibrium systems, the volume in jammed systems is not an externally imposed fixed variable, but rather depends on the microscopic configuration of the grains. Edwards first extraordinary insight was to parametrize the ensemble of jammed states by the volume function  $\mathcal{W}(\{\mathbf{r}_i, \hat{\mathbf{t}}_i\})$ , as a function of the  $N$  particles' positions  $\{\mathbf{r}_i\}$  and orientations  $\{\hat{\mathbf{t}}_i\}$ , as a replacement for the Hamiltonian in the equilibrium ensembles (Edwards and Oakeshott, 1989; Edwards, 1991, 1994; Mehta and Edwards, 1990).

A second crucial point in the development of the Edwards granular statistical mechanics is a proper definition of the jammed state. It is important to note that only jammed configurations  $\{\mathbf{r}_i, \hat{\mathbf{t}}_i\}$  are included in the ensemble. A definition of what we mean by jammed state is not a trivial task and will be treated rigorously in the next section. Assuming that an unambiguous definition of metastable jammed state can be expressed analytically, then a statistical mechanics approach to granular matter proceeds by analogy with equilibrium systems. In this case, the volume function allows for the definition of a granular entropy leading to both microcanonical and

canonical formulations of the volume ensembles. This implies, in particular, the existence of an intensive parameter conjugate to the volume. This temperature-like parameter was called *compactivity* by Edwards.

The full Edwards ensemble is characterized by the macroscopic volume and, further, by the stress of the packing. Since analytical treatments of the full ensemble are challenging, one typically considers suitable approximations. Neglecting correlations between the volume and the stress leads to a volume ensemble under the condition of isostaticity (Song *et al.*, 2008). The core of this review will be devoted to elaborate on a mean-field formulation of the Edwards volume ensemble that can potentially lead to a unifying phase diagram encompassing all jammed matter ranging from systems made of spherical to non-spherical particles, with friction or adhesion to frictionless particles, monodisperse and polydisperse systems and in any dimension. Likewise, we describe frameworks for stress and force statistics alone, such as the stress ensemble (Chakraborty, 2010; Henkes *et al.*, 2007), force network ensemble (Bouchaud, 2002; Snoeijer *et al.*, 2004; Tighe *et al.*, 2010), and belief propagation for force transmission (Bo *et al.*, 2014).

Edwards statistical mechanical ensemble rely on two assumptions: (i) Ergodicity and (ii) Equiprobability of microstates. These assumptions have been scrutinized in the literature, and the questions raised in this context will be reviewed here. Despite these critiques, the Edwards' approach has been used to describe a wide range of jammed and glassy materials. Early works adopted the concept of inherent structures from glasses (Coniglio *et al.*, 2002; Coniglio and Herrmann, 1996; Coniglio and Nicodemi, 2000, 2001; Fierro *et al.*, 2002b) and effective temperatures (Ciamarra *et al.*, 2006; Cugliandolo, 2011; Kurchan, 2000, 2001; Makse and Kurchan, 2002; O'Hern *et al.*, 2004; Ono *et al.*, 2002) with applications to plasticity (Lieou and Langer, 2012). More recent approaches are based on replica theory for hard-sphere glasses (Charbonneau *et al.*, 2017; Parisi and Zamponi, 2010). Valuable insight is gained from models that exhibit both jamming and glass transitions (Ikeda *et al.*, 2012; Krzakala and Kurchan, 2007; Mari *et al.*, 2009). In this review, we emphasize that the Edwards ensemble can be recast as a constraint satisfaction problems, which allows for an unifying view of hard-sphere glasses and spin-glasses through a synthesis applied at the foundation of granular statistical mechanics.

This review is organized as follows. In Sec. II we discuss the foundations of the ensemble approach via the rigorous definition of metastable jammed states, and the construction of microcanonical and canonical ensembles based on the volume function and stress-moment tensor, which play the role of the Hamiltonian in jammed systems. In Sec. III we collect empirical results on the phenomenology of jammed states. Moreover, we review results from experiments, simulations, and theoretical

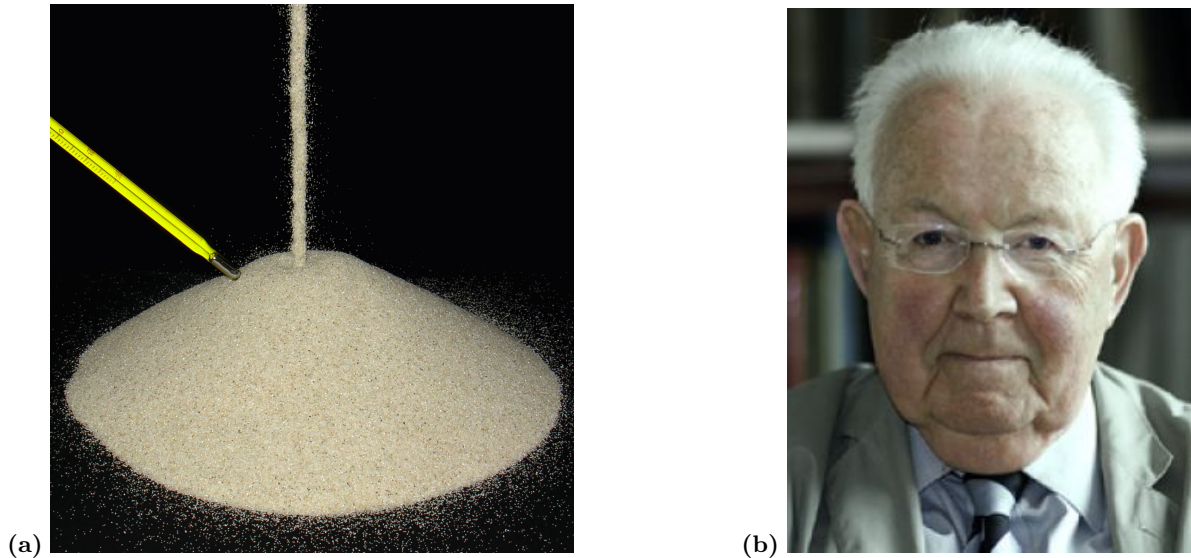


FIG. 1 (a) (Color online) Pouring grains into a sandpile is the simplest example of a jamming transition from a flowing state to a mechanically stable jammed state. However, this simplicity can be deceiving. In this review we show that building sandpiles is at the core of one of the most profound problems in disordered media. From the glass transition to novel phases in anisotropic colloidal systems, pouring grains in a pile is the emblematic system to master with tremendous implications on all sort of soft materials, from glasses, colloids, foams and emulsions to biomatter. Edwards’ endeavour to tame granular matter is condensed in the attempt of measuring the ‘temperature’ of the sandpile. (b) Sir Sam F. Edwards (February 1st 1928 – July 7th 2015) (Warner, 2017). S. F. Edwards first introduced the intriguing idea that a far-from-equilibrium, jammed granular matter could be described using methods from equilibrium statistical mechanics. In the Edwards’ ensemble, macroscopic quantities are computed as flat averages over force- and torque-balanced configurations, which leads to a natural definition of a configurational ‘granular’ temperature known as the compactivity.

models that test the ergodic and uniform measure underlying the ensemble approach. In Sec. IV we consider volume ensembles and their mean-field description, which provides quantitative predictions for ensemble averaged quantities such as the packing fraction of spherical and non-spherical particles. In Sec. V we discuss a unification between the Edwards ensemble of jammed matter and theories based on ideas from glass/spin glass theories under the CSP paradigm. In Sec. VI we finally close with a summary and a collection of open questions for future work.

In recent years a number of reviews have appeared dealing with more specific aspects of granular matter: (Richard *et al.*, 2005) (granular compaction), (Makse *et al.*, 2005) (jammed emulsions), (Bi *et al.*, 2015; Chakraborty, 2010) (stress ensembles), (Tighe *et al.*, 2010) (force network ensemble), (Cugliandolo, 2011; Qiong and Mei-Ying, 2014) (effective temperatures). The present review is also complementary to other reviews on jammed granular matter, which do not specifically discuss the Edwards thermodynamics: (Alexander, 1998; Borzsonyi and Stannarius, 2013; Charbonneau *et al.*, 2017; van Hecke, 2010; Jaeger *et al.*, 1996; Kadanoff, 1999; Liu and Nagel, 2010; Parisi and Zamponi, 2010; Torquato and Stillinger, 2010). Rather than replacing these reviews, our work puts these topics into the general

context of Edwards statistical mechanics and provides an overview of the immense amount of literature related to Edwards ensemble approaches.

## II. STATISTICAL MECHANICS FOR JAMMED GRANULAR MATTER

In a jammed system all particle motion is prevented due to the confinement by the neighbouring particles. The transition to a jammed state is thus not controlled by the temperature as conventional phase transitions in systems at thermal equilibrium, but by geometrical and mechanical constraints imposed by all particles in the system. Therefore, jammed states can be regarded as the set of solutions in the general class of Constraint Satisfaction Problems (CSP), which we term *Jamming Satisfaction Problem* (JSP), where the constraints are fixed by the mechanical stability of the blocked configurations of grains. From this standpoint, the jamming problem has a wider scope than the pure physical significance, encompassing the broader class of CSPs: the unique feature of the packing problem in the large universe of CSPs is that this system allows for a direct and relatively simple experimental test of theoretical predictions.



### A. Definition of jammed states

We consider an assembly of  $N$  (for the sake of simplicity) monodisperse particles described by the configurations of the particles  $\{\mathbf{r}_1, \hat{\mathbf{t}}_1; \dots; \mathbf{r}_N, \hat{\mathbf{t}}_N\}$ , where  $\mathbf{r}_i$  denotes the  $i$ th particle's position (of its center of mass) and  $\hat{\mathbf{t}}_i$  its orientation. The first problem we address concerns the definition of a blocked configuration of the particles, i.e., the jammed states. To be jammed the system has to satisfy both excluded volume and mechanical constraints. The excluded volume constraint enforces that particles do not overlap, and its mathematical implementation depends on the shape of the particles. For a system of monodisperse hard-spheres, this constraint takes on the following form:

$$|\mathbf{r}_i - \mathbf{r}_j| \geq 2R, \quad (\text{equal-size hard spheres}) \quad (1)$$

which means that the centers of any pair of particles  $i$  and  $j$  must be at a distance twice as large as their radius  $R$ . The hard-core constraint in Eq. (1) is valid only for monodisperse spheres, but it can be generalized to polydisperse and nonspherical particles.

The excluded volume constraint is necessary but not sufficient by itself to determine whether a configuration of particles is jammed. Indeed, it has to be supplemented by a constraint enforcing the mechanical stability of the system, requiring that particles satisfy the force and torque balance conditions. We denote by  $\mathbf{d}_a^i$  the vector connecting  $\mathbf{r}_i$  and the  $a$ th contact on the  $i$ th particle. At this contact there is a corresponding force vector  $\mathbf{f}_a^i$  on particle  $i$  arising from the contacting particle. With this notation we can formulate the conditions of force and torque balances for a particle of general shape:

$$\sum_{a \in \partial i} \mathbf{f}_a^i = 0, \quad i = 1, \dots, N \quad (2)$$

$$\sum_{a \in \partial i} \mathbf{d}_a^i \times \mathbf{f}_a^i = 0, \quad i = 1, \dots, N \quad (3)$$

where the notation  $\partial i$  denotes the set of contacts of particle  $i$ . Equations (2–3) apply to both frictional and frictionless particles. In the latter case there is only one single force component in the normal direction

$$\mathbf{f}_a^i = -f_a^i \hat{\mathbf{n}}_a^i \quad (\text{frictionless}), \quad (4)$$

where  $\hat{\mathbf{n}}_a^i$  denotes the normal unit vector at the contact point, which depends on the particle shape. For frictional particles, we can decompose  $\mathbf{f}_a^i$  into a normal component  $f_{a,n}^i$  and a force vector in the tangent plane  $\mathbf{f}_{a,\tau}^i$  (see Fig. 2). Coulomb's law with friction coefficient  $\mu$  is then expressed by the inequality

$$|\mathbf{f}_{a,\tau}^i| \leq \mu f_{a,n}^i \quad (\text{frictional}). \quad (5)$$

If the interparticle forces are purely repulsive, as in most of the cases treated in this review, we also have the condition:

$$\mathbf{d}_a^i \cdot \mathbf{f}_a^i < 0. \quad (6)$$

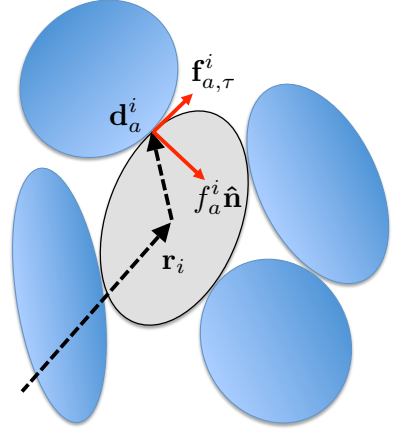


FIG. 2 Parametrization of a jammed configuration involving 5 non-spherical grains. The tangential  $\mathbf{f}_{a,\tau}^i$  and normal force vectors  $f_{a,n}^i \hat{\mathbf{n}}_a^i$  at contact  $a$  on particle  $i$  are shown.  $\mathbf{d}_a^i$  indicates the vector from the center of particle  $i$  to the contact point  $a$  between one of its neighbours.  $\mathbf{r}_i$  gives the location of the center of particle  $i$ . The grey-shaded particle is mechanically stable if all forces and torques generated at the four contact points cancel (see Eqs. (2,3)).

Finally, Newton's third law implies, that two particles  $i, j$  in contact at  $a$  satisfy:

$$\mathbf{f}_a^i = -\mathbf{f}_a^j. \quad (7)$$

### B. Metastability of jammed states

Having defined the necessary and sufficient conditions for a granular system to be jammed, we now provide a finer description of jammed states, based on the concept of metastability, i.e., their stability with respect to particles displacements. A characterization similar to the one proposed here appeared already in (Torquato and Stillinger, 2001), where the authors defined the concept of jamming categories for metastable packings. The similarities with the classification of the jammed states in (Torquato and Stillinger, 2001) are discussed in parallel with the classification presented next.

To define properly the metastable jammed states we need to specify with respect to what type of displacements they are metastable. More precisely, if we start from an initially jammed state satisfying Eqs. (1)–(7) and then displace a set of particles, how do we decide if the initial state is stable under this move? A helpful discriminant is the volume  $V$  or equivalently the volume fraction of the packing  $\phi$  defined as the ratio of the volume occupied by the particles to the total volume of the system and the number of particles involved in the displacement. Thus, consider an initially jammed state, and assume you can displace only one particle at a time. If the volume fraction of the packing is not increasing whatever

particle you move, then we may assert that the packing is stable against any single particle displacement. We call this type of jammed state a 1-Particle-Displacement (1-PD) metastable jammed state, which is defined as a configuration whose volume fraction cannot be increased by the displacement of one single particle, see Fig. 3a. However,  $\phi$  may be increased by moving a set of two or more particles at the same time. The definition of 1-PD metastable jammed states is the same as the definition of *local* jamming in (Torquato and Stillinger, 2001), stating that in a locally jammed configuration no single particle can be displaced while keeping the positions of all other particles fixed.

We can now extend this definition to jammed states which are stable with respect to the simultaneous displacement of multiple particles. Specifically, we define a  $k$ -Particle-Displacement ( $k$ -PD) metastable jammed state as a configuration whose volume fraction cannot be increased by the simultaneous displacement of any contacting subset of  $1, 2, \dots, k$  particles. Again, we find this definition quite similar to the definition of the *collective* jamming category in (Torquato and Stillinger, 2001), which states that in collectively jammed configurations no subset of particles can be simultaneously displaced so that its members move out of contact with one another and with the remaining set. Following the definitions given above a *ground state* of the system is a configuration whose volume fraction cannot be increased by the simultaneous displacement of any finite number of particles. A ground state of jamming corresponds to the  $k \rightarrow \infty$  limit of a  $k$ -PD metastable jammed state, the  $\infty$ -PD jammed ground state.

In the following section we will introduce the volume function  $\mathcal{W}(\mathbf{r})$  to parametrize the system volume as a function of the particles' positions. It is useful then to classify the  $k$ -PD metastable jammed states in terms of the minima of this function. More precisely, we identify the  $k$ -PD metastable jammed states as those states that satisfy the geometrical and mechanical constraints and are local minima of  $\mathcal{W}(\mathbf{r})$ . For example, 1-PD metastable states are those configurations  $\mathbf{r}^*$  for which  $\mathcal{W}(\mathbf{r})$  is convex around  $\mathbf{r}^*$  under 1-Particle-Displacements, but non-convex under  $k$ -Particle-Displacements with  $k > 1$ , see Fig. 4a. Here, convex means that all the eigenvalues of the Hessian of  $\mathcal{W}(\mathbf{r})$  evaluated at the configurations  $\mathbf{r}^*$  are positive, while non-convex means that there exists at least one negative eigenvalue in the spectrum of the Hessian. Similarly,  $k$ -PD metastable states are those configurations  $\mathbf{r}^*$  for which  $\mathcal{W}(\mathbf{r})$  is convex around  $\mathbf{r}^*$  under any  $k'$ -Particle-Displacements with  $k' \leq k$ , and non-convex under any  $k'$ -Particle-Displacements with  $k' > k$ . A simple example of a 1-PD metastable jammed state is shown in Fig. 3a.

Interestingly, in spin-glass systems the (energetically) metastable states can be defined in a similar way, not with respect to volume but with respect to energy. The

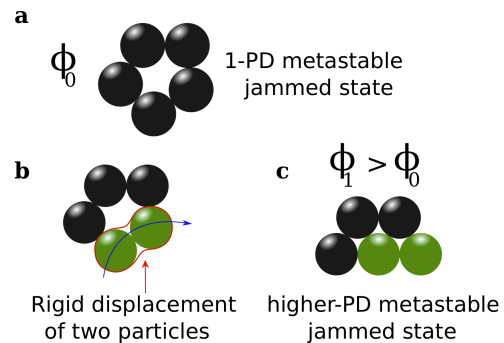


FIG. 3 (a) Example of a 1-Particle-Displacement jammed state: no particle can increase the volume fraction by displacing itself while keeping the others fixed in their positions. It is assumed that a membrane is keeping the particles in place or that they are surrounded and kept in place by a rigid container. (b) The 1-PD metastable state in (a) is not stable under 2PD. Simultaneous displacement of two particles: to escape the 1-PD metastable trap, two contacting particles are displaced while keeping the others fixed in their positions. (c) Higher order metastable jammed state: after the move in (b), a new metastable jammed state is reached having higher stability than the original one in (a).

analog of the 1-PD metastable jammed state is, for a spin glass, the 1-spin-flip (1-SF) metastable state, defined as a configuration whose energy cannot be lowered by the flip of any single spin. Similarly the  $k$ -spin-flip ( $k$ -SF) metastable state, akin to the  $k$ -PD metastable jammed state, is a configuration whose energy cannot be lowered by the flip of any cluster of  $1, 2, \dots, k$  spins. Moreover, for spin glasses, several rigorous results on metastable states are known, including their probabilities, basins of attraction, and how they are sampled by various dynamics (Newman and Stein, 1999). These results are explained in detail in Section V along with their granular counterpart. The analogy between grains, hard-sphere glasses, and spin glasses has been reviewed in (Dauchot, 2007) and is described in Table I and Fig. 4a.

Protocols to generate jammed packings usually lead to a non-zero fraction of particles ( $2 - 5\%$ ), which remain mobile even though all other particles are  $\infty$ -PD jammed. These particles are called *rattlers* and can be displaced within a cage without changing the volume function.

Now that we have a rigorous definition for the jammed states and their metastable classification, we address the crucial problem of how to describe their statistical mechanics. Consider a granular material undergoing vertical tapping. After tapping, the system relaxes into a jammed state. Subsequent tapping will allow the system to explore other jammed states. An important question arises: how does the tapping dynamics sample the jammed states, or what is the probability measure for jammed states obtained from tapping?

	Granular matter	Hard-Sphere Glasses	Spin-Glasses
Thermodynamic descriptor	Volume function $\mathcal{W}(\mathbf{q})$	Density functional $\mathcal{S}[\rho(\mathbf{r})]$	Hamiltonian $\mathcal{H}(\boldsymbol{\sigma})$
Lagrange multiplier	Compactivity $X$	Pressure $P$	Temperature $T$
Entropy	Edwards entropy $S(V)$	Configurational entropy $\Sigma$	Complexity $\Sigma$
Metastable states	Minima of $\mathcal{W}(\mathbf{q})$ + jamming constraint	Minima of $\mathcal{S}[\rho(\mathbf{r})]$	Minima of $\mathcal{H}(\boldsymbol{\sigma})$ at $T = 0$
Local metastable	1-Particle-Displacement	$\phi \in [\phi_{\text{th}}, \phi_{\text{GCP}})$	1-Spin-Flip ( $T = 0$ )
Collective metastable	$k$ -Particle-Displacement		$k$ -Spin-Flip ( $T = 0$ )
Global metastable	$\infty$ -Particle-Displacement $0 \leq \alpha < 1$		$\infty$ -Spin-Flip ( $T = 0$ ) $0 \leq \alpha < 1$
Ground state	$\infty$ -Particle-Displacement $\alpha = 1$	$\phi_{\text{GCP}}$	$\infty$ -Spin-Flip ( $T = 0$ ) $\alpha = 1$

TABLE I Synoptic view of unifying framework to understand the thermodynamics, relevant observables and classification of metastable states in granular matter, hard-sphere glasses and spin-glasses. The four categories of jamming are defined according to their metastability: local metastable (1-PD/SF stable); collective metastable ( $k$ -PD/SF stable with finite  $1 < k < \infty$ ); globally metastable ( $\infty$ -PD/SF stable, but with  $0 \leq \alpha < 1$ , where  $\alpha = k/N$  for  $k, N \rightarrow \infty$ ); and the true global ground state ( $\infty$ -PD/SF stable and  $\alpha = 1$ ).

### C. Edwards statistical ensemble for granular matter

In 1989 Edwards made the remarkable proposal that the macroscopic properties of static granular matter can be calculated as ensemble averages over equiprobable jammed microstates controlled by the system volume (Edwards and Oakeshott, 1989). The thermodynamics of powders was created with this claim (Edwards, 1994):

*“We assume that when  $N$  grains occupy a volume  $V$  they do so in such a way that all configurations are equally weighted. We assume this; it is the analog of the ergodic hypothesis of conventional thermal physics.”*

This idea is very suggestive because it turns a complicated dynamical problem into a relatively simpler equilibrium problem. Such an equilibrium sampling in a non-equilibrium system has been recently also adopted by several authors in the glass community to study the ground state of amorphous packings as the infinite pressure limit of metastable glassy states described by equilibrium sta-

tistical mechanics (Charbonneau *et al.*, 2017; Parisi and Zamponi, 2010). Here, in the so-called Monasson construction (Monasson, 1995), a modified equilibrium average over metastable states is taken, supplemented by the additional assumption that such metastable states become jammed states in the infinite-pressure limit. In such a limit, the states are sampled flatly and the Monasson construction is exactly the Edwards ensemble. Even more, it turns out that mean-field glass models relaxing at zero temperature have exactly Edwards ergodicity property (Kurchan, 2001): at long times any nonequilibrium observable is correctly given by the typical value it takes over all local energy minima of the appropriate energy density. The original idea put forward by Edwards is basically to take the flat average at the end, i.e., in the jammed state.

Under the Edwards ergodic hypothesis, granular matter should be amenable to an equilibrium statistical mechanical treatment, where the role of energy is played by

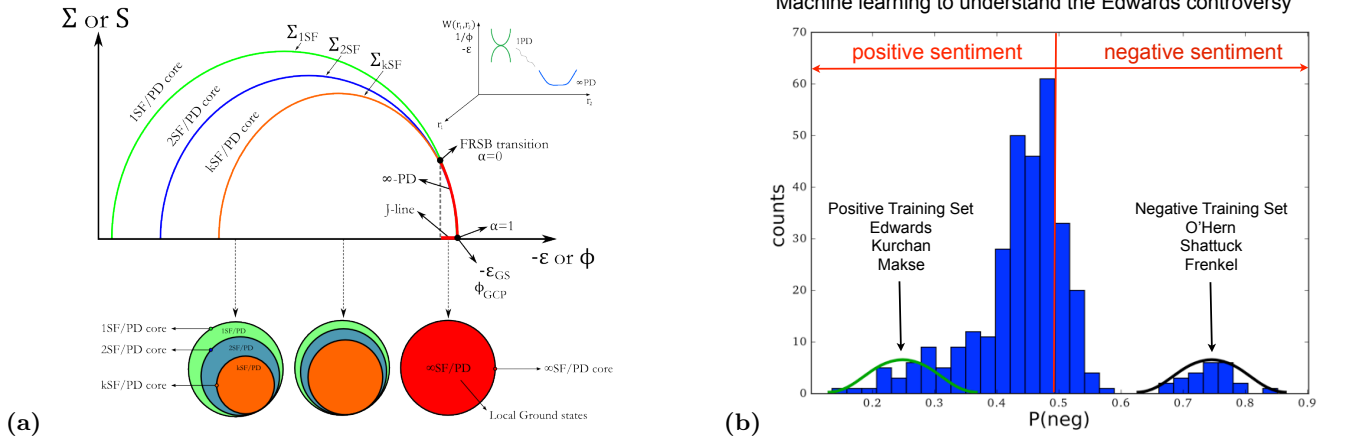


FIG. 4 (Colors online) (a) Unification between Edwards statistical mechanics of jammed matter and the mean field picture of spin glasses. Main panel: Edwards entropy  $S(\phi)$  versus the volume fraction,  $\phi$ , of the metastable states  $k$ -PD and ground state  $\infty$ -PD in the jamming model as well as the analogous complexity  $\Sigma(\epsilon)$  versus the negative energy density,  $-\epsilon$ , in the spin glass models in terms of the equivalent  $k$ -SF metastable and  $\infty$ -SF ground state. The J-line corresponds to the ground states between  $[\phi_{\text{th}}, \phi_{\text{GCP}}]$  and are  $\infty$ -PD states with only positive eigenvalues for the Hessian. This line is obtained by changing  $\alpha = k/N$  between  $[0, 1]$  and  $k \rightarrow \infty$  and  $N \rightarrow \infty$  below the full replica symmetry breaking transition as indicated. Top right panel: Schematic representation of the metastable states 1-PD and ground state  $\infty$ -PD of jamming in the volume landscape (the analogous 1-SF metastable states and the  $\infty$ -SF ground state in the energy landscape of spin glasses is a function of the spin configuration  $\sigma$  instead of  $\mathbf{r}$ ). Lower panel: Organization of the  $k$ -PD metastable states into a hierarchy of successively nested  $k$ -PD cores ( $k$ -cores). (b) Machine learning classifier applied to the abstracts of 581 papers citing the original Edwards paper (Edwards and Oakeshott, 1989) to classify the sentiment of the citing authors regarding the validity of the Edwards ergodic hypothesis. We construct two training sets of papers of the authors indicated in the figure based on the positive sentiment (showing results in agreement with Edwards and assigned  $P(\text{neg}) = 0$ ) and negative sentiment (in disagreement with Edwards, assigned  $P(\text{neg}) = 1$ ). The training sets are then re-classified as indicated. In the negative training set we do not include the recent paper of the Frenkel group showing the validity of Edwards ensemble at the jamming transition (Martiniani *et al.*, 2017) (we thank the authors for allowing us to use their papers as training sets). We use the same machine learning methods from (Bovet *et al.*, 2016) used to predict presidential elections from Twitter activity, see also (Bohannon, 2017), <http://bit.ly/2nSjHuI>. While the majority of authors are neutral, the classifier also identifies two polarized groups; the positive sentiment being the largest one going gradually from neutral to extreme positive. A gap at  $P(\text{neg}) = 0.6$  separates this group from the negative one. Recent work (Martiniani *et al.*, 2017) seems to justify this “wisdom of crowds” effect, see Section III.B.

the volume, and all the jammed states at a fixed volume are equally probable. In granular assemblies consisting of dry particles in a size range above a few microns, the thermal energy at room temperature can be neglected and neither equilibrium entropy nor free energy can be used as thermodynamic potentials to describe the system. Nevertheless, for large enough particle numbers, statistical ideas seem relevant: Macroscopic observables such as the packing fraction are robustly reproduced for a given protocol. If operations manipulating individual particles are neglected, granular assemblies are thus described by well defined macrostates that correspond to many different microscopic configurations. Instead of the energy, one can equivalently take the volume as the key variable characterizing the macrostate of a static assembly. S. F. Edwards insight has suggested to consider the volume of a granular assembly analogous to the energy of an equilibrium system: Unlike in typical equilibrium systems, the volume is not an externally fixed parameter, but depends on the microscopic configuration of the particles

including positions and orientations. This suggests to introduce a volume function  $\mathcal{W}(\{\mathbf{r}_i, \hat{\mathbf{t}}_i\})$  giving the system volume as a function of the particles’ positions  $\mathbf{r}_i$  and orientations  $\hat{\mathbf{t}}_i$  equivalent to the Hamiltonian  $\mathcal{H}(\{\mathbf{p}_i, \mathbf{r}_i\})$ ,  $i = 1, \dots, N$ .

With this analogy, all concepts of equilibrium statistical mechanics can be carried over into the realm of non-thermal static granular systems opening the door for the use of thermal concepts for athermal systems, i.e., there is a whole new statistical mechanics emerging from the point which, in conventional, thermal, statistical mechanics corresponds to  $T = 0$ ,  $S = 0$  (Edwards, 2008). For an in-depth treatment of equilibrium statistical mechanics we refer to standard textbooks (Huang, 1987; Landau and Lifshitz, 1980; Pathria and Beale, 2011). In particular, one can introduce the concept of a granular entropy  $S(V)$  as a measure of the number of microstates  $\Omega(V)$



for a given fixed volume  $V$

$$S(V) = \lambda \log \Omega(V), \quad (8)$$

$$\Omega(V) = \int d\mathbf{q} \delta(V - \mathcal{W}(\mathbf{q})) \Theta_{\text{jam}}. \quad (9)$$

Here, we use the shorthand notation  $\mathbf{q} = \{\mathbf{r}_i, \hat{\mathbf{t}}_i\}$  and  $\int d\mathbf{q} = \prod_{i=1}^N \int d\mathbf{r}_i \oint d\hat{\mathbf{t}}_i$ . The parameter  $\lambda$  ensures the correct dimension of  $S$  as volume (set to unity in the following).

The function  $\Theta_{\text{jam}}$  in Eq. (9) is crucial. It is there to admit only microstates in the ensemble that are jammed by enforcing the excluded volume and mechanical stability constraints in Eqs. (1)–(7). Only these rigid states lead to a static assembly at fixed volume. While this function has been treated lightly in earlier studies of Edwards thermodynamics, it contains most of the interesting physics of the problem and therefore will be treated carefully in the remaining of this review. More precisely,  $\Theta_{\text{jam}}$  admits only the solutions of the Jamming Satisfaction Problem (JSP), which reads for monodisperse hard-spheres:

$$\begin{aligned} \Theta_{\text{jam}} = & \prod_{i,j=1}^N \theta(|\mathbf{r}_i - \mathbf{r}_j| - 2R) && \text{hard - core (spherical)} \\ & \times \prod_{i=1}^N \delta\left(\sum_{a \in \partial i} \mathbf{f}_a^i\right) && \text{force balance} \\ & \times \prod_{i=1}^N \delta\left(\sum_{a \in \partial i} \mathbf{d}_a^i \times \mathbf{f}_a^i\right) && \text{torque balance} \\ & \times \prod_{i=1}^N \prod_{a \in \partial i} \theta(\mu f_{a,n}^i - |\mathbf{f}_{a,\tau}^i|) && \text{Coulomb friction} \\ & \times \prod_{i=1}^N \prod_{a \in \partial i} \theta(-\mathbf{d}_a^i \cdot \mathbf{f}_a^i) && \text{repulsive forces} \\ & \times \prod_{\text{all contacts } a} \delta(\mathbf{f}_a^i + \mathbf{f}_a^j) && \text{Newton 3rd law} \end{aligned} \quad (10)$$

Implicit in this microcanonical description is again the underlying assumption of equiprobability: The distribution of jammed configurations  $\mathbf{q}$  at a given volume is uniform:

$$P_{\text{mic}}(\mathbf{q}) = \Omega(V)^{-1} \delta(V - \mathcal{W}(\mathbf{q})) \Theta_{\text{jam}}. \quad (11)$$

The definition of  $\Theta_{\text{jam}}$  deserves a crucial clarification. According to the classification of metastable jammed states given previously, when constructing the volume ensemble we have to specify what type of metastable jammed states we are considering at the fixed volume  $V$ . The crucial point is that  $k$ -PD jammed states are fundamentally different for different values of  $k$ , and hence there is no reason, in principle, to assign them the same statistical weight across all the values of  $k$ . In other words, when we fix the volume  $V$ , we consider

as equiprobable only the jammed state corresponding to the same metastable class, i.e., with the same  $k$ . This is evident in the language of jammed categories: a locally jammed state ( $=1$ -PD) is substantially different from a collectively jammed state ( $=k$ -PD), and it cannot be claimed, *a priori*, that they are found with equal probability in a tapping experiment, even if they may have the same density. An identical situation applies to metastable states in spin-glasses and disordered ferromagnets where the equiprobability of the metastable states has been rigorously studied (Newman and Stein, 1999).

This clarification is very important, and indeed it is at the origin of many headaches when trying to prove or disprove Edwards conjecture. In the absence of a first principle derivation of Edwards statistical mechanics, there has been a long standing controversy on its validity, as illustrated in Fig. 4b. Even if this condition did not appear in the original formulation by Edwards, it is nevertheless a quite obvious requirement, especially in light of analogous exact results in spin-glasses and hard-sphere glasses (Newman and Stein, 1999; Parisi and Zamponi, 2010). The reason to not make explicit this further condition was presumably the feeling of Edwards that the jammed states that only matter in granular media are the ones corresponding to  $k = \infty$ , i.e. the “ground states” (see however (Edwards *et al.*, 2004) for a more detailed discussion). Here, we extend Edwards idea also to jammed states with  $k < \infty$ . Summing it up, the correct reading of the assumption about the probability measure over jammed states must take into account the restriction to the states within the same  $k$ -PD class, a condition that must be included in the definition of  $\Theta_{\text{jam}}$  as an additional constraint. In practice this can be done after having defined the volume function of the system, which provides an unambiguous definition of mechanically metastable states via its convexity, much in the same way as for spin-glasses, the Hamiltonian allows one to properly define the energetically metastable states, i.e. its local minima (Newman and Stein, 1999). This topic will be discussed in detail in Section V.

In principle the Edwards conjecture can be correct or not, and a case-by-case analysis is required to establish its validity. In granular systems, Liouville’s theorem for the conservation of phase space volume under time evolution (the cornerstone of conventional equilibrium statistical mechanics) does not hold, leading to nonzero phase space compressibility. The reason is the strongly dissipative nature of granular assemblies, which are dominated by static frictional forces; although an intuitive proof for the use of  $\mathcal{W}$  in granular thermodynamics has been sketched by the analogous proof of the Boltzmann equation (H-theorem) (Edwards *et al.*, 2004).

In this ensemble, statistical averages of observables are assumed to be equal to time averages over single trajec-

tories, provided the actual dynamics is ergodic. This can be induced by external drive, such as infinitesimally small tapping or very slow shearing. Since the drive induces fluctuations of the packing configuration, and thus fluctuations of the volume, one can similarly introduce a canonical picture (without change in particle number). The analogue of temperature is called compactivity  $X$ , whose inverse is the derivative of the granular entropy

$$X^{-1} = \frac{\partial S(V)}{\partial V}. \quad (12)$$

For a real granular system, the compactivity can be thought of as a measure of how more compact the system can possibly be. Large values of  $X$  indicate a loose or “fluffy” (but mechanically stable) configuration, whose volume could be reduced further under rearrangement.

The canonical distribution follows from the maximization of the Gibbs entropy just as in thermal equilibrium under the constraint of a fixed average volume

$$V = \int d\mathbf{q} \mathcal{W}(\mathbf{q}) P_{\text{can}}(\mathbf{q}), \quad (13)$$

and has the standard Gibbs form and canonical partition function:

$$P_{\text{can}}(\mathbf{q}) = \frac{1}{\mathcal{Z}} e^{-\mathcal{W}(\mathbf{q})/X} \Theta_{\text{jam}}, \quad (14)$$

$$\mathcal{Z} = \int d\mathbf{q} e^{-\mathcal{W}(\mathbf{q})/X} \Theta_{\text{jam}}. \quad (15)$$

If we follow the analogy with equilibrium thermodynamics, the concepts of granular entropy and compactivity translate into postulated laws of a granular thermodynamics (Edwards *et al.*, 2004):

*Zeroth law.* A consistent picture of compactivity as a temperature-like parameter requires the notion of equilibration: Two systems in physical contact should equilibrate to the same compactivity. The required “volume” transfer is achieved by the external drive, but needs to avoid any mixing of the particles.

*First law.* The analogy with granular matter is not clear as a distinction between heat and work is not useful for jammed granular materials.

*Second law.* In any natural process, the granular entropy always increases. The second law forms the basis of Edwards statistical mechanics.

*Third law.* Our qualitative discussion of compactivity suggests that entropy should thus be a monotonically increasing function of  $X$ : Loose packings at high  $X$  can be realized in many more configurations than dense packings at low  $X$ . In the limit  $X \rightarrow 0$  we can thus postulate that  $S(V) \rightarrow \text{const}$ . The limiting entropy will be finite for any disordered arrangement, while  $S(V) = 0$  is only achieved for a fully ordered non-degenerate crystal structure.

Up to now we have considered only the volume  $V$  as the relevant variable to characterize the jammed state of

a granular system. However, this is not the general case. Indeed, when the system is shaken the grains will fill a volume  $V$  and exert a stress  $\hat{\Sigma}$  on the boundary. Shaking after shaking, the system explores presumably typical configurations in the configuration phase space, which are subject to the constraint on  $V$  and also on  $\hat{\Sigma}$ . Consequently, the entropy of the system  $S(V, \hat{\Sigma})$  must then be computed as a function of those observables, which in the microcanonical ensemble can be defined as

$$S(V, \hat{\Sigma}) = \log \int d\mathbf{q} \delta(V - \mathcal{W}(\mathbf{q})) \delta(V\hat{\Sigma} - \hat{\Phi}(\mathbf{q})) \Theta_{\text{jam}} \quad (16)$$

where

$$\hat{\sigma}_i = \sum_{a \in \partial i} \mathbf{d}_a^i \otimes \mathbf{f}_a^i \quad (17)$$

is the stress tensor associated with particle  $i$  and the sum

$$\hat{\Phi} = \sum_{i=1}^N \hat{\sigma}_i = \sum_{i=1}^N \sum_{a \in \partial i} \mathbf{d}_a^i \otimes \mathbf{f}_a^i \quad (18)$$

is the macroscopic force-moment tensor.

In analogy to the volume ensemble, there should thus exist a temperature-like Lagrange multiplier associated with the stress. Since  $\hat{\Sigma}$  is a tensor, this quantity is also a tensor, which can be defined as

$$\hat{\Lambda}_{ij} = V \frac{\partial \hat{\Sigma}_{ij}}{\partial S}. \quad (19)$$

The tensor  $\hat{\Lambda}$  is referred to as angoricity from the Greek word *ankhos* for stress (Blumenfeld and Edwards, 2009).

A simplification occurs if the stress  $\hat{\Sigma}$  is a simple hydrostatic pressure  $\hat{\Sigma} = p$ . In this case the angoricity degenerates to the scalar quantity  $\Lambda = V \partial p / \partial S$ .

Considerable progress in a theoretical description of granular matter could be achieved from pure volume and stress/force ensembles, which appear as limits of the full description Eq. (16). We discuss these in detail in the following. On the other hand, it has been suggested that volume and stress ensembles are necessarily interdependent, which would require more sophisticated approaches to deal with their correlations (Blumenfeld *et al.*, 2012; Pugnaloni *et al.*, 2010).

#### D. Volume ensemble

Pure volume ensembles neglect the force degrees of freedom. This is reasonable, e.g., in isostatic systems, where all forces are uniquely determined from the configurational degrees of freedom. In this case, the statistical volume ensemble is fully specified by the volume function Eq. (14), which relies on a suitable space tessellation.

## 1. Conventions for space tessellation

In the case of a Hamiltonian there is a unique way to define the energy as a function of the particle configurations, typically in terms of a superposition of all particles' individual kinetic and potential energy plus the energy contribution due to interactions. Such a decomposition is not straightforward in the case of the volume function. Nevertheless, it is natural to express  $\mathcal{W}$  in the form of a superposition

$$\mathcal{W}(\mathbf{q}) = \sum_{i=1}^N \mathcal{W}_i(\mathbf{q}) \quad (20)$$

of non-overlapping volume elements that tessellate the space occupied by the packing.  $\mathcal{W}_i$  is the volume associated with each of the  $N$  particles. Crucially, this volume is not a function of the configuration of the  $i$ th particle only. Naively, one could imagine that  $\mathcal{W}_i$  depends solely on the configurations of particles in the first coordination shell. However, such a restriction is mathematically not sufficient and does not apply in general, e.g., in the Voronoi tessellation. The collective nature of the systems' response to perturbations induces dependencies on particles further away. Moreover, even if one considers only particles in the first coordination shell as a first approximation, a precise definition of  $\mathcal{W}_i$  is not straightforward. The key problem is to reference individual particles, so that their neighbours can be defined. While this is easily achieved in a regular crystalline packing, the difficulties originating from a disordered contact network have been realized early on (Edwards and Oakeshott, 1989; Mounfield and Edwards, 1994). Below we review the different definitions of  $\mathcal{W}_i$  in historical order.

*a. Tensorial formulation* A first solution to the problem of defining  $\mathcal{W}(\mathbf{q})$  was proposed in (Edwards and Grinev, 2001). Introducing the tensor (Edwards and Grinev, 1999a,b)  $\hat{F}_i = \sum_{j \in \partial i} \mathbf{r}_{ij} \otimes \mathbf{r}_{ij}$ , where  $\mathbf{r}_{ij}$  is the separation vector of particles  $i$  and  $j$ , we can define the volume associated with particle  $i$  as  $\mathcal{W}_i = 2\sqrt{\det \hat{F}_i}$ , which involves only contacting particles. The resulting total volume  $\mathcal{W} = \sum_{i=1}^N \mathcal{W}_i$  is thus only an approximation of the exact volume occupied by all  $N$  particles. Formal corrections that allow for an exact definition of  $\mathcal{W}$  have been suggested, but the quantities specifying correlations of tensors belonging to nearest neighbours are intractable for any practical purposes (Edwards and Grinev, 2001).

*b. Quadrons* In 2d, a definition of  $\mathcal{W}_i$ , such that Eq. (20) is exact can be obtained by analysing planar packings in terms of loops and voids (Ball and Blumenfeld, 2002; Blumenfeld and Edwards, 2003), leading to area-tessellating quadrilateral elements referred to as quadrons. In 2d one

can show that the number of quadrons is identical to the number of configurational degrees of freedoms (Blumenfeld and Edwards, 2003, 2006), motivating the use of the quadrons as the elementary “particles” of the system on which the statistical mechanics is based. In 3d this coincidence is no longer valid (Blumenfeld and Edwards, 2006), thus limiting the applicability of the quadrons to realistic systems. Even in 2d it has been noted that the exact tessellation is only valid in the absence of non-convex voids, which are actually present in a gravitational field (Ciamarra, 2007).

*c. Delaunay tessellation* For a set of points specifying, e.g., the centres of spheres in a packing, elementary Delaunay cells are simplexes with vertices at the centres of neighbouring particles. In 2d the simplexes are triangles defined such that no other point lies inside the circumcircle of a given triangle. In 3d the simplexes are likewise tetrahedra defined such that no other point lies inside the circumsphere of a given tetrahedron. In both cases a space filling set of cells is obtained, which, however, is not uniquely associated with a given set of particles. Thus, it is not possible to cast this tessellation into the form of Eq. (20), reducing its applicability to realistic systems. The Delaunay tessellation has been used to analyse the volume statistics of disordered sphere packings (Aste, 2005, 2006; Aste *et al.*, 2007; Finney, 1970; Hiwatari *et al.*, 1984; Klumov *et al.*, 2014), and is the cornerstone in Hales' proof of the Kepler conjecture.

*d. Voronoi tessellation* A straightforward way to tessellate the volume of a packing is to associate that amount of space with particle  $i$  that is closer to it than to any other particle (Fig. 5), thus making full use of the form Eq. (20). This defines the Voronoi tessellation, first introduced by the Ukrainian mathematician G. F. Voronoi in 1908, which is now widely used in mathematics and many applied areas (Aurenhammer, 1991; Okabe *et al.*, 2000). In the case of spheres or points, the Voronoi tessellation is dual to the Delaunay decomposition: the centres of the circumspheres are just the vertices of the Voronoi graph.

Before we define the volume  $\mathcal{W}_i$ , we first introduce the Voronoi boundary (VB). The VB between two particles is defined as the hypersurface that contains all the points that are equidistant to the surfaces of both particles (Baule *et al.*, 2013; Portal *et al.*, 2013; Schaller *et al.*, 2013). If we fix our coordinate system at the centre of mass of particle  $i$  (and also assume its orientation fixed), we can parametrize the VB in terms of the direction  $\hat{\mathbf{c}}$  from particle  $i$  (Fig. 5b). A point on the VB is found at  $s\hat{\mathbf{c}}$ , where  $s$  depends on the relative position  $\mathbf{r}_{ij}$  and orientation  $\hat{\mathbf{t}}_{ij}$  of the two particles:  $s = s(\mathbf{r}_{ij}, \hat{\mathbf{t}}_{ij}; \hat{\mathbf{c}})$ . The value of  $s$  is obtained from two conditions:

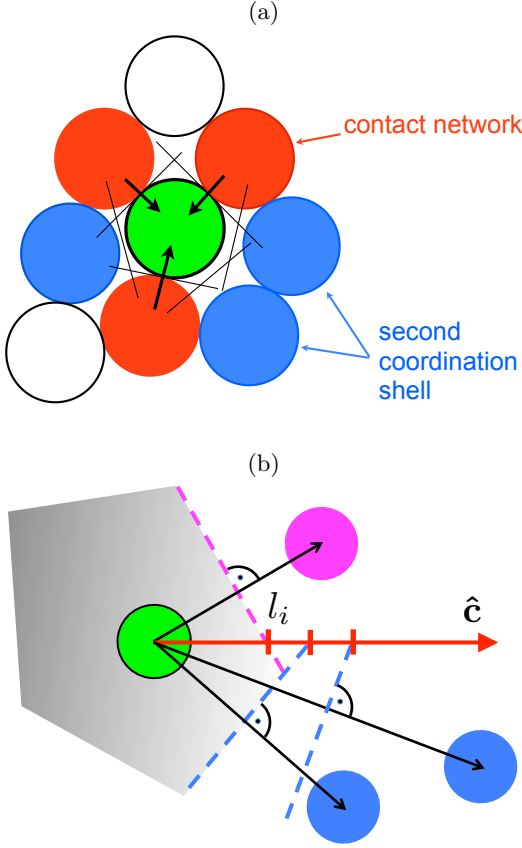


FIG. 5 (Colors online) Illustration of the Voronoi tessellation in a packing of monodisperse disks. (a) In this case the Voronoi boundary (VB) between two particles is the plane perpendicular to the separation vector at half the distance (see Eq. (21)). The VBs of the reference particle (green) with the particles in the first and second coordination shell are indicated with thin black lines. (b) The volume of a Voronoi cell associated with a given particle is defined as the amount of space that is closer to the surface of that particle than to the surface of any other particle. The cell boundary  $l_i(\mathbf{q}, \hat{\mathbf{c}})$  in a given direction  $\hat{\mathbf{c}}$  for a configuration  $\mathbf{q}$  thus follows from the global minimization Eq. (24) and the cell volume from the orientational integral Eq. (23). In the figure the contributed VBs of all particles along  $\hat{\mathbf{c}}$  are indicated. The pink particle contributes the smallest VB, which thus defines the boundary of the Voronoi cell (indicated in grey). We also refer to this particle as “Voronoi particle” along the direction  $\hat{\mathbf{c}}$ .

1. The point  $s\hat{\mathbf{c}}$  has the minimal distance to the surfaces of each of the two objects along the direction  $\hat{\mathbf{c}}$ .
2. Both distances are the same.

As an example, the VB between two spheres of equal radii is the same as the VB between two points at the centres of the spheres. Therefore, condition 1 is trivially satisfied for every  $s$  and condition 2 translates into the

equation  $(s\hat{\mathbf{c}})^2 = (s\hat{\mathbf{c}} - \mathbf{r}_{ij})^2$ , leading to

$$s = \frac{r_{ij}}{2\hat{\mathbf{c}} \cdot \hat{\mathbf{r}}_{ij}}, \quad (21)$$

i.e., the VB is the plane perpendicular to the separation vector  $\mathbf{r}_{ij}$  at half the separation (see Fig. 5a). Already for two spheres of unequal radii, the VB is a curved surface. Taking into account the different radii  $R_i$  and  $R_j$ , the second condition becomes  $s - R_i = \sqrt{(s\hat{\mathbf{c}} - \mathbf{r}_{ij})^2} - R_j$ , which has the solution (Danisch *et al.*, 2010):

$$s = \frac{1}{2} \frac{r_{ij}^2 - (R_i - R_j)^2}{\hat{\mathbf{c}} \cdot \hat{\mathbf{r}}_{ij} - (R_i - R_j)}. \quad (22)$$

Finding a solution for both conditions 1. and 2. for general non-spherical objects is non-trivial (Baule *et al.*, 2013; Portal *et al.*, 2013) and will be discussed in Sec. IV.G.2.

Having defined the VB, the exact mathematical formula for  $\mathcal{W}_i(\mathbf{q})$  in  $d$  dimensions is given by the orientational integral:

$$\mathcal{W}_i(\mathbf{q}) = \frac{1}{d} \oint d\hat{\mathbf{c}} l_i(\mathbf{q}, \hat{\mathbf{c}})^d, \quad (23)$$

where  $l_i(\mathbf{q}, \hat{\mathbf{c}})$  is the boundary of the Voronoi cell in the direction  $\hat{\mathbf{c}}$ . This boundary depends on all  $N$  particle configurations  $\mathbf{q}$  in terms of a global minimization:  $l_i(\mathbf{q}, \hat{\mathbf{c}})$  is the minimum among all VBs in the direction  $\hat{\mathbf{c}}$  between particle  $i$  and all other  $N - 1$  particles in the packing (see Fig. 5b). Formally,

$$l_i(\mathbf{q}, \hat{\mathbf{c}}) = \min_{j:s>0} s(\mathbf{r}_{ij}, \hat{\mathbf{r}}_{ij}, \hat{\mathbf{c}}). \quad (24)$$

Clearly, the global minimization over all particles  $j$  defining  $\mathcal{W}_i$  in Eq. (24) is highly difficult to treat analytically. The Voronoi volume of a particle depends on the position of all the other particles in the packing; clearly, a many-body interaction. The precise knowledge of the microscopic configurations of all particles is intractable in the thermodynamic limit. Nevertheless, the Voronoi convention has been shown to be the most useful way of defining the volume function, since it is well defined for any dimension and captures the effect of different particle shapes. The technical challenges can be circumvented by: (i) decomposing non-spherical shapes into overlapping and intersecting spheres leading to analytically tractable expressions for the VB; (ii) coarse-graining the volume function over a mesoscopic length-scale, which avoids the global minimization problem.

This approach (Baule *et al.*, 2013; Song *et al.*, 2008) turns the volume ensemble into a predictive framework for packings, as discussed in detail in Sec. IV. Interestingly, the Voronoi cell of a particle can be interpreted as its available volume in the packing. This correspondence can be demonstrated by considering a soft interparticle potential and evaluating the free volume for a given potential energy before taking the hard core limit (Song



*et al.*, 2010). Analyzing the statistics of the Voronoi cells also provides deeper insight into structural features of packings, e.g., by quantifying the cell shape anisotropies (Luchnikov *et al.*, 1999; Medvedev and Naberukhin, 1987; Schaller *et al.*, 2015a; Schröder-Turk *et al.*, 2010).

## 2. Statistical mechanics of planar assemblies using quadrons

The quadron convention of the volume function  $\mathcal{W}$  has been used in (Blumenfeld and Edwards, 2003) to calculate the partition function of the volume ensemble explicitly. If correlations between particle positions are neglected, analytical results can be obtained by introducing suitable approximations for  $\Theta_{\text{jam}}$ . The partition function is then analytically tractable and leads likewise to predictions for the average quadron volume and fluctuations (Blumenfeld and Edwards, 2003). The quadron approach also allows to assess the effect of correlations. The lowest order correlations originate from intergranular loops and can thus be considered as background fluctuations. In the case of circular particles with three neighbours one finds that taking into account correlations only due to the intergranular loops reduces the packing density at high compactivity, but increases it at low compactivity. In addition, the difference in density due to correlations is shown to be relatively small at around 2–4%, which suggests that correlation-free models might be sufficiently accurate to capture many packing properties (Blumenfeld and Edwards, 2003).

## 3. $\Gamma$ -distribution of volume cells

The analysis of the statistics of volume cells in sphere packings reveals an interesting universality irrespective of packing protocols and volume conventions. In (Aste, 2006; Aste *et al.*, 2007) experimental packings of  $\sim 145,000$  spherical glass beads were prepared with fluidized bed techniques and structural features investigated with X-ray tomography. The PDFs of cell volumes in the Delaunay convention for 18 different experiments show a surprising collapse onto a unique master curve. The master curve is the  $\Gamma$ -distribution  $f(V, k) = \frac{(V - V_{\min})^{k-1}}{\Gamma(k)\chi^k} e^{-(V - V_{\min})/\chi}$ , with shape parameter  $k$  and scale parameter  $\chi = (\langle V \rangle - V_{\min})/k$ . Such a  $\Gamma$ -distribution has been shown to capture well the volume statistics in a large variety of jammed systems (Aste and Di Matteo, 2008a,b; Aste *et al.*, 2007; Frenkel *et al.*, 2008; Lechenault *et al.*, 2006; Matsushima and Blumenfeld, 2014; Oquendo *et al.*, 2016). Its possible universality has been motivated by statistical mechanical arguments applied to independent elementary volume cells (Aste and Di Matteo, 2008a; Aste *et al.*, 2007) assuming that the cells are uncorrelated. Even though the data collapse on a  $\Gamma$ -distribution is remarkable, it is not clear if it

is indeed a signature of a jammed state. A Poisson point process, e.g., leads likewise to a distribution of Voronoi cell volumes that is well described by a  $\Gamma$ -distribution (Ferenc and Néda, 2007; Kumar *et al.*, 1992; Lazar *et al.*, 2013).

## E. Stress and force ensemble

### 1. Force tilings

It has already been noted in the mid 19th century that the contact forces in a 2d packing can be mapped to a tessellation of the plane, the so called Maxwell-Cremona tessellation (Cremona, 1890; Maxwell, 1864). An individual tile in the tessellation arises from the contact forces acting on a particle  $i$ : the boundary of the tile is constructed by rotating all force vectors by  $\pi/2$  and joining them tip to end leading to a polygon (see Fig. 6a,b). If the forces on the particle all balance the polygon is closed, because its boundary is the sum of all contact forces. Moreover, due to Newton’s third law the tiles of contacting particles always have a side of equal length and orientation, which, for a  $N$  particle packing satisfying force balance leads to a tessellation of the plane without any gaps (Fig. 6c). Note that the condition of torque balance is not required to construct the tiles. The Maxwell-Cremona tessellation underlies the mapping of contact forces to auxiliary forces such as the void forces (Satake, 1993), loop forces (Ball and Blumenfeld, 2002), and height fields (Henkes and Chakraborty, 2005) (see Sec. II.E.3).

An important observation is that any rearrangement of forces changes the area of individual tiles  $A_i$ , but leaves the overall area of the tessellation invariant if force balance is maintained and boundary forces are unchanged. This means that the total area is an invariant under these force rearrangements (Tighe *et al.*, 2008; Tighe and Vlugt, 2010, 2011)

$$\sum_{i=1}^N A_i = \text{const}, \quad (25)$$

where the sum runs over all tiles in the tessellation. Another manifestation is the conservation of the stress-moment tensor (Ball and Blumenfeld, 2002; Henkes and Chakraborty, 2005; Henkes *et al.*, 2007). Eq. (25) only holds for frictionless grains. In frictional systems, the force tiles are non-convex and self-intersecting polygons, which makes the tiling graph non planar and the individual tile areas do not sum up to the overall area (Bi *et al.*, 2015).

Maximum entropy methods in the spirit of E. D. Jaynes information theoretic approach to statistical mechanics (Jaynes, 1957a,b) have been applied to the problem of force statistics in a number of works (Bagi, 1997,

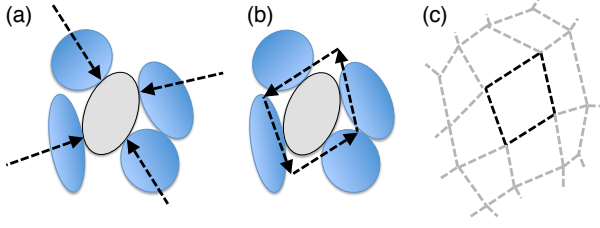


FIG. 6. Illustration of a Maxwell-Cremona tessellation. (a,b) Rotating the contact force vectors by  $\pi/2$  and joining them tip to end leads to a tile that can be associated with an individual particle. (b,c) Due to force balance every tile is closed and the collection of tiles tessellates the plane.

2003; Goddard, 2004; Krut and Rothenburg, 2002; Metzger, 2004; Metzger and Donahue, 2005; Ngan, 2004, 2003; Radeke *et al.*, 2004; Rothenburg and Krut, 2009).

## 2. Force network ensemble

The force network ensemble (FNE) (Snoeijer *et al.*, 2004; Tighe *et al.*, 2008, 2010; Tighe and Vlugt, 2010, 2011) motivated by work of Bouchaud (Bouchaud, 2002) is based on a separation of scales relevant for the particle configurations and forces. In quantitative terms, one can introduce the parameter

$$\epsilon = \frac{\langle f_{ij} \rangle}{\langle r_{ij} \rangle} \left\langle \frac{df_{ij}}{dr_{ij}} \right\rangle^{-1}, \quad (26)$$

where  $\langle \dots \rangle$  denotes an average over all particles in the packing and we introduce the notation  $f_{ij}$  for the normal force component  $f_a^i$  of contact  $a$  on particle  $i$  with particle  $j$ . For  $\epsilon \ll 1$  variations of the forces of order  $\langle f \rangle$  only result in vanishing changes in the particle positions  $\mathbf{r}_{ij}$ . If the forces are underdetermined, i.e., not uniquely fixed by the force and torque balance equations, the forces are thus uncoupled from the configurational degrees of freedom. The FNE considers a fixed contact network (a fixed set of  $\{\mathbf{r}_{ij}\}$ ) and constructs an ensemble of contact forces  $\{f_{ij}\}$  with the following properties: (i) The forces are a priori uniformly distributed as in the Edwards ensemble; (ii) Force and torque balance equations are imposed as constraints; (iii) Forces are repulsive  $\forall f_{ij} \geq 0$  and satisfy the Coulomb condition Eq. (5); (iv) A fixed external pressure  $\mathcal{P}$  sets an overall force scale. For a small number of spheres the resulting force distribution can be derived exactly (Snoeijer *et al.*, 2004). For larger packings maximum entropy arguments can be used (Tighe *et al.*, 2008; Tighe and Vlugt, 2010, 2011). The underlying assumptions imply that the FNE is in principle applicable to frictional hyperstatic systems, but is mathematically well defined also for frictionless particles.

For an isostatic system at jamming the force network ensemble is not needed, since the contact geometry uniquely defines the contact forces (Charbonneau *et al.*,

2015b; Gendelman *et al.*, 2016; Lerner *et al.*, 2013). In this case, an approximation of  $P(f)$  can be calculated with the cavity method assuming a locally tree-like contact geometry corresponding to an assumption of replica symmetry (RS) (Bo *et al.*, 2014). We note that a correct determination of  $P(f)$  requires one to take into account subtle correlations between particle positions that exist at jamming beyond RS, and that are neglected in (Bo *et al.*, 2014), which in the end fails to account for the non-trivial power-laws of  $P(f)$  at jamming. A similar situation appears in the approximative calculation at 1RSB using replicas, which also fails to predict the correct exponents (Parisi and Zamponi, 2010). As discussed in Sec. V.A, the correct calculation needs to be performed at the full-RSB level since the jamming line is deep in the Gardner phase of the model.

## 3. Stress ensemble

A statistical ensemble based on the stress-moment tensor is conveniently constructed by introducing auxiliary force variables based on the voids surrounded by contacting particles in 2d (Ball and Blumenfeld, 2002; Henkes and Chakraborty, 2005). If we choose the centre of an arbitrary void as the origin of a height field, we can construct the height vectors  $\mathbf{h}_\nu$  iteratively as (Henkes and Chakraborty, 2005)

$$\mathbf{h}_\nu = \mathbf{f}_a^i + \mathbf{h}_\mu. \quad (27)$$

Here,  $\mu, \nu$  label voids and  $\mathbf{f}_a^i$  is the force vector at the contact that is crossed when going from the centre of void  $\mu$  to the centre of void  $\nu$ . Since the contact forces on a particle sum to zero due to force balance, the height vectors are well defined and represent a one-to-one mapping of the contact forces. The microscopic stress tensor of a single grain, Eq. (17),  $\hat{\sigma}_i$  can then be expressed in terms of the height fields (Ball and Blumenfeld, 2002)

$$\hat{\sigma}_i = \sum_{a \in \partial i} (\mathbf{r}_{a1} + \mathbf{r}_{a2}) \otimes \mathbf{h}_\mu, \quad (28)$$

where  $\mathbf{r}_{a1}$  and  $\mathbf{r}_{a2}$  denote the vectors connecting void  $a$  with the contact points. The macroscopic force-moment tensor Eq. (18) of a macroscopic assembly of  $N$  particles occupying area  $A$  in the quadron convention is thus

$$\hat{\Phi} = \sum_{i=1}^N \hat{\sigma}_i = \sum_{\mu \in \partial A} (\mathbf{r}_{\mu 1} + \mathbf{r}_{\mu 2}) \otimes \mathbf{h}_\mu. \quad (29)$$

The sum in the last expressions runs only over all voids defining the boundary of the area  $A$ , since all contributions from particles in the bulk cancel. We see that  $\hat{\Phi}$  is conserved under rearrangement of the contact forces in the bulk that preserve force balance, which is a manifestation of the area conservation Eq. (25). Therefore, packings with different values of  $\hat{\Phi}$  can not be transformed

into each other by rearranging the bulk forces. This allows us to define a granular entropy  $S = \log \Omega(A, \Phi, N)$  via the number of force configurations  $\Omega(A, \Phi, N)$  leading to a given  $\Phi$ .

In order to obtain the canonical distribution, we divide the system into a small partition of size  $m$  and the remaining system  $N - m$ , which acts as a reservoir. For frictionless isotropic systems the only independent part of  $\Phi$  is the trace  $\Gamma = \text{tr } \Phi$ , which represents a simple hydrostatic pressure  $p = \Gamma/A$ . In this case, the formalism simplifies and the canonical distribution is (Henkes and Chakraborty, 2009; Henkes *et al.*, 2007)

$$P(\Gamma_m) = \frac{\Omega_m(\Gamma_m)}{\mathcal{Z}(\alpha)} e^{-\alpha \Gamma_m}, \quad \Gamma_m = \sum_{i,j} d_{ij} F_{ij}, \quad (30)$$

where  $\alpha = \log \Omega_N(\Gamma)/\partial \Gamma$  and the sum is taken over all contact vectors and forces in the  $m$ -particle cluster.

Eq. (30) leads to the following testable predictions:

- All subregions in an equilibrated packing  $k$  should have the same granular temperature  $\alpha_k$ . Thus measuring  $P(\Gamma_m)$  in two packings  $k$  and  $k'$  yields the ratio (Henkes *et al.*, 2007)

$$\log \left[ \frac{P_k(\Gamma_m) P_{k'}(\Gamma'_m)}{P_k(\Gamma'_m) P_{k'}(\Gamma_m)} \right] = (\alpha_k - \alpha_{k'}) (\Gamma_m - \Gamma'_m). \quad (31)$$

Moreover, the distribution  $P_k(\Gamma_m)$  satisfies the scaling (Henkes *et al.*, 2007)

$$P_k(\Gamma_m) = P_{k'}(\Gamma_m) e^{-(\alpha_k - \alpha_{k'}) \Gamma_m}. \quad (32)$$

Eqs. (31,32) require that packings  $k$  and  $k'$  are sufficiently close in density to neglect changes in  $\Omega$  due to different volumes.

- At the isostatic point the partition sum  $Z(\alpha)$  can be evaluated analytically by summing over all force degrees of freedom assuming a uniform distribution. In a monodisperse system of spheres, this yields the predictions (Henkes and Chakraborty, 2009):  $\Omega(\Gamma_m) = \Gamma^{2m}$  for  $m \gg 1$  and

$$\alpha = \frac{N z_{\text{iso}}}{2 \langle \Gamma \rangle}, \quad (33)$$

where  $\langle \Gamma \rangle = -\partial \log Z / \partial \alpha$ . We also obtain the exponential force distribution

$$P(F) \propto e^{-\alpha r_0 F}, \quad (34)$$

where  $r_0$  is the sphere radius.

Simulations of soft sphere systems have confirmed predictions Eqs. (31,32) for different packing densities (Henkes *et al.*, 2007). Eq. (33) has also been shown close to the  $J$ -point, but deviations are observed for larger densities, where instead the relation  $\alpha = N a \langle z \rangle / \Gamma_N$  is observed. Here,  $a$  increases monotonically from  $a = 2$  for  $\langle z \rangle > z_{\text{iso}}$  (Henkes and Chakraborty, 2009).

### III. PHENOMENOLOGY OF JAMMED STATES AND SCRUTINIZATION OF THE EDWARDS ENSEMBLE

In this section we first describe the phenomenological results characterizing the jammed states and then proceed to review work dedicated to test the Edwards assumption of equiprobability of jammed states.

#### A. Jamming in soft and hard sphere systems

Over the past two decades, considerable progress has been made in our understanding of jammed particles packings. Here we summarize the main results of this work needed for the remainder of this review. One can refer to several recent review articles for more details. (Bi *et al.*, 2015; Charbonneau *et al.*, 2017; van Hecke, 2010; Liu and Nagel, 2010; Torquato and Stillinger, 2010)

##### 1. Isostaticity in jammed packings

The average coordination number in packings is approximately estimated by naive Maxwell counting arguments (Alexander, 1998; Maxwell, 1870) which consider the force variables constrained only by force and torque balance Eqs. (2,3) and Newton's third law Eq. (7), but ignore the crucial constraints of Coulomb, Eqs. (5), and repulsive forces, Eq. (6). In particular, attractive forces are allowed, contradicting the fact that the forces are purely repulsive, Eq. (6). With these caveats in mind, one obtains an estimation of the average coordination number  $z$  assuming: (i) all degrees of freedom (dofs) in the packing are constrained by contacts (for periodic boundary conditions); (ii) the number of contacts will be minimal for a generic disordered packing. As a consequence, packings of frictionless particles should satisfy (see appendix A)

$$z = 2d_f. \quad (35)$$

When Eq. (35) is satisfied the packing is *isostatic* under the naive Maxwell counting argument: the number of force and torque balance equations exactly equals the number of contact force components. Therefore, the configurational dofs fully determine the force dofs and vice versa, which allows to construct ensembles based on only configurational or force dofs. Since isostatic packings have the minimal number of contacts for a geometrically rigid packings they are also referred to as marginally stable (Müller and Wyart, 2015). Packings with  $z$  smaller or larger than the isostatic value are referred to as hypostatic and hyperstatic, respectively.

Equation (35) predicts that packings of frictionless spheres have  $z = 6$ , while rotationally symmetric shapes such as spheroids and spherocylinders have  $z = 10$  and fully asymmetric shapes have  $z = 12$ . The isostaticity for spheres is indeed widely observed to hold very closely

in experiments and simulations for both soft and hard sphere systems. In fact it has been shown (Moukarzel, 1998) that non-cohesive sphere packings become exactly isostatic, when their stiffness goes to infinity. However, if we consider a small deformation from the spherical shape to, e.g., a spheroid, the isostatic condition would predict a discontinuous jump in the average coordination number from  $z = 6$  to  $z = 10$ . Instead, one finds that packings of non-spherical shapes are in general hypostatic with a smooth increase from the spherical isostatic  $z$  value under deformation (Donev *et al.*, 2004, 2007; Schreck *et al.*, 2012; Williams and Philipse, 2003; Wouterse *et al.*, 2009). These hypostatic packings are indeed mechanically stable if the effect of the shape curvature at the contact point is taken into account (Donev *et al.*, 2007; Roux, 2000). As a consequence, one can construct configurations that are mechanically stable even though there are fewer contacts than configurational dofs per particle (see Sec. IV.G.3). Interestingly, also for larger aspect ratios the average coordination number generally stays below the isostatic value, which is just slightly lower for spheroids and fully asymmetric ellipsoids (Donev *et al.*, 2004), but exhibits a much stronger decrease for spherocylinders (Baule *et al.*, 2013; Williams and Philipse, 2003; Wouterse *et al.*, 2009; Zhao *et al.*, 2012).

For polyhedral particles with flat faces and edges the above counting arguments need to be modified, since, e.g., two touching faces constrain more than a single configurational dof. In (Jaoshvili *et al.*, 2010) it has been suggested to associate every contact with the number of configurational dofs that are constrained by it: Contact of two faces  $\rightarrow 3$  constraints; face and edge contact  $\rightarrow 2$  constraints; face and vertex, edge and edge contacts  $\rightarrow 1$  constraint. With these correspondences the isostaticity of disordered jammed packings of tetrahedra and other Platonic solids could indeed be demonstrated (Jaoshvili *et al.*, 2010; Jiao and Torquato, 2011; Smith *et al.*, 2011).

For frictional particles the contact counting argument provides the range of coordination numbers  $4 \leq z \leq 6$  for spheres and  $4 \leq z \leq 12$  for general shapes (see appendix A). For spheres it is generally observed that  $z \rightarrow 6$  for a friction coefficient  $\mu \rightarrow 0$  (frictionless limit) and  $z \rightarrow 4$  for  $\mu \rightarrow \infty$  (infinitely rough spheres) (see Sec. III.A). For intermediate  $\mu$  sphere packings are thus generally hyperstatic. Hyperstaticity is also found for frictional ellipsoids (Schaller *et al.*, 2015b) and frictional tetrahedra, when the different types of contact are translated into constraints on the configurational dofs (Neudecker *et al.*, 2013).

The Coulomb condition Eq. (5) restricts the possible force configurations compared with the infinitely rough limit: A stable force configuration with a certain  $z(\mu)$  is also stable for all larger  $\mu$  values. Any determined value  $z(\mu)$  is thus in principle a lower bound on the possible combinations of  $z$  and  $\mu$ , although it might not be possible to generate these combinations in practice. This high-

lights that  $z(\mu)$  is not unique and depends strongly on the history of the packing generation. It should be stressed that the above isostatic conjectures are valid only under the naive Maxwell counting argument ignoring the repulsive nature of the interactions and the inequalities derived from Coulomb conditions. A model generalizing Maxwell arguments to this more realistic scenario was proposed in (Bo *et al.*, 2014) suggesting the existence of a well defined lower bound on  $z(\mu)$  (see Sec. V.A).

## 2. Packing of soft spheres

So far we have treated only hard spheres. A packing of soft spheres with radius  $R$  is modelled by repulsive normal forces: (Johnson, 1985; Landau *et al.*, 1986):

$$f_{a,n}^i = k_n \xi^\alpha, \quad (36)$$

where the normal overlap is  $\xi = (1/2)[2R - |\mathbf{r}_1 - \mathbf{r}_2|] > 0$ , and  $\mathbf{r}_{1,2}$  are the positions of the grain centres. The normal force acts only in compression,  $f_{a,n}^i = 0$  when  $\xi < 0$ . The effective stiffness  $k_n = \frac{8}{3}\mu_g R^{1/2}/(1 - \pi_g)$  is defined in terms of the shear modulus of the grains  $\mu_g$  and the Poisson ratio  $\pi_g$  of the material from which the grains are made (typically  $\mu_g = 29$  GPa and  $\pi_g = 0.2$ , for spherical glass beads). The exponent  $\alpha$  is typically chosen among two possibilities: (i)  $\alpha = 1$  for simple harmonic springs, and (ii)  $\alpha = 3/2$  for 3d spherical geometries at the contact (Hertz forces).

The situation in the presence of a tangential force,  $\mathbf{f}_{a,\tau}^i$ , is more complicated. In the case of spheres under oblique loading, the tangential contact force was calculated by Mindlin (Mindlin, 1949). For the special case where the partial increments do not involve microslip at the contact surface (i.e.,  $|\Delta f_{a,\tau}^i| < \mu \Delta f_{a,n}^i$ , where  $\mu$  is the static friction coefficient between the spheres, typically  $\mu = 0.3$ ) Mindlin (Mindlin, 1949) showed that the incremental tangential force is

$$\Delta f_{a,\tau}^i = k_t \xi^{1/2} \Delta s, \quad (37)$$

where  $k_t = 8\mu_g R^{1/2}/(2 - \pi_g)$ , and the variable  $s$  is defined such that the relative shear displacement between the two grain centers is  $2s$ . This is called the Mindlin “no-slip” solution.

Typical packing preparation protocols employ Molecular Dynamics compressing an initially loose gas (Makse *et al.*, 2004, 1999, 2000). In 2d it is necessary to use bidisperse mixtures in order to avoid crystallization. Other protocols start from a random configuration corresponding to a large “temperature”  $T = \infty$  initial state. Jammed packings at  $T = 0$  are generated by bringing the system to the closest energy minimum using conjugate-gradient techniques to minimize the energy of the system, which is well defined for frictionless systems (O’Hern



*et al.*, 2002). Another protocol for numerically constructing jammed states consists in putting particles at random positions above the packing at a certain height and letting particles settle under gravity (Herrmann, 1993). Also sophisticated experimental realizations of this procedure have been developed (Pouliquen *et al.*, 1997).

In the  $T = 0$  limit or the mechanical equilibrium state assemblies of these particles exhibit a transition to the jammed state. There exists in particular a critical packing density  $\phi_c$  characterizing the onset of jamming at which the static shear moduli  $G_\infty$  and the pressure  $p$  (and therefore, the static bulk modulus as well) become zero simultaneously (under decompression) and the coordination number attains the isostatic value (Makse *et al.*, 1999). For finite  $N$  the precise value of  $\phi_c$  depends on the initial  $T$  state and the protocol employed, but scaling behavior of  $G_\infty$  and  $p$  for each of the different  $\alpha$  values is observed when using the distance to jamming  $\phi - \phi_c$  as a control parameter for packings near isostaticity. The critical density  $\phi_c$  in the  $T = 0$  limit and zero shear stress is referred to as *J-point* (O'Hern *et al.*, 2002). For quenches starting at infinite temperature, in the thermodynamic limit  $N \rightarrow \infty$  the distribution of  $\phi_c$  values converges to a delta function at a value  $\phi^* = 0.639 \pm 0.001$  for frictionless monodisperse spheres in 3d. The J-point thus obtained is close to values typically found for random close packings (RCP) of hard spheres.

The following power-law scalings have been observed by many studies and are independent of polydispersity or dimensionality (van Hecke, 2010; Liu and Nagel, 2010; Majmudar *et al.*, 2007; Makse *et al.*, 2004, 1999, 2000; O'Hern *et al.*, 2003, 2002; Zhang and Makse, 2005):

- Pressure:

$$p \sim (\phi - \phi_c)^\alpha \quad (38)$$

- Static bulk modulus:

$$B_\infty \sim (\phi - \phi_c)^{\alpha-1} \quad (39)$$

- Static shear modulus:

$$G_\infty \sim (\phi - \phi_c)^{\alpha-1/2} \quad (40)$$

- Average coordination number:

$$z - z_c \sim (\phi - \phi_c)^{1/2}, \quad (41)$$

where  $z_c$ , the critical coordination number measured at  $\phi_c$ , agrees in fact with the isostatic value  $z = 2d_f$ .

The square root scaling of  $z - z_c$  is observed for all  $\alpha$  values, which indicates that this scaling is only due to

the packing geometry independent of the interaction potential. The scaling of the pressure can be interpreted as an affine response of the packing to deformations. This argument, which is usually referred as the Effective Medium Approximation in granular matter (DeGiuli *et al.*, 2014a,b, 2015; Digby, 1981; During *et al.*, 2013; Jenkins *et al.*, 2005; Makse *et al.*, 2004, 1999; Norris and Johnson, 1997; Walton, 1987; Wyart, 2010), also predicts an exponent  $\alpha - 1$  for the bulk modulus Eq. (39) (proportional to the second derivative of the energy) as observed (although the scaling law has a different prefactor as expected from affine deformations). However, the shear modulus should then also scale with an exponent  $\alpha - 2$ , which is not observed in Eq. (40), highlighting the effects of non-affine motion under shear (Magnanimo *et al.*, 2008; Makse *et al.*, 2004, 1999). The observed scaling of the shear modulus has been reproduced in models of disordered solids by taking into account the non-affine response within an approximate analytical scheme (Zaccone and Scossa-Romano, 2011). Equation (41) has been shown to be a bound for stability in (Wyart *et al.*, 2005b) based on physical arguments and confirmed analytically in a replica calculation of the perceptron model of jamming (Franz *et al.*, 2015). Lattice models that exhibit critical behavior related to Eqs. (39)–(41) capture the jamming transition in terms of a percolation transition ( $k$ -core or bootstrap percolation) (Schwarz *et al.*, 2006; Toninelli *et al.*, 2006).

Anomalous behavior at point J is also indicated in the density of normal mode frequencies (Charbonneau *et al.*, 2015a; DeGiuli *et al.*, 2014b; O'Hern *et al.*, 2003; Silbert *et al.*, 2005, 2009; Wyart *et al.*, 2005a,b). In a crystal the low frequency excitations are sound modes with a vibrational density of states  $\sim \omega^{d-1}$  (Debye scaling). In a disordered packing theoretical arguments based on marginal stability predict instead (DeGiuli *et al.*, 2014b)

$$D(\omega) \sim \begin{cases} \omega^{d-1} & \omega \ll \omega_0 \\ \omega^2/\omega^{*2} & \omega_0 \ll \omega \ll \omega^* \\ \text{constant} & \omega \gg \omega^* \end{cases}, \quad (42)$$

which is also exhibited by the perceptron model (Franz *et al.*, 2015) and found in simulations of jammed soft spheres in dimensions 3–7 (Charbonneau *et al.*, 2015a; Lerner *et al.*, 2016; Mizuno *et al.*, 2017). The  $\omega^2/\omega^{*2}$  scaling has also been observed in emulsion experiments (Lin *et al.*, 2016). In Eq. (42),  $\omega^*$  is a characteristic frequency that vanishes at jamming as

$$\omega^* \sim z - z_c \quad (43)$$

and  $\omega_0$  is a small threshold frequency.

At jamming the density of states thus stays non-zero for arbitrary small frequencies. This highlights that at point J there is an excess of low frequency modes compared with crystals. This anomaly is sometimes seen

analogous to the Boson peak observed in glassy materials (Franz *et al.*, 2015). The vanishing crossover frequency  $\omega^*$  allows to identify a length scale  $l^*$ , which diverges upon reaching point J as:  $l^* \sim (z - z_c)^{-1}$  (Wyart *et al.*, 2005a). Such a diverging length scale has been observed numerically in the vibrational eigenmodes and in the response to point perturbations (Ellenbroek *et al.*, 2009, 2006; Silbert *et al.*, 2005). However, theoretical arguments predict for point responses  $l^* \sim (z - z_c)^{-1/2}$  (Lerner *et al.*, 2014). The length scale  $l^*$  has been computed in (Doring *et al.*, 2013; Wyart, 2010). Diverging length scales when approaching point J from below have also been identified related to velocity correlation functions (Olsson and Teitel, 2007) and clusters of moving particles (Drocco *et al.*, 2005). When approaching point J from above finite point correlation functions are not sufficient to detect such a length scale. Instead, point to set correlation functions are necessary, which can provide a quantitative description of the sensitivity of force propagation in granular materials to boundary conditions (Mailman and Chakraborty, 2011, 2012).

The concept of frequency dependent complex-valued effective mass  $M_{\text{eff}}(\omega)$  (Hsu *et al.*, 2009) obtained as the packing is subjected to a vertical acceleration at a given frequency is directly related to the vibrational density of states (Hu *et al.*, 2014a). Indeed, the vibrational density of states can be accessed experimentally through the measurement of  $M_{\text{eff}}(\omega)$  via a pole decomposition of the normal modes of the system (Hu *et al.*, 2014a). By measuring the stress dependence of the effective mass, it was shown that the scaling of the characteristic frequency  $\omega^*$  deviates from the mean field prediction Eq. (43) in real frictional packings (Hu *et al.*, 2014a). Furthermore, the presence of dissipative modes can be studied via the imaginary part of the complex valued effective mass (Hu *et al.*, 2014b; Johnson *et al.*, 2015).

When friction is added, the observed packing densities and coordination numbers at point J are generally smaller than RCP (Kasahara and Nakanishi, 2004; Makse *et al.*, 2000; Papanikolaou *et al.*, 2013; Shen *et al.*, 2014; Shundyak *et al.*, 2007; Silbert, 2010; Silbert *et al.*, 2002a). As a function of the friction coefficient  $\mu$  the densities decrease monotonically from  $\phi \approx 0.64$  for frictionless spheres to  $\phi \approx 0.55$  in the limit of infinitely rough spheres. Experiments find much lower packing fractions in the large friction limit (Farrell *et al.*, 2010). The densities are also dependent on the packing preparation for the same  $\mu$  highlighting the history dependence of frictional packings. An open question is whether there is a well-defined lower bound on the packing density for a given  $\mu$ , which could specify random loose packing (RLP) densities (Makse *et al.*, 2000; Onoda and Liniger, 1990): the lowest density packings that are mechanically stable. Extremely low density mechanically stable packings can be generated with additional attractive interactions, e.g., due to adhesion. Adhesive packings of spheres are

discussed in Sec. IV.F.

Likewise, the coordination number decreases monotonically for  $\mu \geq 0$  from the isostatic frictionless value  $2d_f$ , reaching the frictional isostatic value  $z_{\text{iso}}^\mu = d + 1$  in the limit  $\mu \rightarrow \infty$ . Frictional packings are thus in general hyperstatic, so that particle configurations do not uniquely determine the contact forces. How this indeterminacy depends on the friction coefficient and affects the mechanical properties has been investigated in detail using contact dynamics by (Unger *et al.*, 2005). It was also found that the contacts with large indeterminacy are also those contacts that make up force chains (McNamara and Herrmann, 2004).

The following scaling results at point J have been obtained in simulations of frictional soft spheres with Hertz-Mindlin forces (Henkes *et al.*, 2010; Makse *et al.*, 2000; Shundyak *et al.*, 2007; Silbert, 2010; Somfai *et al.*, 2007; Zhang and Makse, 2005). For the coordination number one finds a scaling analogous to Eq. (41)

$$z - z_c \sim z_0(\mu)(\phi - \phi_c)^{1/2}, \quad (44)$$

where  $z_c \approx 2d_f$  is the frictionless isostatic value at point J and  $z_0(\mu)$  a weakly  $\mu$ -dependent prefactor. However, other quantities like the critical frequency  $\omega^*$  and the bulk/shear modulus do not scale with  $\phi - \phi_c$  contrary to the frictionless case. One finds

$$\omega^* \sim z - z_{\text{iso}}^\mu, \quad G_\infty/B_\infty \sim z - z_{\text{iso}}^\mu. \quad (45)$$

By comparison, Eqs. (39,40,41) predict the scaling  $G_\infty/B_\infty \sim z - z_c$ . Therefore, one can conclude that the critical observables generally scale with the distance to isostaticity (Wyart, 2005).

### 3. Packing of hard spheres

The structural properties of packings have been investigated in considerable detail with computer simulations and experiments of hard spheres satisfying constraints Eq. (1). Hard sphere results should coincide with soft spheres at zero pressure. A widely used simulation algorithm for jammed hard particles is the Lubachevsky-Stillinger (LS) algorithm (Lubachevsky and Stillinger, 1990). Here, starting from a random initial configuration of spheres in a volume with periodic boundary conditions generated, e.g., by random sequential addition of spheres, the sphere radii are expanded uniformly with a rate  $\lambda$ . Collisions occur due to the expansion of the particles, which are resolved in an event-driven manner. Forces can be calculated from the rate of exchange of momentum per unit time. Eventually, a jammed state is reached with diverging collision rates at the contacts and typically 2-3% of rattlers that remain unjammed. The properties of the final state are then independent of the random initial state, but depend on the expansion rate. For  $\lambda \rightarrow 0$  the system is in equilibrium leading to crystallization, while for small  $\lambda > 0$  the system

is able to reach a quasiequilibrium jammed state with a density  $\phi(\lambda)$ . These states have been characterized as long-lived metastable glass states which in infinite dimensions are described (Parisi and Zamponi, 2010) by the replica symmetry breaking (RSB) theory adapted from the solution of the Sherrington-Kirkpatrick (SK) model of spin-glasses (Sherrington and Kirkpatrick, 1975) (see Secs. III.A.4 and V).

An advanced numerical technique that can deal with perfectly rigid particles and at the same time obtain the contact forces precisely is Contact Dynamics (CD), as reviewed for instance in (Radjai and Richefeu, 2009). In fact, granular structures turn out to be more stable under gravity when using CD than any other numerical method (McNamara and Herrmann, 2004). CD has been used extensively to explore force networks, their fluctuations and their indeterminacies in frictional packings, see e.g. (Unger *et al.*, 2005).

Experiments of hard sphere packings go back to the seminal work by Bernal and Scott (Bernal, 1960; Bernal and Mason, 1960; Scott, 1960, 1962). Indeed, in the old days Mason, a postgraduate student of Bernal, took on the task of shaking glass balls in a sack and ‘freezing’ the resulting configuration by pouring wax over the whole system. He would then carefully take the packing apart, ball by ball, noting the positions of contacts for each particle. Since this labor-intensive method patented half a century ago, yet still used in recent studies (Donev *et al.*, 2004), other groups have extracted data at the level of the constituent particles using x-ray tomography (Aste *et al.*, 2004, 2005; Richard *et al.*, 2003; Saadatfar *et al.*, 2012). The most sophisticated experiment for granular matter to date has resolved coordinates of up to 380000 spheres using X-ray tomography (Aste *et al.*, 2004, 2005). The packing densities achieved are in general sensitive to the packing protocol, friction, and polydispersity. The effect of boundary walls can be reduced by focusing the analysis on bulk particles or preparing the walls with randomly glued spheres. Mechanically stable disordered packings of spheres are typically found in the range  $\phi \approx 0.55 - 0.64$ . Empirical studies have shown that one can identify different density regions depending on variations in the protocol (Aste, 2005): (i)  $\phi \approx 0.55 - 0.58$ : packings are only created by reducing the effect of gravity (Onoda and Liniger, 1990); (ii)  $\phi \approx 0.58 - 0.61$ : packings are unstable under tapping; (iii)  $\phi \approx 0.61 - 0.64$ : packings are generated by tapping and compression (Knight *et al.*, 1995; Nowak *et al.*, 1998, 1997; Philippe and Bideau, 2002). Packings in the range  $\phi \approx 0.64 - 0.74$ , i.e., up to the FCC crystal density are usually only generated by introducing local crystalline order. This has been achieved experimentally by pouring spheres of equal size homogeneously over plate, that vibrates horizontally at a very low frequency (Pouliquen *et al.*, 1997). The attained density depends on the frequency. A similar range of densities is obtained by flux deposition of spheres into a

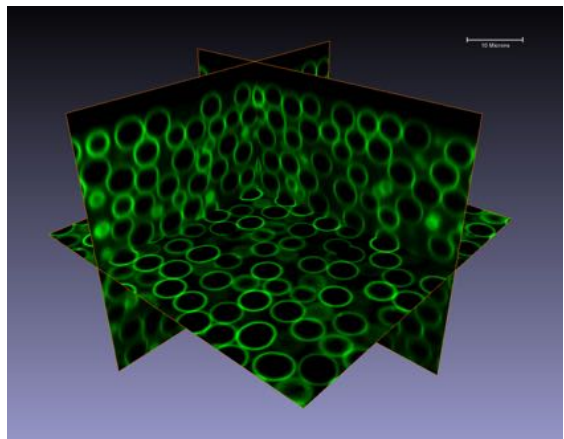


FIG. 7 3D confocal image of a colloidal packing showing green fluorescence on the particles’ surface. The method of (Kyeyune-Nyombi *et al.*, 2018) improves detection resolution of the particle contact network using fluorescent exclusion effects at the contact point. Structural properties of the colloidal packing near marginal stability that required high resolution contact detection thus become experimentally accessible (see Table IV). From (Kyeyune-Nyombi *et al.*, 2018).

container with a templated surface (Panaiteescu and Kudrolli, 2014).

Establishing the number of contacting spheres in experiments is somewhat challenging. The celebrated Bernal packings (Bernal and Mason, 1960) find a coordination number close to  $z = 6$ , while compressed jammed emulsions near the jamming transition studied by confocal microscopy (Brujić *et al.*, 2007) finds an average coordination  $\langle z \rangle = 6.08$ , close to the isostatic conjecture. One generally finds that larger densities coincide with larger values of  $z$  exhibiting a monotonic increase over the range  $\phi \approx 0.55 - 0.64$  from  $z \approx 4 - 7$  (Aste, 2005; Aste *et al.*, 2004, 2005, 2006) largely in agreement with simulation results on frictional soft-sphere systems at small pressure. A new method for contact detection in jammed colloids using fluorescent exclusion effects at the contact point has been developed in (Kyeyune-Nyombi *et al.*, 2018). The method improves detection resolution and allows precise determination of the small force distributions, coordination number, vibrational density of states, and pair correlations (see Fig. 7).

The following consensus on the structural properties of the pair correlation function  $g_2(r)$  of jammed hard-spheres has been reached from simulations and experiments for a variety of protocols:

- A delta function peak at  $r = \sigma$  due to contacting particles, where  $\sigma = 2R$  is the contact radius. The area under the peak is the average coordination number, which has the isostatic value  $z_{\text{iso}} = 2d_f = 6$  at jamming in frictionless systems.
- A power-law divergence due to a large number of

near-contacting particles

$$g_2(r) \sim (r - \sigma)^{-\gamma}. \quad (46)$$

The exponent  $\gamma$  has been measured as  $\gamma \approx 0.4$  in simulations of hard spheres (Charbonneau *et al.*, 2012; Donev *et al.*, 2005b; Lerner *et al.*, 2013; Skoge *et al.*, 2006) and  $\gamma \approx 0.5$  in simulations of stiff soft spheres (O'Hern *et al.*, 2003; Silbert *et al.*, 2002b, 2006). The value depends on whether rattlers are included or not in the numerical protocol. Theoretical arguments based on the marginal stability of jammed packings provide (Müller and Wyart, 2015)

$$\gamma = 1/(2 + \theta), \quad (47)$$

where  $\theta$  is the exponent of the force distribution:  $P(f) \sim f^\theta$ . Empirical studies find  $\theta \approx 0.2 - 0.5$  (see Sec. III.A.5).

- A split second peak at  $r = \sqrt{3}\sigma$  and  $r = 2\sigma$  away from contact. The precise shapes of the two peaks have not been clearly established yet. Simulations show a strong asymmetry of the  $r = 2\sigma$  peak. The values  $2\sigma$  and  $\sqrt{3}\sigma$  have been related to the contact network:  $2\sigma$  is the maximal distance between two particles sharing one neighbour, while  $\sqrt{3}\sigma$  is the maximal distance between two particles sharing two (Clarke and Jónsson, 1993). The split-second peak is indicative of structural order between the first and second coordination shells. However, no signs of crystalline order have been observed.
- Long-range order  $g_2(r) - 1 \sim -r^{-4}$  for  $r \rightarrow \infty$  (Donev *et al.*, 2005a). This is equivalent to a non-analytic behavior of the structure factor  $S(k) \sim |k|$  for  $k \rightarrow 0$ , which is typically only seen in systems with long-range interactions and is uncharacteristic for liquids. The fact that  $S(0) = 0$  is characteristic of a hyperuniform system (Torquato and Stillinger, 2003). However, the validity of hyperuniformity at jamming has recently been questioned (Ikeda and Berthier, 2015; Ikeda *et al.*, 2017; Ozawa *et al.*, 2017; Wu *et al.*, 2015).

#### 4. The nature of random close packing

The nature of RCP of frictionless hard spheres and whether it is indeed a well-defined concept has been a long-standing issue. In (Torquato *et al.*, 2000) it has been argued that “random” and “close-packed” are at odds with each other, since inducing partial order typically increases packing densities, such that both can not be maximized simultaneously. As an alternative it has been suggested to use a more quantitative approach

based, e.g., on a metric detecting bond-orientational order (Steinhardt *et al.*, 1983). RCP can then be replaced by the concept of a “maximally random jammed” (MRJ) packing: The packing with the minimal order among all jammed ones. In practice, all possible order metrics would need to be checked to identify a truly random state, which is of course not feasible. Nevertheless, many different packing protocols and algorithms seem to robustly achieve disordered packings with maximal densities around  $\phi \approx 0.64$ , which coincides with the densities of MRJ packings for many different order parameters (Torquato and Stillinger, 2010). Despite early attempts to explain this reproducibility, e.g., based on maximum entropy arguments (O'Hern *et al.*, 2003, 2002) and liquid state theory (Aste and Coniglio, 2004; Kamien and Liu, 2007), there is now a general consensus that jamming densities can be obtained over a range of densities depending on the preparation protocol if crystallization is suppressed (Charbonneau *et al.*, 2012; Chaudhuri *et al.*, 2010; Ciamarra *et al.*, 2010; Hermes and Dijkstra, 2010; Ozawa *et al.*, 2012; Skoge *et al.*, 2006). This leads to the concept of a *J-line*, which was first proposed theoretically in the context of a replica solution of hard sphere glasses at the mean-field level ( $d \rightarrow \infty$ ) (Parisi and Zamponi, 2005) and other fully connected models (Mari *et al.*, 2009). In the presence of polydispersity in the particle size or in higher dimensions, crystallization is strongly suppressed and the physics of the glass transition is expected to dominate the corresponding jamming transition. If jamming is approached from the equilibrium fluid phase, the resulting jammed states are then essentially the infinite pressure limits of glassy states. A deep understanding of jamming in this scenario has been provided by exact solutions for  $d \rightarrow \infty$  using both dynamical mode-coupling type approaches (Kurchan *et al.*, 2016; Maimbourg *et al.*, 2016) and static approaches adapted from the solution of the Sherrington-Kirkpatrick model of spin-glasses (Charbonneau *et al.*, 2014a,b; Franz *et al.*, 2015; Parisi and Zamponi, 2010; Rainone and Urbani, 2016). Remarkably, the full RSB  $d \rightarrow \infty$  solution predicts scaling exponents for  $g_2(r)$ , Eq. (46), and the force distribution  $P(f)$ , Eq. (48) (see next section), that are in agreement with finite dimensional measurements for a range of  $d$  values even in 3d (Charbonneau *et al.*, 2014a,b). This remarkable agreement between an infinite dimensional mean-field theory and 3d simulations indicates that, at jamming, there is a strong suppression of fluctuations, first of all thermal fluctuations by definition, but, more importantly, sample to sample fluctuations which are known to be stronger than thermal fluctuations. Similar agreement between an infinite-dimensional result and finite dimensions is not observed for the finite-temperature glass transition. Thus, the critical properties of jamming related to marginal stability appear independent of dimensionality. For a recent review on the  $d \rightarrow \infty$  solution of hard sphere glasses, we



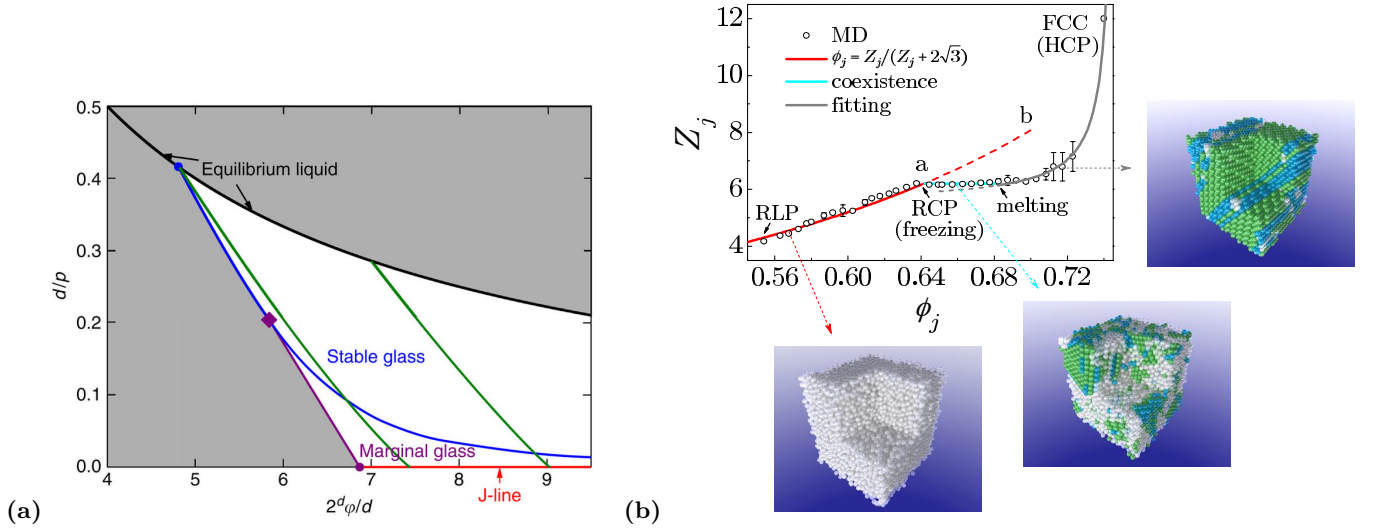


FIG. 8 (Colors online) (a) Phase diagram in  $d \rightarrow \infty$  obtained from the non-equilibrium sampling of glassy states (Charbonneau *et al.*, 2017). Glassy states exist in the white region between the continuation of the equilibrium equation of state (black) and the infinite pressure J-line. The blue line denotes the Gardner phase transition separating stable and marginally stable glass states. Glass states are possible for densities  $> \phi_d$  at which metastable states first appear in the liquid. Compressing the glass states to  $p \rightarrow \infty$  yields jammed states on the J-line  $\phi_j \in [\phi_{th}, \phi_{GCP}]$ . From (Charbonneau *et al.*, 2014b). (b) Interpretation of RCP in a 3d system made of monodisperse spheres as a first order freezing transition between disordered and ordered phases. In low dimensional systems (3d and specially 2d) crystallization prevails around RCP and precludes the appearance of the J-line as discussed in (Parisi and Zamponi, 2010). The coordination number  $z_j$  is plotted versus the volume fraction  $\phi_j$  for each packing at jamming. One can identify: (i) a disordered branch which can be fitted by the equation of state (75) derived in Sec. IV.A; (ii) a coexistence region; and (iii) an ordered branch. White particles are random clusters, light blue are HCP and green are FCC clusters. The dashed line from  $a \rightarrow b$  denotes the states beyond crystallization, which can be reached upon deformation of the particles (see Fig. 20). From (Jin and Makse, 2010).

Density	Definition	Value in $d = 3$
$\phi_d$	The liquid state splits in an exponential number of states	$\approx 0.58$
$\phi_K$	Ideal glass phase transition – jump in compressibility	$\approx 0.62$
$\phi_{th}$	Divergence of the pressure of the less dense states	$\approx 0.64$
$\phi_{GCP}$	Divergence of the pressure of the ideal glass	$\approx 0.68$

TABLE II Density values when compressing a liquid state until jamming avoiding crystallization (Charbonneau *et al.*, 2017; Parisi and Zamponi, 2010).

refer to (Charbonneau *et al.*, 2017). An overview of the different density values discussed in the following is given in Tables II,III.

Briefly, in this scenario a glass transition interrupts the continuation of the liquid equation of state considered in (Aste and Coniglio, 2004; Kamien and Liu, 2007) at densities  $\phi_j \in [\phi_d, \phi_K]$ , where  $\phi_d$  signals the dynamical glass transition at the density at which many metastable states first appear in the liquid phase and  $\phi_K$  is the Kauzmann density of the ideal glass. Upon compression of the metastable states (taking some care in the preparation protocol (Charbonneau *et al.*, 2017)) the pressure diverges at jamming densities  $\phi_j \in [\phi_{th}, \phi_{GCP}]$ . The lower limit is the threshold density  $\phi_{th} \approx 0.64$  calculated in (Parisi and Zamponi, 2010), although it should be noted that the values calculated with replica theory

come with a large error bar due to the approximation of the liquid equation of state (Mangeat and Zamponi, 2016). The maximal density is the glass close packing  $\phi_{GCP} \approx 0.68$  corresponding to the infinite pressure limit of the ideal glass  $\phi_K$ . Therefore, the ground state of jamming can be achieved in a whole range of densities along a J-line  $\phi_j \in [\phi_{th}, \phi_{GCP}]$  depending on the density of the metastable glass phase  $\phi \in [\phi_d, \phi_K]$  that is compressed to jamming. Before jamming is reached the glass undergoes a transition to a Gardner phase, where the configuration space is fragmented into an infinite fractal hierarchy of disconnected regions, which, in turn, brings about isostaticity and marginal stability (Charbonneau *et al.*, 2014a,b). Indeed the states on the J-line are all stable under all possible particle rearrangements with  $k \rightarrow \infty$  in the thermodynamic limit  $N \rightarrow \infty$ , thus corresponding

Density	Definition	Value in $d = 3$
$\phi_{\text{rlp}}$	Random loose packing: lowest density of a mechanically stable packing	$\frac{1}{1+\sqrt{3}/2} = 0.536\dots$ (Song <i>et al.</i> , 2008)
$\phi_{\text{rcp}}$	Random close packing	$\frac{1}{1+1/\sqrt{3}} = 0.634\dots$ (Song <i>et al.</i> , 2008)
$\phi_{\text{f}}$	Packing freezing point of a 1st order transition	$\approx 0.64$ (Jin and Makse, 2010)
$\phi_{\text{m}}$	Packing melting point of a 1st order transition	$\approx 0.68$ (Jin and Makse, 2010)
$\phi_{\text{fcc}}$	Density of the FCC crystal	$\pi/(3\sqrt{2}) = 0.74048\dots$

TABLE III Density values when crystallization is not suppressed. The values for  $\phi_{\text{rlp}}$  and  $\phi_{\text{rcp}}$  are determined within the Edwards ensemble using a coarse-grained volume function (Jin and Makse, 2010; Song *et al.*, 2008) (see Sec. IV.B).

to the ground state of jamming, as discussed in Fig. 4a. On the other hand, they differ in the fraction  $\alpha = k/N \sim \text{const.}$  of particle rearrangements required for stability.

Such a viewpoint is motivated by analogy with the full RSB solution of the  $p$ -spin glass (Crisanti and Leuzzi, 2006), which is the spin glass model corresponding to the full-RSB solution of infinite dimensional spheres underlying the J-line (Charbonneau *et al.*, 2014a). By varying  $\alpha$  one obtains states on the J-line: the value  $\alpha = 0$  corresponds to the states at the lower density  $\phi_{\text{th}}$ , while  $\alpha = 1$  corresponds to the true global ground state of jamming at the largest density  $\phi_{\text{GCP}}$ . Metastable  $k$ -PD states with finite  $k$  are achieved with lower packing fractions as depicted in Fig. 4a and in Table I.

We conclude that the truly global ground state is actually only one of the possible  $\infty$ -PD stable states and corresponds to the point  $\alpha = 1$ , which is at  $\phi_{\text{GCP}}$ . The other states along the J-line, obtained by varying  $0 \leq \alpha < 1$ , can be thought of as globally metastable (in reality they also belong to the ground state of the J-line). On the basis of this picture, we propose four categories of jamming according to their metastability as explained in Table I: local metastable (1-PD stable), collective metastable ( $k$ -PD stable with finite  $1 < k < \infty$ ), globally metastable ( $\infty$ -PD stable but with  $0 \leq \alpha < 1$ , and the true global ground state ( $\infty$ -PD stable and  $\alpha = 1$ ). In particular the J-line corresponds to globally metastable states ( $\infty$ -stable) while the ground state corresponds to  $\phi_{\text{GCP}}$ .

Interestingly, the phase diagram that arises from the  $d \rightarrow \infty$  solution, which corresponds to a particular packing protocol, can be reproduced by sampling over glassy states with a modified (non-equilibrium) measure (Charbonneau *et al.*, 2014a, 2017; Parisi and Zamponi, 2010) (see Fig. 8a). Possible glass states are then predicted in the white region of Fig. 8a bounded by the metastable continuation of the equilibrium liquid and the J-line. In this approach the Gardner transition (blue line) separates stable and marginally stable states. Crucially, for infinite pressure this non-equilibrium sampling assigns equal probability to each jammed state at a given density, i.e., it agrees with Edwards uniform measure. Therefore, the non-equilibrium sampling of glassy states at the ground state is another generalization of the Edwards ensemble to finite pressures. Since the critical jamming exponents

calculated in this approach are the same as those from the full RSB solution (Rainone and Urbani, 2016), we conclude that the observed phenomenology of jamming is at least consistent with Edwards assumption of equiprobability in the values of the exponents. Edwards statistical mechanics thus captures key features of the jamming phenomenology, a fact that is increasingly being recognized (Charbonneau *et al.*, 2017; Sharma *et al.*, 2016). Highly sophisticated simulations have recently confirmed the validity of Edwards assumptions at the jamming transition as well (Martiniani *et al.*, 2017) (see Sec. III.B).

Furthermore, these results highlight the fact that packing problems, and more generally CSPs, undergo a phase transition separating a satisfiable (SAT) (hypostatic or under-constrained) regime from an unsatisfiable (UNSAT) (hyperstatic or over-constrained) phase, as one varies the ratio of constraints over variables. The jamming transition is equivalent to this SAT-UNSAT phase transition in the broad class of continuous CSPs, which are conjectured to belong to the same "super-universality" class based on models displaying SAT/UNSAT like the celebrated perceptron model (Franz and Parisi, 2016; Franz *et al.*, 2015) which admits a much simpler solution at the full RSB level than the hard-sphere glass.

If crystallization is *not* suppressed, compressing an equilibrium liquid of monodisperse spheres can lead to partial crystalline order (Anikeenko and Medvedev, 2007; Anikeenko *et al.*, 2008; Francois *et al.*, 2013; Hanifpour *et al.*, 2015, 2014; Jin and Makse, 2010; Kapfer *et al.*, 2012; Klumov *et al.*, 2014, 2011; Radin, 2008). Using the granular entropy of Edwards statistical mechanics as treated in Sec. II.C, then allows to identify the onset of crystalline order with the freezing point of a first order transition, which is found at  $\phi_{\text{f}} \approx 0.64$  (Jin and Makse, 2010). Likewise, a melting point appears at  $\phi_{\text{m}} \approx 0.68$ . Between these two densities a coexistence of disordered and ordered states exists at the coordination number of isostaticity  $z = 6$  (see Fig. 8b). Defining RCP in this scenario as the freezing point, two branches then exist: a disordered branch from the RLP at  $\phi_{\text{rlp}} \approx 0.54$  up to the freezing point  $\phi_{\text{f}} \approx 0.64$  and an ordered branch from the melting point  $\phi_{\text{m}} \approx 0.68$  to FCC at  $\phi_{\text{fcc}} = 0.74\dots$ . The signature of this disorder-order transition is a disconti-

nity in the entropy density of jammed configurations as a function of the compactivity. This highlights the fact that beyond RCP, denser packing fractions of monodisperse spheres can only be reached by partial crystallization up to the homogeneous FCC crystal phase in agreement with the interpretation of RCP as a MRJ state (Torquato *et al.*, 2000). Indeed, RCPs are known to display sharp structural changes (Anikeenko and Medvedev, 2007; Anikeenko *et al.*, 2008; Aristoff and Radin, 2009; Kapfer *et al.*, 2012; Klumov *et al.*, 2014, 2011; Radin, 2008) signalling the onset of crystallization (Torquato and Stillinger, 2010). The first-order transition scenario observed numerically in (Jin and Makse, 2010) has been verified in a set of experiments of 3d hard sphere packings (Francois *et al.*, 2013; Hanifpour *et al.*, 2015, 2014). In (Francois *et al.*, 2013) the onset of crystallization at the freezing point  $\phi_f \approx 0.64$  has been identified from the variance of the Voronoi volume fluctuations (Jin and Makse, 2010), a “granular specific heat” (Aste and Di Matteo, 2008a), and the frequency of polytetrahedral structures. The coexistence line at isostaticity between  $\phi_f \approx 0.64$  and  $\phi_m \approx 0.68$  has been observed not only for frictionless packings but also for frictional ones, where high densities have been achieved by applying intense vibrations (Hanifpour *et al.*, 2015, 2014).

The existence of the first-order crystallization transition at RCP is expected to be dominant in a finite dimensional 3d system of equal size spheres and therefore excludes the appearance of the interesting glassy phases discussed above unless crystallization is suppressed by heterogeneities like polydispersity. Interestingly, the values of the limiting densities  $[\phi_{th}, \phi_{GCP}]$  coincide approximately with the densities of the melting and freezing points in the first-order transition obtained for monodisperse 3d systems (Jin and Makse, 2010). However, this coincidence is most likely coincidental since these states are unrelated. It should be noted that the analysis of structure and order parameters is generally supportive of the existence of a glass-crystal coexistence mixture in the density region  $0.64 \leq \phi \leq 0.68$  in monodisperse sphere packings where crystallization dominates over the glass phase. All the (maximally random) jammed states along the segment  $[\phi_{th}, \phi_{GCP}]$  can be made denser at the cost of introducing some partial crystalline order. Support for an order/disorder transition at  $\phi_f$  is also obtained from the increase of polytetrahedral substructures up to RCP and its consequent decrease upon crystallization (Anikeenko *et al.*, 2008).

The connection of the replica approach with the Edwards ensemble for jammed disordered states is summarized in Table I and Fig. 4a and will be discussed in detail in Sec. V. The hierarchy of metastable jammed states  $k$ -PD with  $k \in [1, \infty)$  is analogous to  $k$ -SF with  $k \in [1, \infty)$  metastable states in spin-glasses which in turn are related to the continuity of jammed states along the J-line. This is the picture emerging from a full RSB solution, at

the mean-field level of fully connected systems, like the SK model of spin-glasses (Sherrington and Kirkpatrick, 1975). Thus, we expect that a continuous jamming line of states should emerge from the Edwards ensemble solution of the JSP, since it is another realization of a typical NP-hard CSP.

On the other hand, the mean field solution of the Edwards volume ensemble (Song *et al.*, 2008) reviewed in Sec. IV predicts a single jamming point at RCP, Eq. (82),  $\phi_{rcp} = \frac{1}{1+1/\sqrt{3}} \approx 0.634$  for  $z = 6$ . This prediction corresponds to the ensemble average over a coarse-grained Voronoi volume for a fixed coordination number. Since an ensemble average over all packings at a fixed coordination number is performed in the coarse-graining of the volume function, the obtained volume fractions  $\phi_{rcp}$  are in fact averaged over the J-line predicted by the replica method. Thus,  $\phi_{rcp}$  can be associated to the state with the largest entropy (largest complexity) along  $[\phi_{th}, \phi_{GCP}]$ , expected to be near the highest entropic state  $\phi_{th}$  in the replica theory picture. Indeed, high-dimensional calculations performed in Sec. IV.C support this conjecture: the scaling obtained with dimension  $d$  of the Edwards prediction for RCP and  $\phi_{th}$  agree within a prefactor, see Eqs. (95) and (99) below.

New possibilities to study densely packed states are opened up by including activity on the particle level (self-propulsion), which shifts the glass transition closer to random close packing (Ni *et al.*, 2013).

## 5. Force statistics

It has been realized early on that jammed granular aggregates exhibit non-uniform stress fields due to arching effects (Cates *et al.*, 1998; Jaeger *et al.*, 1996). More recent work has focused on the interparticle contact force network. The key quantity is the force distribution  $P(f)$ , which exhibits characteristic features at jamming as observed in both experiments (Brujić *et al.*, 2003a,b; Corwin *et al.*, 2005; Erikson *et al.*, 2002; Kyeyune-Nyombi *et al.*, 2018; Liu *et al.*, 1995; Løvøll *et al.*, 1999; Makse *et al.*, 2000; Mueth *et al.*, 1998; Zhou *et al.*, 2006) and simulations (Makse *et al.*, 2000; O’Hern *et al.*, 2001; Radjai *et al.*, 1996; Tkachenko and Witten, 2000):

- $P(f)$  has a peak at small forces (approximately at the mean force  $\langle f \rangle$ ). This peak has been argued to represent a characteristic signature of jamming (O’Hern *et al.*, 2001).
- For large forces, the decay of  $P(f)$  has been generally measured as exponential. Although a faster than exponential decay has also been observed in experiments (Majmudar and Behringer, 2005) and simulations (van Eerd *et al.*, 2007).

These properties are observed in both hard and soft sphere systems, largely independent of the force law.

For  $f \rightarrow 0^+$ ,  $P(f)$  converges to a power-law

$$P(f) \sim f^\theta, \quad f \rightarrow 0^+, \quad (48)$$

with some uncertainty regarding the value of the exponent:  $\theta \approx 0.2 - 0.5$ . The existence of this power-law has been explained by the marginal stability of the packing which is controlled by small forces (Wyart, 2012). As a consequence,  $\theta$  is related to the exponent  $\gamma$  of near contacting neighbours by Eq. (47). A more detailed investigation of the excitation modes related to the opening and closing of contacts suggests that there are in fact two relevant exponents  $\theta_e$  and  $\theta_l$  (Lerner *et al.*, 2013):  $\theta_e$  corresponding to motions of particles extending through the entire systems; and  $\theta_l$  corresponding to a local buckling of particles. A marginal stability analysis provides  $\gamma = (2 + \theta_e)^{-1} = (1 - \theta_l)/2$  (Müller and Wyart, 2015), which has also been demonstrated numerically (Lerner *et al.*, 2013). Asymptotically  $\theta = \min(\theta_l, \theta_e)$  and thus  $\theta = \theta_l \approx 0.2$  for  $\gamma \approx 0.4$ .

Theoretically, one step replica symmetry 1RSB theory for fully connected hard sphere packings in infinite dimensions predicts  $\theta = 0$  (Parisi and Zamponi, 2010), while the full RSB calculation provides a non-zero  $\theta = 0.42..$  and  $\gamma = 0.41..$  (Charbonneau *et al.*, 2014a,b), a result corroborated theoretically with a simpler jamming model, the Perceptron model from machine learning, which exhibits a jamming transition as well (Franz and Parisi, 2016; Franz *et al.*, 2015). This result further indicates the importance of the jamming transition to general CSPs. The full-RSB values are seemingly in disagreement with the scaling relations from marginal stability in the presence of localized modes, since they predict  $\theta_l = 0.17..$  However, based on simulation results it has been shown that the probability of localized modes decreases exponentially with dimension and thus they do not contribute to the full RSB solution for  $d \rightarrow \infty$  (Charbonneau *et al.*, 2015b). Thus, in 3d simulations the so called bucklers (particles with all forces except one, usually the smallest, approximately aligned in a plane) are removed from the distribution decreasing the small force counting and changing the exponent from 0.17 to 0.42 in agreement with the full RSB replica theory. As a consequence,  $\theta = \theta_e$  in agreement with the scaling relations.

High-resolution measurements of the contact network in 3d allow for the experimental determination of the exponents  $\theta$  and  $\gamma$ , see Table IV and Fig. 7 (Kyeyune-Nyombi *et al.*, 2018). Here, the value of the small force exponent can be estimated due to the high resolution of contact detection. Values in the range  $\theta \approx 0.11 - 0.17$  below the full RSB prediction are found even when bucklers are removed. Instead of the equality Eq. (47), the inequality  $\gamma \geq 1/(2 + \theta)$  is still observed, except for one packing A which is presumably hyperstatic. On the other limit of sparse graphs, replica symmetry calculations gives  $\theta = 0$  in the thermodynamic limit using population dynamics implying that RS calculations do not

capture the full physics of the jamming point (Bo *et al.*, 2014) (discussed in Sec. V.A).

Packing	$N$	$z$	$\phi$	$\theta$	$\gamma$	$1/(2 + \theta)$
A	1393	7.57	0.66(8)	0.110(5)	0.42(2)	0.474(1)
B	1263	6.79	0.62(4)	0.143(4)	0.62(2)	0.467(1)
C	1486	6.64	0.64(7)	0.170(6)	0.75(3)	0.461(1)

TABLE IV Structural properties of a 3d colloidal packing near marginal stability using high-resolution measurements of the contact network (Kyeyune-Nyombi *et al.*, 2018). Three slightly different packing protocols have been used. Instead of the equality (47), the weak force exponent  $\theta$  (Eq. (48)) and the small gap exponent  $\gamma$  (Eq. (46)) are found to satisfy the inequality  $\gamma \geq 1/(2 + \theta)$  (Wyart, 2012) (except for Packing A which might be hyperstatic). The exponent  $\theta$  does not change appreciable whether bucklers are included or not.

## B. Test of ergodicity and the uniform measure in the Edwards ensemble

Assuming ergodicity for a jammed system of grains as proposed by Edwards (see Sec. II.C) seems contradictory at first, but has become meaningful in the first place in light of certain seminal compaction experiments developed over the years starting from the work of Nowak *et al.* in the 90's (Brujić *et al.*, 2005; Chakravarty *et al.*, 2003; Knight *et al.*, 1995; Makse *et al.*, 2005; Nowak *et al.*, 1998, 1997; Philippe and Bideau, 2002; Richard *et al.*, 2005).

Nowak, *et al.* (Nowak *et al.*, 1998, 1997) performed a set of experiments of the compaction of spherical glass beads as a function of increasing and decreasing vertical tapping intensity. Figure 9 shows their results for the packing fraction  $\rho$  versus the tapping intensity  $\Gamma$  (normalized by the acceleration due to gravity). The key observation is that the system, after initial transient behavior on the ‘irreversible branch’, reaches a ‘reversible branch’ on which it retraces the variation of the packing fraction upon increasing and decreasing the intensity. The initial tapping breaks the frictional contacts that support loose packed configurations and store information about the system preparation. On the reversible branch, small tapping intensities induce denser packings with packing fractions slightly above random close packing for equal-sized spheres.

In principle, we can interpret the reversible packings as equilibrium-like states, in which the details of the microscopic configurations and the compaction protocol are irrelevant, as demonstrated by the reversible nature of the states evidenced by the unique branch traveled by the system as the external intensity is increased



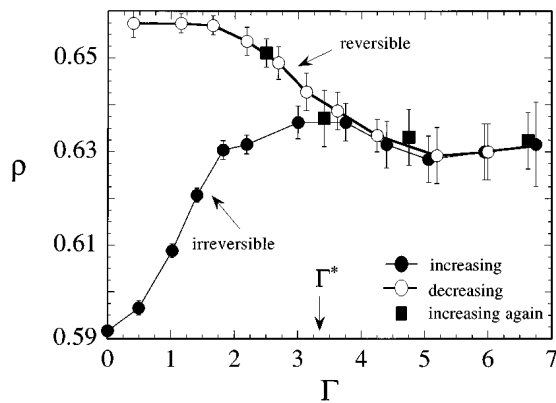


FIG. 9 The packing fraction  $\rho$  plotted as a function of the shaking intensity  $\Gamma$  from experiments of granular packings undergoing vertical tapping (Nowak *et al.*, 1998). The intensity is defined as the ratio of the peak acceleration during a single tap to the gravitational acceleration. The system is prepared initially at low packing fraction and subjected to taps of increasing intensity. The tapping intensity is then successively reduced, and the system falls on a reversible branch, where the system retraces the density versus intensity behavior upon subsequent increases and decreases of the intensity. From (Nowak *et al.*, 1998).

and decreased. These are the states for which we expect, in principle, a statistical mechanical formalism to hold. The existence of such a reversible branch has been corroborated in a number of experimental systems with different compaction techniques, e.g., under mechanical oscillations and vibrations, shearing, or pressure waves (Brujić *et al.*, 2005; Chakravarty *et al.*, 2003; Philippe and Bideau, 2002) and studied with theory and modelling (Caglioti *et al.*, 1997; Krapivsky and BenNaim, 1994; Nicodemi, 1999; Nicodemi *et al.*, 1997a,b,c, 1999; Prados *et al.*, 2000). However, this interpretation has been challenged in a number of studies of ergodicity in jammed matter.

Systems that are subjected to a constant drive such as infinitesimal tapping or also small shear are able to explore their phase space dynamically, such that ergodicity can be tested directly by comparing time averages and averages with respect to the constant volume ensemble. We stress here, that only infinitesimal driving forces should be applied to test equiprobable states (see discussion in Sec. VI). An agreement of the two averages has indeed been observed in simple models (Berg *et al.*, 2002; Gradenigo *et al.*, 2015), as well as soft sphere systems with a small number of particles  $N = 30$  (Wang *et al.*, 2010a, 2012).

Some recent systematic results are more controversial though, motivating a continued investigation of this fascinating concept (Irastorza *et al.*, 2013). A very detailed and rigorous numerical analysis confirms that at low tapping intensities, the system can not be considered to be ergodic: Two different realizations of the same prepa-

ration protocol do not correspond to the same stationary distribution, indicated by a statistical test of data for both the packing density (Paillusson, 2015; Paillusson and Frenkel, 2012) using volume histograms sample over time (McNamara *et al.*, 2009a,b), and the trace of the force-moment tensor (Gago *et al.*, 2016). When considering the fraction of persistent contacts as a function of tapping intensity, one observes that the non-ergodic regime coincides with a larger percentage of persistent contacts, while such contacts are almost absent in the ergodic regime (Gago *et al.*, 2016). The picture that emerges is that the breakdown of ergodicity is connected to the presence of contacts that do not break under the effect of the tapping. In accordance with physical intuition, the system can then not sample its whole phase space, but is stuck in specific regions with the consequent breaking of ergodicity. An additional reason to doubt the validity of ergodicity is the violation of the time reversal symmetry due to dissipation (Dauchot, 2007).

Ergodicity is also intimately related to the existence of non-equilibrium fluctuation-dissipation relations (FDR) characterized by an effective temperature (Cugliandolo, 2011). For equilibrium systems, the FDR is a very general result relating time correlations and responses through the temperature of the thermal environment. Non-equilibrium FDRs have been shown to hold in a wide range of systems starting with the work of Ref. (Cugliandolo *et al.*, 1997), e.g., for glassy systems (Bellon and Ciliberto, 2002; Crisanti and Ritort, 2003; Leuzzi, 2009) and models of driven matter (Berthier *et al.*, 2000; Loi *et al.*, 2008) (see also the review (Marconi *et al.*, 2008)). It has recently also been demonstrated in single molecule DNA driven out of equilibrium by an optical tweezer (Dieterich *et al.*, 2015). Non-equilibrium FDRs and effective temperatures are often linked to the slow modes of the relaxation in a glassy phase (Cugliandolo *et al.*, 1997). In granular compaction, the relaxation to the final density is similarly slow, following, e.g., an inverse logarithmic law under tapping (Krapivsky and BenNaim, 1994; Nowak *et al.*, 1998, 1997) and a Kohlrausch-Williams-Watts law under shear (Lu *et al.*, 2008a). The fluctuations induced by the continuous driving allow for the definition of an effective temperature, which, in an ergodic system, should agree with the granular temperature associated with the canonical volume ensemble (Cugliandolo, 2011). This allows for an indirect test of ergodicity, which has been established in a number of systems, both toy models (Barrat *et al.*, 2000; Brey *et al.*, 2000; Coniglio *et al.*, 2004; Dean and Lefèvre, 2001; Fierro *et al.*, 2002a, 2003; Lefèvre, 2002; Lefèvre and Dean, 2002; Nicodemi, 1999; Nicodemi *et al.*, 2004; Prados and Brey, 2002; Tarjus and Viot, 2004) and more realistic ones using MD simulation of slowly sheared granular materials (Makse and Kurchan, 2002), as well as experiments measuring effective temperatures in colloidal jammed systems (Song *et al.*, 2005) and slowly sheared granular materials in a vertical

Couette cell (Potiguar and Makse, 2006; Wang *et al.*, 2008, 2006) and vibrating cells (Ribiere *et al.*, 2007). The observation of ratcheting in packings of polygonal particles under cyclic load (Alonso-Marroquín and Herrmann, 2004) sheds however some doubts about the exploration of configuration space due to systematic irreversible displacements on the grain scale: not only is time reversibility violated, but a steady state does not seem to be reached.

The concept of granular temperature or compactivity  $X$  raises the question whether it is a well defined quantity at all. There are essentially two different methods to calculate  $X$  from packing data: (i) From the statistics of elementary volume cells. Exploiting the analogy with equilibrium statistical mechanics,  $X$  can be derived by thermodynamic integration over the inverse volume fluctuations (Briscoe *et al.*, 2008; Jin and Makse, 2010; Lechenault *et al.*, 2006; Nowak *et al.*, 1998; Ribiere *et al.*, 2007; Schröter *et al.*, 2005). Alternatively, one can use analytical expressions either for the volume distribution, such as the  $\Gamma$ -distribution (Aste and Di Matteo, 2008a,b; Aste *et al.*, 2007) or for  $X$  itself, derived e.g. from idealized solutions using quadrons (Blumenfeld and Edwards, 2003; Blumenfeld *et al.*, 2012). (ii) Using an overlapping histograms approach (Dean and Lefevre, 2003; McNamara *et al.*, 2009a). The protocol independence of  $X$  obtained from a fit to the quadron solution has been shown in (Becker and Kassner, 2015). In (Zhao and Schröter, 2014) four different ways of measuring  $X$  from the same experimental data set of a binary disk packing have been systematically compared. Interestingly, only two of the methods have been shown to agree quantitatively once the density of states is also included as an experimental input. This highlights possible inconsistencies between different definitions of  $X$ .

The equilibration of the temperature-like parameters in Edwards statistical mechanics has been demonstrated in experiments (Jorjadze *et al.*, 2011; Puckett and Daniels, 2013; Schröter *et al.*, 2005). However, in (Puckett and Daniels, 2013) only the angoricity and not the compactivity has been shown to equilibrate. An upper bound on the Edwards entropy in frictional hard-sphere packings has recently been suggested (Baranau *et al.*, 2016).

Recent criticism in (Blumenfeld *et al.*, 2016) has claimed that the volume function is *per se* not suitable as the central concept for a statistical mechanical approach, since the volume is defined by the boundary particles and  $\mathcal{W}$  is thus independent of the configurations of bulk particles, i.e.,  $\partial\mathcal{W}/\partial\mathbf{q}_i = 0$  for these degrees of freedom. As a consequence, the resulting entropy would be miscalculated due to miscounting of these configurations. However, in (Becker and Kassner, 2017) it has been shown that the vanishing derivatives are still consistent with statistical mechanics. Even if  $\mathcal{W}$  is independent of some degrees of freedom, the resulting partition function still

takes these into account and thus allows the correct calculation of macroscopic observables in terms of expectation values.

Related to ergodicity, the second controversial concept underlying Edwards statistical mechanics is the assumption of equiprobability of jammed microstates, Fig. 4a. Since Edwards' initial conjecture, most studies have focused on testing the validity of the consequences of this assumption rather than testing it directly. On the other hand, a direct test requires the evaluation of all possible jammed configurations and counting the occurrence of distinct microstates, which is possible in model systems (Bowles and Ashwin, 2011; Slobinsky and Pagnaloni, 2015a,b). For more realistic packings, such a direct test has long been restricted to small numbers of particles due to the prohibitively large number of resulting jammed states. Some of the first direct tests for up to  $N = 14$  particles have shown a highly non-uniform distribution, suggesting that the structural and mechanical properties of dense granular media are not dominated equally by all possible configurations as Edwards assumed, but by the most frequent ones (Gao *et al.*, 2006, 2009; Xu *et al.*, 2005). It has been argued that the non-uniformity, which is manifest in a broad distribution of basin volumes in the energy landscape that identify jammed states, is due to the fast quench into the energy minima (Wang *et al.*, 2012). Moreover, it is not clear if the non-uniformity survives for larger system sizes.

Remarkable recent progress has been able to conclusively validate Edwards' equiprobability assumption for realistic system sizes. Advances in numerical methods have enabled a direct computation of basin volumes of distinct jammed states of up to  $N = 128$  polydisperse frictionless spheres in both 2d and 3d with a hard core and soft shell (Asenjo *et al.*, 2014; Martiniani *et al.*, 2017, 2016a,b,c; Xu *et al.*, 2011). The spheres are jammed by equilibrating the fluid phase, inflating the particles and then minimizing the energy to produce mechanically stable packings at a given packing density. The minimization procedure finds individual packings with a probability  $p_i$  proportional to the volume  $v_i$  of their basin of attraction. The number of jammed states is  $\Omega(\phi) = V_J(\phi)/\langle v \rangle(\phi)$ , where  $\langle v \rangle(\phi)$  is the average basin volume and  $V_J(\phi)$  the total phase space volume. The observation that different basins have different volumes for a range of  $\phi$  values already implies that they will not be equally populated and thus equiprobability breaks down for these densities. However, as shown in (Asenjo *et al.*, 2014), the granular entropy still satisfies extensivity if one considers the Gibbs entropy

$$S_G^* = - \sum_i p_i \log p_i - \log N! \quad (49)$$

The subtracted term  $\log N!$  ensures that two systems in identical macrostates are in equilibrium under an exchange of particles and is required for extensivity (Cates

and Manoharan, 2015; Frenkel, 2014; Swendsen, 2006). In order to test equiprobability one can compare  $S_G^*$  with the likewise modified Boltzmann expression  $S_B^* = \log \Omega(V) - \log N!$ . The Gibbs entropy satisfies  $S_G^* \leq S_B^*$  with equality when all  $p_i$  are equal,  $p_i = 1/\Omega$ . Remarkably,  $S_G^*$  indeed approaches  $S_B^*$  as  $\phi \rightarrow \phi^*$  for a specific packing density  $\phi^*$  (see Fig. 10) (Martiniani *et al.*, 2017). At  $\phi^*$  the basin volumes decorrelate from structural observables such as pressure, coordination number, etc. Furthermore using a finite size scaling analysis one can show that  $\phi^*$  coincides with the density at which pressure fluctuations diverge as  $N \rightarrow \infty$ , which is only possible at the jamming transition  $\phi^J$ :  $\phi_{N \rightarrow \infty}^* = \phi_{N \rightarrow \infty}^J$ . The comprehensive study in (Martiniani *et al.*, 2017) thus demonstrates that Edwards assumption of equiprobability indeed holds at the jamming transition, which corresponds to the point of maximum entropy. Moreover, it is shown that equiprobability is still satisfied over the whole range of  $\phi$  values if one conditions on a fixed value of the pressure indicating that the generalized stress-volume Edwards ensemble is also a robust description.

In general, it is important to keep in mind that equiprobability will not hold for all possible packing algorithms. For example, the protocol used in (Atkinson *et al.*, 2014) to generate maximally random jammed monodisperse disk packings based on a linear programming algorithm (Torquato and Jiao, 2010) samples a particular subset of all possible jammed states, which have only a very low probability of occurrence in the Edwards ensemble. In (Charbonneau *et al.*, 2017) it is shown that the configurational entropy of jammed packings resulting from adiabatic compression of glassy states is systematically smaller than the one obtained from Edwards uniform measure. Hence, this protocol generates exponentially fewer packings than are possible. A framework to include protocol dependence in an Edwards-type ensemble has been suggested (Paillusson, 2015). Even without such an extension, recent theoretical work has shown that the predictions resulting from Edwards assumptions are indeed in excellent agreement with empirical data, confirming, e.g., the critical properties of hard spheres at jamming (Charbonneau *et al.*, 2017) (see Sec. III.A.4), and jamming densities in a wide range of different systems as reviewed in the next Section IV. Conceptually, it is possible to resolve the problem of protocol dependence if one starts from the very beginning by defining the metastable jammed states and not the protocols, then one avoids the whole question of the ergodic hypothesis or protocol dependence or similar issues, which are not really essential for Edwards' statistics. We will discuss in detail this line of reasoning in Section V by exploiting an analogy between metastable jammed states with the metastable states of spin-glass systems.

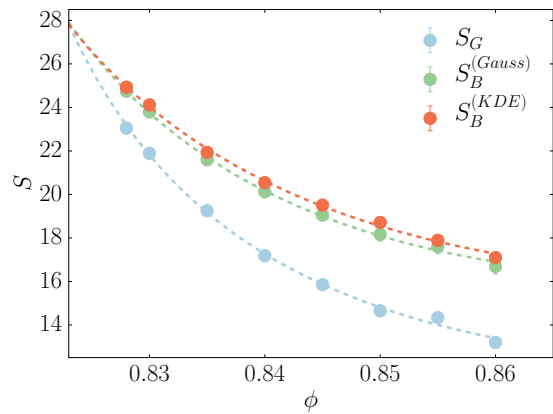


FIG. 10 (Colors online) Recent numerical results confirm Edwards equiprobability assumption at the jamming transition (Martiniani *et al.*, 2017). Gibbs entropy Eq. (49) and Boltzmann entropy  $S_B^* = \log \Omega(V) - \log N!$  demonstrating equiprobability at  $\phi^* \approx 0.82$  for  $N = 64$  particles.  $S_B^*$  is computed parametrically (“Gauss”) and non-parametrically using a kernel density estimate (“KDE”). From (Martiniani *et al.*, 2017).

#### IV. EDWARDS VOLUME ENSEMBLE

In this chapter we focus on the Voronoi convention to define the microscopic volume function of an assembly of jammed particles. As we discuss in detail, Edwards statistical mechanics of a restricted volume ensemble can then be cast into a predictive framework to determine packing densities for both spherical and non-spherical particles. In the next sections we outline the mean-field statistical mechanical approach based on a coarse-graining of the Voronoi volume function Eq. (23). In Secs. IV.C–IV.F, we discuss different aspects of packings of spheres, such as the effects of dimensionality, bidispersity, and adhesion. In Sec. IV.G we focus on packings of non-spherical shapes. A comprehensive phase diagram classifying packings of frictional, frictionless, adhesive spheres and non-spherical shapes is presented in Sec. IV.H.

##### A. Mean-field calculation of the microscopic volume function

The key question is how analytical progress can be made with the volume function Eq. (23). The global minimization in the definition of  $l_i(\hat{c})$ , Eq. (24), implies that the volume function is a complicated non-local function. This global character indicates the existence of strong correlations and greatly complicates the calculation of, e.g., the partition function in the Edwards ensemble approach. In order to circumvent these difficulties, we review here a mean-field geometrical viewpoint developed in a series of papers (Baule and Makse, 2014; Baule *et al.*,

2013; Bo *et al.*, 2014; Briscoe *et al.*, 2008, 2010; Liu *et al.*, 2015; Meyer *et al.*, 2010; Portal *et al.*, 2013; Song *et al.*, 2010, 2008; Wang *et al.*, 2010a,b, 2011, 2010c), where the central quantity is not the exact microscopic volume function, but rather the average or coarse-grained volume of an individual cell in the Voronoi tessellation. The packing density  $\phi$  of a system of monodisperse particle of volume  $V_0$  is given by

$$\phi = \frac{NV_0}{\sum_{i=1}^N \mathcal{W}_i} = \frac{V_0}{\frac{1}{N} \sum_{i=1}^N \mathcal{W}_i}. \quad (50)$$

In the limit  $N \rightarrow \infty$  we replace the denominator by the ensemble averaged volume of an individual cell  $\overline{W} = \langle \mathcal{W}_i \rangle_i$ :  $\frac{1}{N} \sum_{i=1}^N \mathcal{W}_i \rightarrow \overline{W}$  as  $N \rightarrow \infty$ . As a result the volume fraction is simply

$$\phi = V_0/\overline{W}. \quad (51)$$

Considering Eq. (23), we can perform an ensemble average to obtain:

$$\begin{aligned} \overline{W} &= \left\langle \frac{1}{d} \oint d\hat{\mathbf{c}} l_i(\hat{\mathbf{c}})^d \right\rangle_i = \frac{1}{d} \oint d\hat{\mathbf{c}} \langle l_i(\hat{\mathbf{c}})^d \rangle_i \\ &= \frac{1}{d} \oint d\hat{\mathbf{c}} \int_{c^*}^{\infty} dc c^d p(\mathbf{c}, z). \end{aligned} \quad (52)$$

In the last step we have introduced the pdf  $p(\mathbf{c}, z)$  which is the probability density to find the Voronoi boundary VB at a value  $c$  in the direction  $\hat{\mathbf{c}}$ . This involves a lower cut-off  $c^*$  in the direction  $\hat{\mathbf{c}}$  due to the hard-core boundary of the particles. Crucially, we assume that the pdf is a function of  $\mathbf{c}$  and the coordination number  $z$  only rather than a function of the exact particle configurations in the packing. This is the key step in the coarse-graining procedure, which replaces the exact microscopic information contained in  $l_i(\hat{\mathbf{c}})$  by a probabilistic quantity. In the following, we focus on spheres, where  $p(\mathbf{c}, z) = p(c, z)$  and  $c^*(\hat{\mathbf{c}}) = R$  due to the statistical isotropy of the packing and the isotropy of the reference particle itself. More complicated shapes will be treated in subsequent sections.

We now introduce the cumulative distribution function (CDF)  $P_>(c, z)$  via the usual definition  $p(c, z) = -\frac{d}{dc} P_>(c, z)$ . Eq. (52) becomes then in 3d

$$\begin{aligned} \overline{W}(z) &= \frac{4\pi}{3} \int_R^{\infty} dc c^3 p(c, z) \\ &= V_0 + 4\pi \int_R^{\infty} dc c^2 P_>(c, z), \end{aligned} \quad (53)$$

where  $V_0 = \frac{4\pi}{3} R^3$ . The advantage of using the CDF  $P_>$  rather than the pdf, is that the CDF has a simple geometrical interpretation. We notice first that  $P_>$  contains the probability to find the VB in a given direction  $\hat{\mathbf{c}}$  at a value larger than  $c$ , given  $z$  contacting particles. But this probability equals the probability that  $N-1$  particles are outside a volume  $\Omega$  centered at  $\mathbf{c}$  relative to

the reference particle (Fig. 11). Otherwise, if they were inside that volume, they would contribute a VB smaller than  $c$ . The volume  $\Omega$  is thus defined as

$$\Omega(\mathbf{c}) = \int d\mathbf{r} \Theta(c - s(\mathbf{r}, \hat{\mathbf{c}})) \Theta(s(\mathbf{r}, \hat{\mathbf{c}})), \quad (54)$$

where  $s(\mathbf{r}, \hat{\mathbf{c}})$  parametrizes the VB in the direction  $\hat{\mathbf{c}}$  for two spheres of relative position  $\mathbf{r}$ .  $\Theta(x)$  denotes the usual Heavyside step function. Due to the isotropy of spheres, the direction  $\hat{\mathbf{c}}$  can be chosen arbitrarily. We refer to  $\Omega$  as the *Voronoi excluded volume*, which extends the standard concept of the hard-core excluded volume  $V_{\text{ex}}$  that dominates the phase behavior of interacting particle systems at thermal equilibrium (Onsager, 1949).

This geometrical interpretation allows us to connect  $P_>(c, z)$  with the  $N$ -particle pdf  $P_N(\{\mathbf{r}_1, \mathbf{r}_2, \dots, \mathbf{r}_N\})$  in an exact way. Without loss of generality we denote the reference particle  $i$  as particle 1. Then,  $P_>(c, z) = P_>(\mathbf{r}_1; \Omega)$ , i.e., the probability that the  $N-1$  particles apart from particle 1 are outside the volume  $\Omega$ . Since  $P_N(\{\mathbf{r}_1, \mathbf{r}_2, \dots, \mathbf{r}_N\})$  expresses the probability to find particle 1 at  $\mathbf{r}_1$ , particle 2 at  $\mathbf{r}_2$ , etc., we have (Jin *et al.*, 2010)

$$\begin{aligned} P_>(\mathbf{r}_1; \Omega) &= \mathcal{C} \int d\mathbf{r}^{N-1} P_N(\{\mathbf{r}_1, \mathbf{r}_2, \dots, \mathbf{r}_N\}) \\ &\quad \times \prod_{i=2}^N [1 - m(\mathbf{r}_i - \mathbf{r}_1; \Omega)], \end{aligned} \quad (55)$$

where  $\mathcal{C}$  ensures proper normalization. The indicator function  $m(\mathbf{r}; \Omega)$  is given by

$$m(\mathbf{r}; \Omega) = \begin{cases} 1, & \mathbf{r} \in \Omega \\ 0, & \mathbf{r} \notin \Omega \end{cases} \quad (56)$$

Equation (55) is the starting point for the calculation of  $P_>(c, z)$  from a systematic treatment of the particle correlations as discussed in Sec. IV.D for 2d packings (Jin *et al.*, 2014) and in Sec. IV.C for high-dimensional packings (Jin *et al.*, 2010). Here, we proceed with a phenomenological approach based on an exact treatment in 1d which is used as an approximation to the 3d case, as originally developed in (Song *et al.*, 2008).

We can first separate contributions to  $P_>$  stemming from bulk and contacting particles. We introduce two CDFs, the bulk contribution  $P_B$  and the contact contribution  $P_C$ :

- $P_B$  denotes the probability that spheres in the bulk are located outside the Moon-phase grey volume  $V^*$  in Fig. 11. The volume  $V^*$  is the volume excluded by  $\Omega$  for bulk particles and takes into account the overlap between  $\Omega$  and the hard-core excluded volume  $V_{\text{ex}}$ :

$$\begin{aligned} V^* &= \Omega - \Omega \cap V_{\text{ex}} \\ &= \int d\mathbf{r} \Theta(r - 2R) \Theta(c - s(\mathbf{r}, \hat{\mathbf{c}})) \Theta(s(\mathbf{r}, \hat{\mathbf{c}})). \end{aligned} \quad (57)$$



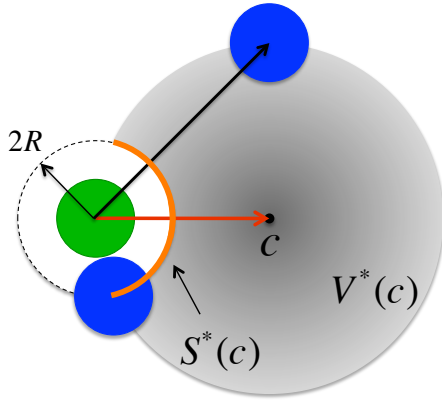


FIG. 11 (Colors online) The condition to have the VB in the direction  $\hat{s}$  from the reference particle (green sphere) at the value  $c$  is geometrically related to the exclusion volume  $\Omega$  for all other particles (blue spheres). Taking into account the conventional hard-core excluded volume leads to the Voronoi excluded volume Eq. (57) (the Moon phase - grey volume  $V^*$ ) and Voronoi excluded surface Eq. (57) (orange line).

We call  $V^*$  the Voronoi excluded volume.

- $P_C$  denotes the probability that contacting spheres are located outside the boundary of the grey area indicated in orange in Fig. 11 and denoted  $S^*$ . The surface  $S^*$  is the surface excluded by  $\Omega$  for contacting particles:

$$S^* = \partial V_{\text{ex}} \cap \Omega$$

$$= \oint d\mathbf{r} \Theta(c - s(\mathbf{r}, \hat{\mathbf{c}})) \Theta(s(\mathbf{r}, \hat{\mathbf{c}})) \Big|_{r=2R}, \quad (58)$$

where  $\partial V_{\text{ex}}$  denotes the boundary of  $V_{\text{ex}}$ .

A key assumption to make analytical progress is to assume  $P_B$  and  $P_C$  to be statistically independent, thus  $P_{>} = P_B P_C$ . There is no a priori reason why this should be the case, so the independence should be checked a posteriori from simulation data. For spheres and non-spherical particles close to the spherical aspect ratio, it has been verified that independence is a reasonable assumption (Baule *et al.*, 2013; Song *et al.*, 2008). It is then natural to consider only  $P_C$  to be a function of  $z$ . Therefore,

$$P_{>}(c, z) = P_B(c) \times P_C(c, z). \quad (59)$$

We now derive a functional form of the  $P_B$  term. In 1d, the distribution of possible arrangements of  $N$  hard rods in a volume  $V$  can be mapped to the distribution of ideal gas particles by removing the occupied volume  $NV_0$  (Krapivsky and BenNaim, 1994; Palásti, 1960; Rényi, 1958; Tarjus and Viot, 2004). The probability to locate one particle at random outside the volume  $V^*$  in a system

of volume  $V - NV_0$  is then  $P_{>}(1) = 1 - V^*/(V - NV_0)$ . For  $N$  ideal particles, we obtain

$$P_{>}(N) = \left(1 - \frac{V^*}{V - NV_0}\right)^N. \quad (60)$$

The particle density is  $\tilde{\rho} = N/(V - NV_0)$ . Therefore

$$\lim_{N \rightarrow \infty} P_{>}(N) = \lim_{N \rightarrow \infty} \left(1 - \frac{\tilde{\rho} V^*}{N}\right)^N = e^{-\tilde{\rho} V^*}. \quad (61)$$

In the thermodynamic limit the probability to observe  $N$  particles outside the volume  $V^*$  is given by a Boltzmann-like exponential distribution. In this limit, the particle density becomes

$$\tilde{\rho} = \lim_{N \rightarrow \infty} \frac{1}{\frac{1}{N} \sum_{i=1}^N \mathcal{W}_i - V_0} = \frac{1}{\overline{W} - V_0}. \quad (62)$$

While the above derivation is exact in 1d, the extension to higher dimensions is an approximation: Even if there is a void with a large enough volume, it might not be possible to insert a particle due to the constraint imposed by the geometrical shape of the particles (which does not exist in 1d). Nevertheless, in what follows, we assume the exponential distribution of Eq. (61) to be valid in 3d as well and write

$$P_B(c) = e^{-\tilde{\rho} V^*(c)}, \quad (63)$$

where the Voronoi excluded volume can be calculated explicitly from Eq. (57):

$$V^*(c) = V_0 \left( \left( \frac{c}{R} \right)^3 - 4 + 3 \frac{R}{c} \right). \quad (64)$$

Furthermore, we also assume  $P_C$  to have the same exponential form as Eq. (63), despite not having the large number approximation leading to it (the maximum coordination is the kissing number 12). Introducing a surface density  $\sigma(z)$ , we write

$$P_C(c) = e^{-\sigma(z) S^*(c)}, \quad (65)$$

where the Voronoi excluded surface follows from Eq. (58):

$$S^*(c) = 2S_0 \left( 1 - \frac{R}{c} \right), \quad (66)$$

where  $S_0 = 4\pi R^2$ . To obtain an expression for  $\sigma(z)$  we calculate the average  $\langle S^* \rangle$  with respect to the pdf  $-\frac{d}{dc} P_C(c)$ , which yields a simple result (Song *et al.*, 2010, 2008; Wang *et al.*, 2011)

$$\langle S^* \rangle \approx 1/\sigma(z). \quad (67)$$

In turn,  $\langle S^* \rangle$  is defined as the average of the solid angles of the gaps left between  $z$  contacting spheres around the reference sphere. An alternative operational definition assuming an isotropic distribution of contact particles is:

- (i) Generate  $z$  contacting particles at random.

- (ii) For a given direction  $\hat{\mathbf{c}}$ , determine the minimal value of the VB, denoted by  $c_m$ .
- (iii) The average  $\langle S^* \rangle$  follows as a Monte-Carlo average in the limit.

$$\langle S^* \rangle = \lim_{n \rightarrow \infty} \frac{1}{n} \sum_{i=1}^n S^*(c_{m,i}), \quad (68)$$

where  $c_{m,i}$  is the  $c_m$  value of the  $i$ th sample. Simulations following this procedure and considering  $z = 1$  up to the kissing number  $z = 12$  suggest that

$$\sigma(z) \approx \frac{z}{4\pi} \sqrt{3}, \quad z > 1, \quad (69)$$

for a chosen radius  $R = 1/2$ . The exact constants appearing in this expression are motivated from an exact treatment of the single particle case plus corrections due to the occupied surface of contact particles (Song *et al.*, 2010; Wang *et al.*, 2011).

Due to the dependence of  $\bar{\rho}$  on  $\bar{W}$ , the CDF  $P_>$  is thus

$$P_>(c, z) = \exp \left[ -\frac{V^*(c)}{\bar{W} - V_0} - \sigma(z) S^*(c) \right], \quad (70)$$

where  $V^*$ ,  $S^*$ , and  $\sigma$  are given by Eqs. (64,66,69). Overall, Eq. (70) with Eq. (53) leads to a self-consistent equation to determine  $\bar{W}$  as a function of  $z$ :

$$\begin{aligned} \bar{W}(z) = V_0 + 4\pi \int_R^\infty dc c^2 \exp \left[ -\frac{V_0}{\bar{W}(z) - V_0} \times \right. \\ \left. \times \left( \frac{c^3}{R^3} - 4 + 3\frac{R}{c} \right) - \sigma(z) 2S_0 \left( 1 - \frac{R}{c} \right) \right] \end{aligned} \quad (71)$$

for which, remarkably, an analytical solution can be found. By using Eqs. (64,66), Eq. (71) is satisfied when (Song *et al.*, 2008):

$$\frac{d}{dc} \left( \frac{1}{w} \left( 3\frac{R}{c} \right) + \sigma(z) S^*(c) \right) = 0, \quad (72)$$

where the free volume is  $w \equiv (\bar{W} - V_0)/V_0$ . Then, with Eq. (66) we obtain the solution for  $w$

$$w(z) = \frac{3}{2S_0\sigma(z)} = \frac{2\sqrt{3}}{z}, \quad (73)$$

using Eq. (69) and setting  $R = 1/2$  for consistency.

As the final result of this section, we arrive at the coarse-grained mesoscopic volume function

$$\bar{W}(z) = V_0 + \frac{2\sqrt{3}}{z} V_0, \quad (74)$$

which is a function of the observable coordination number  $z$  rather than the microscopic configurations of all the particles in the packing. With Eq. (50), we also obtain the packing density as a function of  $z$

$$\phi(z) = \frac{V_0}{\bar{W}} = \frac{z}{z + 2\sqrt{3}}. \quad (75)$$

Equation (75) can be interpreted as an equation of state of disordered sphere packings. In the next section we will show that it corresponds to the equation of state in  $z$ - $\phi$  space in the limit of infinite compactivity.

## B. Packing of jammed spheres

In the hard sphere limit angoricity can be neglected, such that the statistical mechanics of the packing is described by the volume function alone. The partition function is then given by Edwards' canonical one, Eq. (15). With the result on the coarse-grained volume function it is possible to go over from the fully microscopic partition function Eq. (15) to a mesoscopic one (Song *et al.*, 2008; Wang *et al.*, 2011). To this end we change the integration variables in Eq. (15) from the set of microscopic configurations  $\mathbf{q} = \{\mathbf{q}_1, \dots, \mathbf{q}_N\}$  (positions and orientations of the  $N$  particles) to the volumes  $\mathcal{W}_i(\mathbf{q})$ , Eq. 23, of each cell in the Voronoi tessellation. Since the microscopic volume function is given as a superposition of the individual cells, Eq. (20), the partition function Eq. (15) can be expressed as

$$\mathcal{Z} = \prod_{i=1}^N \int d\mathcal{W}_i g(\mathcal{W}) e^{-\sum_{i=1}^N \mathcal{W}_i/X} \Theta_{\text{jam}}. \quad (76)$$

Here, the function  $g(\mathcal{W})$  for  $\mathcal{W} = \{\mathcal{W}_1, \dots, \mathcal{W}_N\}$  denotes the density of states. In the coarse-grained picture all the volume cells are non-interacting and effectively replaced by the volume function Eq. (74). The partition function thus factorizes  $\mathcal{Z} = \mathcal{Z}_i^N$ , where

$$\mathcal{Z}_i(X) = \left( \int dW g(W) e^{-W/X} \Theta_{\text{jam}} \right)^N \quad (77)$$

Averages over the volume ensemble as well as all thermodynamic information is thus accessible via Eq. (77). The crucial step to go from the full microscopic partition function Eq. (15) to Eq. (77) is to introduce the density of states  $g(W)$  for a given volume  $W$ . Although this step formally simplifies the integral, the complexity of the problem is now transferred to determining  $g(W)$ , which is in principle as difficult to solve as the model itself. In Eq. (77),  $X$  is the compactivity measured in units of the particle volume  $V_0$ , and  $\Theta_{\text{jam}}$  imposes the condition of jamming.

In the mean-field view developed in the previous section,  $W$  is directly related to the geometrical coordination number  $z$  via Eq. (74). Therefore, we map  $g(W)$  to  $g(z)$ , the density of states for a given  $z$  via a change of variables  $g(W) = \int P(W|z) g(z) dz$ , where  $P(W|z)$  is the conditional probability of a volume  $W$  for a given  $z$ , which, with Eq. (74), is given by  $P(W|z) = \delta(W - \bar{W}(z))$ , where we have neglected fluctuations in  $z$ , see (Wang *et al.*, 2010c). Substituting these two equations into Eq. (77) effectively changes the integration variable from  $W$  to  $z$  leading to the single particle (isostatic) partition function

$$\mathcal{Z}_{\text{iso}}(X, Z_m) = \int_{Z_m}^6 g(z) \exp \left[ -\frac{2\sqrt{3}}{zX} \right] dz. \quad (78)$$

The jamming condition is now absorbed into the integration range, which constrains the coordination number to isostatic packings (therefore the name isostatic partition function). Notice that in this mesoscopic mean-field approach the force and torque balance jamming conditions from  $\Theta_{\text{jam}}$  Eq. (10) are incorporated when we set the coordination number to the isostatic value. Thus, in this way, we circumvent the most difficult problem of implementing the force jamming condition Eq. (10).

More precisely, the geometric and force/torque constraints from Eq. (10) imply that there are two types of coordination numbers: (i) the geometrical coordination number  $z$ , parametrizing the free volume function Eq. (73) as a function of all contacting particles, constraining the position of the particle via the hard-core geometrical interaction Eq. (1). (ii) The mechanical coordination number  $Z_m$ , counting only the geometrical contacts  $z$  that at the same time carry non-zero force (Oron and Herrmann, 1999, 1998) and therefore takes into account the force and torque balance conditions Eqs. (2)-(7) via the isostatic condition.

From the definition we have  $z \geq Z_m$  since there could be a geometric contact that constraints the motion of the particle but carries no force. This distinction makes sense when there is friction in the packing. For instance, imagine a frictionless particle at the isostatic point  $z = Z_m = 6$  (although isostatic is a global property). Now add friction to the interactions. The mechanical coordination number can be as low as  $Z_m = 4$ , but still  $z = 6$ ; the geometrical constraints are the same, only two forces have been set to zero, allowing for tangential forces to appear in the remaining 4 contacts.

For frictionless packings, we have  $z = Z_m$ . Furthermore, in the limit of infinite compactivity, where the entropy of the packings is maximum and therefore, the packings are the most probable to find in experiments, we will see that again  $z = Z_m$  and the distinction between mechanical and geometrical coordination number disappears. In what follows, we will consider the consequences of considering the two coordination numbers only for the following 3d monodisperse system of spheres. The distinction between  $z$  and  $Z_m$  will allow us to describe the phase diagram for all compactivities as in Fig. 12a, below. In the remaining sections where we treat non-spherical particles and others, either we will assume frictionless particles or packings at infinite compactivity for which we simply set  $z = Z_m$  and get a single equation of state rather than the yellow area in Fig. 12a.

The mechanical coordination  $Z_m$  defines isostatic packings, which, strictly applies only to the two limits  $Z_m = 2d = 6$  for frictionless particles with friction  $\mu \rightarrow 0$  and  $Z_m = d + 1 = 4$  for infinitely rough particles  $\mu \rightarrow \infty$ . An important assumption is that  $Z_m$  varies continuously as a function of  $\mu$

$$4 \leq Z_m(\mu) \leq z \leq 6. \quad (79)$$

In fact, a universal  $Z_m(\mu)$  curve has been observed for a range of different packing protocols (Song *et al.*, 2008) and calculated analytically in (Bo *et al.*, 2014). The upper bound of  $z$  is the frictionless isostatic limit. This effectively excludes from the ensemble the partially crystalline packings, which are characterized by larger  $z$ .

The remaining unknown is the density of states  $g(z)$ , which can be determined using analogies with a quantum mechanical system (see appendix B) leading to

$$g(z) = (h_z)^{z-\mathcal{D}}, \quad (80)$$

where  $\mathcal{D}$  is the dimension per particle of the configuration space and  $h_z$  a typical distance between jammed configurations in this space. Note that the factor  $(h_z)^{-\mathcal{D}}$  will drop out when performing ensemble averages. Physically, we expect  $h_z \ll 1$ . The exact value of  $h_z$  can be determined by a fitting of the theoretical values to the simulation data, but it is not important as long as we take the limit at the end:  $h_z \rightarrow 0$ .

Having defined the jammed ensemble via the partition function  $\mathcal{Z}_{\text{iso}}$ , we can calculate the ensemble averaged packing density  $\phi(X, Z_m) = \langle \phi(z) \rangle$  as

$$\phi(X, Z_m) = \frac{1}{\mathcal{Z}_{\text{iso}}} \int_{Z_m}^6 \frac{z}{z + 2\sqrt{3}} e^{-\frac{2\sqrt{3}}{zX} + z \log h_z} dz. \quad (81)$$

Equation (81) gives predictions on the packing densities as a function of  $X$  over the whole range of friction values  $\mu \in [0, \infty)$  since  $Z_m(\mu)$  is determined by friction (Song *et al.*, 2008). We can identify three distinct regimes (see Fig. 12):

1. In the limit of vanishing compactivity ( $X \rightarrow 0$ ), only the minimum volume at  $z = 6$  contributes. The density is the RCP limit  $\phi_{\text{rcp}} = \phi(X = 0, Z)$ :

$$\phi_{\text{rcp}} = \frac{1}{1 + 1/\sqrt{3}} = 0.634\ldots, \quad Z_m(\mu) \in [4, 6], \quad (82)$$

and the corresponding RCP free volume is

$$w_{\text{rcp}} = \frac{1}{\sqrt{3}}. \quad (83)$$

$\phi_{\text{rcp}}$  defines a vertical line in the phase diagram ending at the  $J$ -point: (0.634, 6). Here, RCP is identified as the ground state of the jammed ensemble with maximal density and coordination number. Notice that this result is also obtained from Eq. (75) at  $z = 6$ .

2. In the limit of infinite compactivity ( $X \rightarrow \infty$ ), the Boltzmann factor  $\exp[-2\sqrt{3}/(zX)] \rightarrow 1$ , and the average in Eq. (81) is taken over all states with equal probability. The  $X \rightarrow \infty$  limit defines the

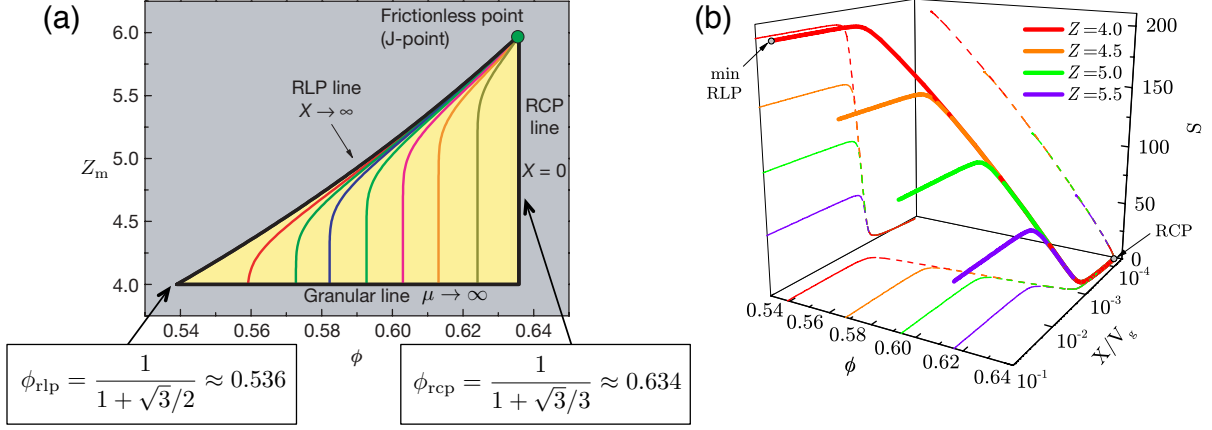


FIG. 12 (Colors online) (a) Theoretical prediction of the statistical theory Eq. (81). All disordered packings of spheres lie within the yellow triangle demarcated by the RCP line at  $\phi_{\text{rcp}} = 0.634$ , the RLP line parametrized by Eq. (84) and the lower limit for stable packings at  $Z = 4$  (granular line) for  $\mu \rightarrow \infty$ . Lines of constant finite compactivity  $X$  are in colour. Packings are forbidden in the grey area. (b) Predictions of the equation of state of jammed matter in the  $(X, \phi, s)$ -space determined with Eq. (86). Each line corresponds to a different system with  $Z_m(\mu)$  as indicated. The projections in the  $(\phi, s)$  and  $(X, s)$  planes show that RCP ( $X = 0$ ) is less disordered than RLP ( $X \rightarrow \infty$ ). Adapted from (Song *et al.*, 2008).

random loose packing equation of state  $\phi_{\text{rlp}}(Z) = \phi(X \rightarrow \infty, Z_m)$  as a function of  $Z_m$ :

$$\phi_{\text{rlp}}(Z_m) = \frac{1}{Z_{\text{iso}}(\infty, Z_m)} \int_{Z_m}^6 \frac{z}{z + 2\sqrt{3}} e^{z \ln h_z} dz \approx \frac{Z_m}{Z_m + 2\sqrt{3}}, \quad Z_m(\mu) \in [4, 6]. \quad (84)$$

The approximation comes from  $h_z \rightarrow 0$ . For small but finite  $h_z \ll 1$ , an interesting regime appears of negative compactivity (Briscoe *et al.*, 2010), yet unstable, leading to the limit of RLP when  $X \rightarrow 0^-$  which has been termed as the random very loose packing (Ciamarra and Coniglio, 2008). Thus,  $\phi_{\text{rlp}}$  spans a whole line in the phase diagram between the frictionless value  $\phi_{\text{rcp}}$  upto the limit  $\mu \rightarrow \infty$  at:

$$\phi_{\text{rlp}}^{\text{min}} = \frac{1}{1 + \sqrt{3}/2} = 0.536\ldots, \quad \text{for } Z_m = 4. \quad (85)$$

The corresponding RLP free-volume is  $w_{\text{rlp}}^{\text{min}} = \sqrt{3}/2$ . These values are interpreted as the minimal density of mechanically stable sphere packings appearing at  $Z_m = 4$ . We notice that Eq. (84) can be obtained from the single particle Eq. (75), by setting  $z = Z_m$ . Indeed, in the limit of infinite compactivity the mechanical coordination takes the value of the geometrical one.

3. Finite compactivity  $X$  defines the packings inside the triangle bounded by the RCP and RLP lines and the limit for isostaticity  $Z_m = 4$  as  $\mu \rightarrow \infty$

(granular line) are characterized. In this case, Eq. (81) can be solved numerically. Figure 12a shows the lines of constant compactivity plotted parametrically as a function of  $Z_m$ .

Further thermodynamic characterisation is obtained by considering the entropy of the jammed configurations, which can be identified by analogy with the equilibrium framework. In equilibrium statistical mechanics we have  $F = E - TS$ , such that  $S = E/T + \ln \mathcal{Z}$  using the free energy expression  $F = -T \ln \mathcal{Z}$  (setting  $k_B$  to unity). By analogy we obtain the entropy density of the jammed configuration  $s(X, Z_m)$  (entropy per particle) (Briscoe *et al.*, 2008, 2010; Brujić *et al.*, 2007):

$$s(X, Z_m) = \langle W \rangle / X + \ln \mathcal{Z}_{\text{iso}} \quad (86)$$

substituting the partition function Eq. (78) in the last step. In Fig. 12b each curve corresponds to a packing with a different  $Z_m$  value determined by Eq. (86). The projections  $s(\phi)$  and  $s(X)$  characterize the nature of randomness in the packings. When comparing all the packings, the maximum entropy is at  $\phi_{\text{rlp}}$  for  $X \rightarrow \infty$ , while the entropy is minimum at  $\phi_{\text{rcp}}$  for  $X \rightarrow 0$ . Following the granular line in the phase diagram we obtain the entropy for infinitely rough spheres showing a larger entropy for the RLP than the RCP. The same conclusion is obtained for the other packings at finite friction ( $4 < Z_m < 6$ ). We conclude that the RLP states are more disordered than the RCP states.

As stated, in the following results we will focus always on the  $X \rightarrow \infty$  regime, where the volume function that is obtained from the solution of the self-consistent equation is also the equation of state, since we simply have  $z \rightarrow Z_m$  for  $X \rightarrow \infty$  when calculating the ensemble



averaged packing density (compare Eqs. (75) and (84)). Therefore, we can drop the distinction between  $Z_m$  and  $z$  (for simplicity we consider  $z$ ), while keeping in mind that there exist further packing states for finite  $X$  that are implied but not explicitly discussed in the next sections (e.g., in the full phase diagram Fig. 20).

### C. Packing of high-dimensional spheres

According to Eq. (53), the key quantity to calculate exactly the average volume  $\bar{W}$  is the CDF  $P_>(\mathbf{r}_1; \Omega)$  as defined in Eq. (55). This CDF has been approximated in the work of (Song *et al.*, 2008) reviewed in previous Section IV.A by using a simple one dimensional gas-like model which is analogous in 1d to a parking lot model (Krapivsky and BenNaim, 1994; Palásti, 1960; Rényi, 1958; Tarjus and Viot, 2004), leading to the exponential form (70). It turns out that in the opposite limit of infinite dimensions (mean-field), a closed form of  $P_>$  can be obtained as well, based on general considerations of correlations in liquid state theory. In this mean-field high- $d$  limit, the form obtained in (Song *et al.*, 2008) can be determined as a limiting case, with the added possibility to develop a systematic expansion of  $P_>$  in terms of pair distribution functions allowing to include higher order correlations which were neglected in (Song *et al.*, 2008). Furthermore, the high- $d$  limit is important to compare the predictions of the Edwards ensemble to other mean-field theories such as the RSB solution of hard-sphere packings (Parisi and Zamponi, 2010). The high-dimensional limit is treated next (Jin *et al.*, 2010).

In large dimensions, the effect of metastability between amorphous and crystalline phases is strongly reduced, because nucleation is increasingly suppressed for large  $d$  (van Meel *et al.*, 2009a,b; Skoge *et al.*, 2006). Moreover, mean-field theory becomes exact for  $d \rightarrow \infty$ , because each degree of freedom interacts with a large number of neighbours (Parisi, 1988) opening up the possibility for exact solutions.

In the following, we discuss the mean-field high-dimensional limit of the coarse-grained Voronoi volume theory starting from liquid state theory. We only sketch the main steps in the calculation, for full details we refer to (Jin *et al.*, 2010). Assuming translational invariance of the system, Eq. (55) can be rewritten as

$$P_>(\mathbf{r}_1; \Omega) = 1 + \sum_{k=1}^{N-1} (-1)^k \frac{\rho^k}{k!} \times \int_{\Omega} g_{k+1}(\mathbf{r}_{12}, \dots, \mathbf{r}_{1(k+1)}) d\mathbf{r}_{1i} \cdots d\mathbf{r}_{1(k+1)}, \quad (87)$$

where  $g_n$  denotes the  $n$ -particle correlation function

$$g_n(\mathbf{r}_{12}, \mathbf{r}_{13}, \dots, \mathbf{r}_{1n}) = \frac{N!}{\rho^n (N-n)!} \int P_N(\mathbf{r}^n, \mathbf{r}^{N-n}) d\mathbf{r}^{N-n}, \quad (88)$$

with  $\rho = N/V$  the particle density. The integrals in Eq. (87) express the probabilities of finding a pair, triplet, etc., of spheres within the volume  $\Omega$ . For an exact calculation of  $P_>$ , we thus need the exact form of  $g_n(\mathbf{r}_{12}, \mathbf{r}_{13}, \dots, \mathbf{r}_{1n})$  to all orders, which is not available. However, assuming the generalized Kirkwood superposition approximation from liquid theory (Kirkwood, 1935), we can approximate  $g_n$  in high dimensions by a simple factorized form (Jin *et al.*, 2010):

$$g_n(\mathbf{r}_{12}, \mathbf{r}_{13}, \dots, \mathbf{r}_{1n}) \approx \prod_{i=2}^n g_2(\mathbf{r}_{1i}), \quad (89)$$

where  $g_2$  is the pair correlation function.

Equation (89) indicates that spheres 2, ...,  $n$  are correlated with the central sphere 1 but not with each other, which is reasonable for large  $d$  since the sphere surface is then large compared with the occupied surface. The term  $S_{d-1}$  in Eq. (91) denotes the surface of a  $d$ -dimensional sphere with radius  $2R$ . Substituting Eq. (89) in Eq. (87) yields

$$P_>(\mathbf{r}_1; \Omega) = \sum_{k=0}^{N-1} (-1)^k \frac{\rho^k}{k!} \left( \int_{\Omega} g_2(\mathbf{r}) d\mathbf{r} \right)^k = \exp \left[ -\rho \int_{\Omega} g_2(\mathbf{r}) d\mathbf{r} \right], \quad (90)$$

in the limit  $N \rightarrow \infty$  ( $\rho \rightarrow 1/\bar{W}$ ).

Thus, we see that calculating the CDF  $P_>$  reduces to know the form of the pair correlation function. Indeed, the exponential form calculated in Section IV.A using a 1d model, Eq. (70), is obtained from Eq. (90) by assuming the following simplified pair correlation function (which has been considered also in (Torquato and Stillinger, 2006)):

$$g_2(r) = \frac{z}{\rho S_{d-1}} \delta(r - 2R) + \Theta(r - 2R). \quad (91)$$

This form corresponds to assuming a set of  $z$  contacting particles contributing to the delta-peak at  $2R$  plus a set of uncorrelated bulk particles contributing to a flat (gas-like) distribution characterized by the  $\Theta$ -function. This form, depicted in Fig. 13, further assumes the factorization of the contact and bulk distribution and represents the simplest form of the pair correlation function, yet, it gives rise to accurate results for the predicted packing densities. The important point is that the high-d result Eq. (90) allows to express more accurate pair correlation functions than Eq. (91) into the formalism to systematically capture higher order features in the correlations, thus allowing for an improvement of the theoretical results. Such improvements are treated in Sections IV.D and IV.F.

Using Eq. (91) and the definition of  $\Omega$ , Eq. (54), we see that the volume integral  $\int_{\Omega} g_2(\mathbf{r}) d\mathbf{r}$  becomes

$$\int_{\Omega} g_2(\mathbf{r}) d\mathbf{r} = \frac{z S^*(c)}{\rho S_{d-1}} + V^*(c), \quad (92)$$

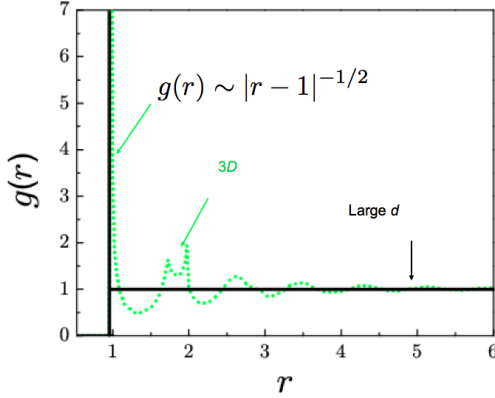


FIG. 13 (Colors online) At the core of the mean-field approach developed in (Song *et al.*, 2008) to calculate the volume fraction of 3d packings is the approximation of the real pair correlation function (green curve) with its characteristic peaks indicating short-range correlations in the packing and the power-law decay of the near contacting particles, Eq. (46), by a simple delta-function (black curve) at the contacting point plus a flat distribution characterizing a gas-like bulk of uncorrelated particles. Surprisingly, such an approximation, which is expected to work better at high dimensions than at low dimensions, gives accurate results for the volume fraction in 3d, as shown in Section IV.A. High-dimensional analyses allow to treat higher-order correlations neglected in (Song *et al.*, 2008) to improve the theoretical predictions in a systematic way as shown in Secs. IV.C, IV.D and IV.F.

where  $V^*$  and  $S^*$  are the Voronoi excluded volume and surface, Eqs. (57,58), for general  $d$ . We thus recover the same factorized form of the CDF as in 3d, Eq. (70), but now generalized to any dimension  $d$ , separating bulk and contact contributions

$$P_{>}(c, z) = \exp \left[ -\rho V^*(c) - \frac{z S^*(c)}{S_{d-1}} \right], \quad (93)$$

whose validity should increase with increasing dimension. The Voronoi excluded volume and surface,  $V^*$  and  $S^*$ , can be calculated with Eqs. (57,58) for general  $d$ . The term  $z/S_{d-1}$  can be interpreted as the surface density  $\sigma(z)$  in the 3d theory.

The  $d$ -dimensional generalization of Eq. (53) is

$$\bar{W} = V_0^{(d)} + \frac{V_0^{(d)} d}{R^d} \int_R^\infty dc c^{d-1} P_{>}(c, z). \quad (94)$$

For large  $d$  an analytical solution of Eq. (94) can be obtained. In terms of  $w = (\bar{W} - V_0^{(d)})/V_0^{(d)}$  one obtains the following asymptotic predictions of the Edwards ensemble in high-d (Jin *et al.*, 2010) for the free volume:  $w_{\text{Edw}} = \frac{3}{4d} 2^d$ , and the volume fraction in the Edwards

ensemble is

$$\phi_{\text{Edw}} = \frac{4}{3} d 2^{-d}. \quad (95)$$

The scaling  $\phi \sim d 2^{-d}$  is also found in other approaches for jammed spheres in high dimensions. In principle, it satisfies the Minkowski lower bound (Torquato and Stillinger, 2010):

$$\phi_{\text{Mink}} = \frac{\zeta(d)}{2} 2^{-d}, \quad (96)$$

where  $\zeta(d)$  is the Riemann zeta function,  $\zeta(d) = \sum_{k=1}^\infty \frac{1}{k^d}$ , although this can be regarded as a minimal requirement. Density functional theory predicts (Kirkpatrick and Wolynes, 1987):

$$\phi_{\text{dft}} \sim 4.13 d 2^{-d}. \quad (97)$$

Mode-coupling theory with a Gaussian correction predicts (Ikeda and Miyazaki, 2010; Kirkpatrick and Wolynes, 1987):

$$\phi_{\text{mct}} \sim 8.26 d 2^{-d}. \quad (98)$$

Replica symmetry breaking theory at the 1 step predicts (Parisi and Zamponi, 2010)

$$\phi_{\text{th}}^{\text{1RSB}} \sim 6.26 d 2^{-d}, \quad (99)$$

and the full RSB solution predicts (Charbonneau *et al.*, 2014b)

$$\phi_{\text{th}}^{\text{fullRSB}} \sim 6.85 d 2^{-d} \quad (100)$$

as the lower limit of jamming in the J-line ( $\phi_j \in [\phi_{\text{th}}, \phi_{\text{GCP}}]$ ).

In general, we see that the Edwards prediction has the same asymptotic dependence on  $d$ , Eq. (95), as the competing theories. However the prefactors are in disagreement, especially with the 1RSB calculation. While Edwards ensemble predicts a prefactor  $4/3$ , the 1RSB prediction is 6.26. A comparison of the large  $d$  results for  $P_B$  and  $P_C$  with those in 3d indicates that the low  $d$  corrections are primarily manifest in the expressions for particle density  $\rho$  and the surface density  $\sigma(z) = z/S_{d-1}$  (Jin *et al.*, 2010). In 3d, the density exhibits van der Waals like corrections due to the particle volume:  $\rho \rightarrow \tilde{\rho} = 1/(\bar{W} - V_0)$ . Likewise, there are small corrections to the surface density  $z/4\pi \rightarrow \langle S^* \rangle^{-1} \approx (z/4\pi)\sqrt{3}$ . The origin of the additional  $\sqrt{3}$  factor is not clear. In 2d, further corrections are needed to obtain agreement of the theory with simulation data, a case that is treated next.

#### D. Packing of disks

The high-dimensional treatment discussed in the previous section shows that improvements on the mean field approach of (Song *et al.*, 2008) can be achieved through

better approximations to the pair distribution function by including neglected correlations between neighboring particles. These correlations become crucial in low-dimensional systems, in particular in 2d systems of disk packings. Interestingly, below we show that the 2d case allows for a systematic improvement of the predictions based on a systematic layer expansion of the pair distribution function through a dimensional reduction of the problem to a one-dimensional one, as treated next.

In principle, disordered packings of monodisperse disks are difficult to investigate in 2d, since crystallization typically prevents the formation of an amorphous jammed state. In (Berryman, 1983) the density of jammed disks has been estimated as  $\phi_{\text{rcp}} = 0.82 \pm 0.02$  by extrapolating from the liquid phase. Only recently, MRJ states of disks have been generated in simulations using a linear programming algorithm (Torquato and Jiao, 2010). These packings achieve a packing fraction of  $\phi_{\text{mrj}} = 0.826$  including rattlers and exhibit an isostatic jammed backbone (Atkinson *et al.*, 2014). By comparison, the densest crystalline arrangement of disks is a triangular lattice with  $\phi = \frac{\pi}{\sqrt{12}} \approx 0.9069$ , which has already been proven by Thue (Thue, 1892). For disordered packings, replica theory predicts the J-line in 2d from  $\phi_{\text{th}} = 0.8165$  to the maximum density of glass close packing at  $\phi_{\text{GCP}} = 0.8745$  (Parisi and Zamponi, 2010), although these values have a large error bar due to the liquid theory approximation used in the calculation. A recent theory based on the geometric structure approach estimates  $\phi_{\text{mrj}} = 0.834$  (Tian *et al.*, 2015).

In order to elucidate the 2d problem from the viewpoint of the Edwards ensemble, one can adapt as a first approach the same statistical theory developed for 3d spheres in Sec. IV.A to the 2d case. This would lead to a self-consistent equation for the average Voronoi volume as in Eq. (53) (Meyer *et al.*, 2010):

$$\bar{W}(z) = V_0 + 2\pi \int_R^\infty dc c P_>(c, z), \quad (101)$$

where  $P_>(c, z)$  has the form of Eq. (70) with  $V_0 = \pi R^2$  and the 2d analogues of  $V^*$  and  $S^*$  are easily calculated. The surface density  $\sigma(z)$  follows from simulations of local configurations via Eq. (67). In the relevant  $z$  range between the isostatic frictionless value  $z = 2d = 4$  and the lower limit  $z = d + 1 = 3$  for frictional disks,  $\sigma(z)$  is found to be approximately linear:  $\sigma(z) = (z - 0.5)/\pi$  for  $R = 1/2$  (Meyer *et al.*, 2010).

Overall, such an implementation would predict a RCP density of 2d frictionless disks of  $\phi_{\text{rcp}} \approx 0.89$  greatly exceeding the empirical values. The reason for the discrepancy are much stronger correlations between the contact and bulk particles in low dimensions, such that the assumed independence of the CDFs  $P_B$  and  $P_C$  in Eq. (59) is no longer valid. A phenomenological way to quantify the correlations by coupling bulk and surface terms has

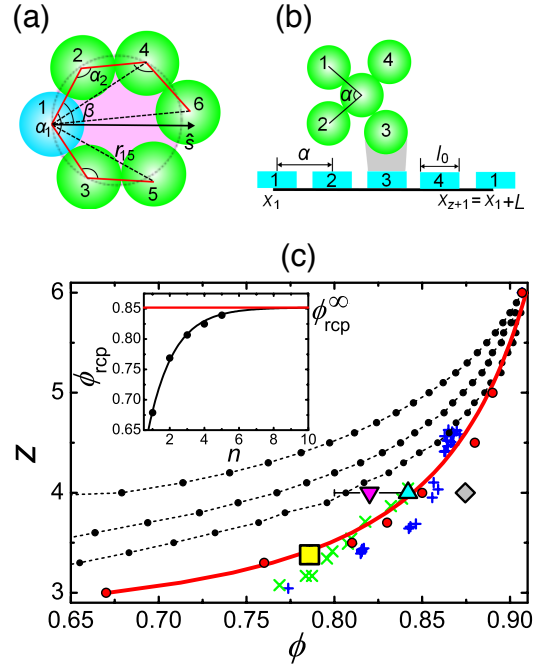


FIG. 14 (Colors online) (a) An illustration of the geometrical quantities used in the calculation of  $P_>$ , Eq. (102). The  $\alpha_j$  are the angles between any two Voronoi particles for a given  $\hat{s}$ . (b) Mapping monodisperse contact disks to 1d rods. The 2d exclusive angle  $\alpha$  corresponds to the 1d gap. (c) Phase diagram of 2d packings. Theoretical results for  $n = 1, 2, 3$  (line points, from left to right) and  $\phi_{\text{rcp}}^\infty$  (red) are compared to (i) values in the literature: (Berryman, 1983) (down triangle), (Parisi and Zamponi, 2010) (diamond), and (O'Hern *et al.*, 2002) (up triangle), (ii) simulations of  $10^4$  monodisperse disks (crosses), and polydisperse disks (pluses), and (iii) experimental data of frictional disks (square). (Inset) The theoretical RCP volume fraction  $\phi_{\text{rcp}}(n)$  as a function of  $n$ . The points are fitted to a function  $\phi(n) = \phi_{\text{rcp}}^\infty - k_1 e^{-k_2 n}$ , where  $k_1 = 0.34 \pm 0.02$ ,  $k_2 = 0.67 \pm 0.06$  and  $\phi_{\text{rcp}}^\infty = 0.85 \pm 0.01$ . Adapted from (Jin *et al.*, 2014).

been discussed in (Meyer *et al.*, 2010) leading to better agreement with simulation data.

A systematic way of dealing with the correlations can be developed by focusing only on particles close to the direction  $\hat{c}$ , i.e., particles that could contribute a VB, and then constructing a layer expansion into coordination shells (Jin *et al.*, 2014). We denote these particles as Voronoi particles. In the exact Eq. (55), one can then consider the exclusion condition  $\prod_{i=2}^{\tilde{n}} [1 - m(\mathbf{r}_i - \mathbf{r}_1; \Omega)]$  over  $\tilde{n}$  Voronoi particles (including the reference particle) rather than all  $N$  particles in the packing. In 2d, the Voronoi particles are located on the two closest branches to the direction  $\hat{c}$  and can be described by a correlation function of angles  $G_{\tilde{n}}(\alpha_1, \alpha_2, \dots, \alpha_n)$ . Using angles instead of the position coordinates is a suitable parametrization of the Voronoi particles provided the underlying contact network is assumed fixed only al-

lowing fluctuations in the angles without destroying contacts. For such a fixed contact network the degree of freedom per particle is thus reduced by one and allows to map the  $\tilde{n} - 1$  position vectors  $\mathbf{r}_{12}, \mathbf{r}_{13}, \dots, \mathbf{r}_{1\tilde{n}}$  onto the angles  $\alpha_1, \alpha_2, \dots, \alpha_n$  of contacting Voronoi particles plus the angle  $\beta$  describing the direction  $\hat{\mathbf{c}}$  (see Fig. 14). This requires  $\tilde{n} - 1 = n + 1$ . Transforming variables from  $(\mathbf{r}_{12}, \mathbf{r}_{13}, \dots, \mathbf{r}_{1\tilde{n}})$  to  $(\beta, \alpha_1, \alpha_2, \dots, \alpha_n)$  in Eq. (55) leads to (Jin *et al.*, 2014)

$$P_{>}(c) = \lim_{n \rightarrow \infty} \mathcal{C}' \int \dots \int \Theta(\alpha_1 - \beta) G_n(\alpha_1, \dots, \alpha_n) \times \prod_{j=2}^{n+2} \Theta\left(\frac{r_{1j}}{2\hat{\mathbf{c}} \cdot \hat{\mathbf{r}}_{1j}} - c\right) d\beta d\alpha_1 \dots d\alpha_n, \quad (102)$$

where the constant  $\mathcal{C}' = z/L$  with  $L = 2\pi$  ensures the normalization  $P_{>}(R) = 1$ . Equation (102) becomes exact as  $n \rightarrow \infty$  and provides a systematic approximation for finite  $n$ . In particular,  $n$  can be related to the coordination layers above and below  $\hat{\mathbf{c}}$ .

One can then make two key assumptions to make this approach tractable (Jin *et al.*, 2014). Firstly, one applies the Kirkwood superposition approximation as in the high-dimensional case for  $G_n$ :  $G_n(\alpha_1, \dots, \alpha_n) \approx \prod_{j=1}^n G(\alpha_j)$ . Secondly, the system of contacting Voronoi particles is mapped onto a system of 1d interacting hard rods with an effective potential  $V(x)$  (see Fig. 14). Considering the particles in the first coordination shell (Fig. 14b) leads to a set of  $z$  rods at positions  $x_i$ ,  $i = 1, \dots, z$ , where the rods are of length  $l_0 = \pi/3$  and the system size is  $L = 6l_0$  with periodic boundary conditions. In addition, the local jamming condition requires that each particle has at least  $d+1$  contacting neighbours, which can not all be in the same ‘‘hemisphere’’. In 2d, this implies that  $z \geq 3$  and  $\alpha_j \leq \pi$ . In the rod system, this constraint induces an upper limit  $3l_0$  on possible rod separations. Thus, the jamming condition is equivalent to introducing an infinite square-well potential between two hard rods. Crucially, the partition function  $Q(L, z)$  can then be calculated exactly in 1d (Jin *et al.*, 2014):

$$Q(L, z) = \sum_{k=0}^{\lfloor \frac{L/l_0 - z}{2} \rfloor} (-1)^k \binom{z}{k} \frac{[L/l_0 - z - 2k]^{z-1}}{(z-1)!} \times \Theta(L/l_0 - z) \Theta(3z - L/l_0), \quad (103)$$

where  $\lfloor x \rfloor$  is the integer part of  $x$  and the inverse temperature has been set to unity since it is irrelevant. This allows to determine the distribution of angles (gaps)  $G(\alpha) = \langle \delta(x_2 - x_1 - \alpha) \rangle$

$$G(\alpha) = \frac{Q(\alpha, 1) Q(L - \alpha, z - 1)}{Q(L, z)}. \quad (104)$$

In the limit  $a \rightarrow \infty$  the system becomes the classical Tonks gas of 1d hard rods (Tonks, 1936). In the thermodynamic limit ( $L \rightarrow \infty$  and  $z \rightarrow \infty$ ), the gap distribution

is  $G_{\text{HR}}(\alpha) = \rho_f e^{-\rho_f(\alpha/l_0 - 1)}$ , where  $\rho_f = z/(L/l_0 - z)$  is the free density.

The density of 2d disk packings follows by solving Eq. (101) with Eqs. (102,104) numerically using Monte-Carlo (Fig. 14c). The formalism reproduces the highest density of 2d spheres in a triangular lattice at  $\phi \approx 0.91$  for  $z = 6$ . For disordered packings one obtains the RCP volume fraction:

$$\phi_{\text{rcp}}^{2d} = 0.85 \pm 0.01, \quad \text{for } z = 4, \quad (105)$$

and the RLP volume fraction as:

$$\phi_{\text{rlp}}^{2d} = 0.67 \pm 0.01, \quad \text{for } z = 3. \quad (106)$$

We see that the prediction of the frictionless RCP point is close to the numerical results and the result of the 1RSB theory  $\phi_{\text{th}} = 0.8165$ , while a new prediction of RLP at the infinite friction limit is obtained.

## E. Packing of bidisperse spheres

Polydispersity with a smooth distribution of sizes typically occurs in industrial particle synthesis and thus affects packings in many applications. Qualitatively, one expects an increase in packing densities due to size variations: The smaller particles can fill those voids that are not accessible by the larger particles leading to more efficient packing arrangements, which is indeed observed empirically (Brouwers, 2006; Desmond and Weeks, 2014; Santiso and Müller, 2002; Sohn and Moreland, 1968). Simulations have shown that the jamming density in polydisperse systems depends also on the compression rate without crystallization (Hermes and Dijkstra, 2010) and the skewness of the size distribution (Desmond and Weeks, 2014). Since these issues are important in technological applications, as for instance the proportioning of concrete, very efficient phenomenological models have been developed to predict volume fractions of mixtures of various types of grains (de Larrard, 1999). For size distributions following a power-law, space-filling packings can be constructed (Herrmann *et al.*, 1990). On the theoretical side, a ‘granocentric’ model has been shown to reproduce the packing characteristics of polydisperse emulsion droplets (Clusel *et al.*, 2009; Corwin *et al.*, 2010; Jorjadze *et al.*, 2011; Newhall *et al.*, 2011; Puckett *et al.*, 2011). Here, the packing generation is modelled as a random walk in the first coordination shell with only two parameters, the available solid angle around each particle and the ratio of contacts to neighbors, which can both be calibrated to experimental data.

The simpler case of a bidisperse packing with two types of spheres with different radii has been investigated in (Clarke and Wiley, 1987; Hopkins *et al.*, 2013; de Lange Kristiansen *et al.*, 2005; Santiso and Müller, 2002) using simulations. Here, one can generally observe packing densities that increase from the monodisperse value as both the size ratio and concentration of



small spheres is varied. In (Hopkins *et al.*, 2013) mechanically stable packings with a large range of densities  $0.634 \leq \phi \leq 0.829$  have been generated using a linear programming algorithm. Interestingly, for a given size ratio, the density is non-monotonic, exhibiting a peak at a specific concentration. A theoretical approach that is able to reproduce the density peak in the bidisperse case has been developed in (Danisch *et al.*, 2010) based on the volume ensemble. The key idea is to treat the spheres of radii  $R_1 < R_2$  as different species 1 and 2 with independent statistical properties. If we denote by  $x_1$  the fraction of small spheres 1, then  $x_1 = N_1/(N_1 + N_2)$ , with  $N_i$  the number of spheres  $i$  in the packing. Likewise,  $x_2 = 1 - x_1$ . The overall packing density is

$$\phi = \frac{\bar{V}_g}{\bar{W}}, \quad \bar{V}_g = \sum_{i=1}^2 x_i V_g^{(i)} \quad (107)$$

where  $V_g^{(i)} = \frac{4\pi}{3} R_i^3$  and  $\bar{W}$  is the average volume of a Voronoi cell as before. The average now includes averaging over the different species, so that

$$\bar{W} = \sum_{i=1}^2 x_i \bar{W}_i, \quad (108)$$

$$\bar{W}_i = V_g^{(i)} + 4\pi \int_{R_i}^{\infty} dc c^2 P_{>}^{(i)}(c, z), \quad i = 1, 2 \quad (109)$$

as a straightforward extension of Eq. (53). The CDF  $P_{>}^{(i)}(c, z)$  contains the probability that, for a Voronoi cell of species  $i$ , the boundary is found at a value larger than  $c$ . This probability depends, of course, on both species. Assuming statistical independence we can introduce a factorization into bulk and contact particles of both species (Danisch *et al.*, 2010) analogously to the monodisperse case Eq. (59):

$$P_{>}^{(i)}(c, z) = P_B^{(i1)}(c) P_C^{(i1)}(c, z) P_B^{(i2)}(c) P_C^{(i2)}(c, z) \quad (110)$$

Here,  $P_B^{(ij)}$  denotes the CDF due to contributions of bulk particles of species  $j$  to a Voronoi cell of species  $i$ . Likewise  $P_C^{(ij)}$  refers to the contact particles. We express each of these terms in analogy to the monodisperse case, i.e., Eqs. (63,65),

$$P_B^{(ij)} = \exp[-\tilde{\rho}_j V_{ij}^*(c)], \quad (111)$$

$$P_C^{(ij)} = \exp[-\sigma_{ij}(z) S_{ij}^*(c)]. \quad (112)$$

The Voronoi excluded volume and surface,  $V_{ij}^*$  and  $S_{ij}^*$ , are defined by Eqs. (57,58), where now  $s(\mathbf{r}, \hat{\mathbf{c}})$  denotes the VB between spheres of radii  $R_i$  and  $R_j$ , as parametrized by Eq. (22). The particle densities  $\tilde{\rho}_j$  are given by

$$\tilde{\rho}_j = \frac{x_j}{\bar{W} - \bar{V}_g}, \quad j = 1, 2. \quad (113)$$

The main challenge is to obtain an expression for the surface density  $\sigma_{ij}(z)$ . For this, it is first necessary to

distinguish different average contact numbers:  $z_{ij}$  is the average number of spheres  $j$  in contact with a sphere  $i$ . It follows that the average number of contacts of sphere  $i$ , denoted by  $z_i$ , is

$$z_i = z_{i1} + z_{i2}, \quad z = \sum_{i=1}^2 x_i z_i. \quad (114)$$

By relating the contact numbers  $z_i$  to the average occupied surface on sphere  $i$ ,  $\langle S_i^{\text{occ}} \rangle$ , one can obtain the following equations to relate  $z_{ij}$  with  $z$

$$z_1 = \frac{z}{x_1 + x_2 \frac{\langle S_1^{\text{occ}} \rangle}{\langle S_2^{\text{occ}} \rangle}}, \quad z_2 = \frac{z}{x_1 \frac{\langle S_2^{\text{occ}} \rangle}{\langle S_1^{\text{occ}} \rangle} + x_2}. \quad (115)$$

and

$$z_{11} = \frac{z_1^2 x_1}{z}, \quad z_{12} = \frac{z_1 z_2 x_2}{z}, \quad (116)$$

$$z_{21} = \frac{z_1 z_2 x_1}{z}, \quad z_{22} = \frac{z_2^2 x_2}{z}. \quad (117)$$

where  $\langle S_i^{\text{occ}} \rangle$  is approximated as  $\langle S_i^{\text{occ}} \rangle = \sum_{j=1}^2 x_j S_{ij}^{\text{occ}}$  with the exact expression for the occupied surface (see Fig. 15a)

$$S_{ij}^{\text{occ}} = 2\pi \left( 1 - \sqrt{1 - \left( \frac{R_j}{R_i + R_j} \right)^2} \right). \quad (118)$$

Eqs. (115–117) imply that we can express  $z_{ij}$  as a function of  $z$ :  $z_{ij} = z_{ij}(z)$ . As before,  $\sigma_{ij}$  can in principle be obtained from simulations using Eq. (67). However, a direct simulation of  $\langle S_{ij}^* \rangle$  as a function of  $z$  contacting particles ignores the dependence of the different species that is not resolved in  $z$ . Therefore,  $\tilde{\sigma}_{ij}$  is introduced via

$$\sigma_{ij}(z) = \tilde{\sigma}_{ij}(z_{ij}(z)). \quad (119)$$

In turn, we obtain  $\tilde{\sigma}_{ij} = \langle S_{ij}^* \rangle^{-1}$  as a function of  $z_{ij}$  by generating configurations around sphere  $i$  with the proportions  $z_{i1}/z_i$  of spheres 1 and  $z_{i2}/z_i$  of spheres 2.  $\langle S_{ij}^* \rangle$  follows operationally again as the Monte-Carlo average Eq. (68).

Overall, the packing density of the bi-disperse packing of spheres can be calculated by solving the following self-consistent equation for the free volume  $w = \bar{W} - \bar{V}_g$

$$w = 4\pi \sum_{i=1}^2 x_i \int_{R_i}^{\infty} dc c^2 \times \exp \left\{ - \sum_{j=1}^2 \left[ \frac{x_j}{w} V_{ij}^*(c) + \sigma_{ij}(z) S_{ij}^*(c) \right] \right\} \quad (120)$$

We notice that Eq. (120) is the generalization of Eq. (71) from monodisperse to bidisperse packings. While the monodisperse self-consistent Eq. (71) admits a closed analytical solution, the bidisperse Eq. (120) does

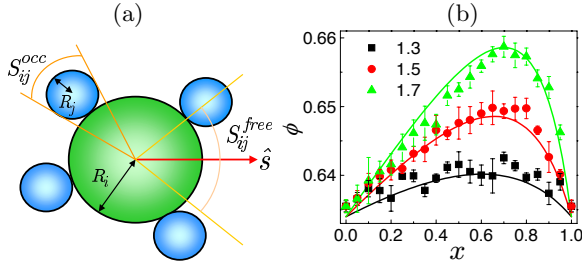


FIG. 15 (Colors online) (a) The occupied surface Eq. (118) and the Voronoi excluded surface  $S_{ij}^*$ . (b) Comparison between theory and numerical simulations of Hertzian packings at RCP vs the concentration  $x$  of small spheres. Different symbols denote different ratios  $R_1/R_2$ . Adapted from (Danisch *et al.*, 2010).

not. Thus, we resort to a numerical solution of this equation, and therefore the equation of state  $w(z)$  is obtained numerically in these cases rather than in closed form as obtained for monodisperse spheres Eq. (73).

Calculations for all systems (from spheres to non-spheres, monodisperse or polydisperse and beyond) that use the present mean-field theory in the Edwards ensemble will end up with a self-consistent equation for the free volume of the form Eq. (71) or Eq. (120). However, so far, the only self-consistent equation that admits a closed analytical solution is the 3d monodisperse case leading to Eq. (73). The remaining equations of state for all systems studied so far are too involved and need to be solved numerically.

Results of numerical solutions of Eq. (120) are shown in Fig. 15b demonstrating good agreement with simulation data as well as the predictions of the 1RSB hard-sphere glasses calculations (Biazzo *et al.*, 2009). We observe the pronounced peak as a function of the species concentration  $x = x_1 \in [0, 1]$ . The extension of the theory to higher-order mixtures is straightforward in principle. The main challenge is to obtain the generalizations of Eqs. (115, 116, 117). Determining  $\tilde{\sigma}_{ij}(z_{ij})$  from simulations of local packing configurations becomes also an increasingly complex task.

## F. Packing of attractive colloids

Packings of particles with diameters of around  $10\mu\text{m}$  or smaller enter the domain of colloids and are often dominated by adhesive van der Waals forces in addition to friction and hard-core interactions. In fact, packings of adhesive colloidal particles appear in many areas of engineering as well biological systems (Jorjadze *et al.*, 2011; Marshall and Li, 2014) and exhibit different macroscopic structural properties compared with non-adhesive packings of large grains treated so far, where attractive van der Waals forces are negligible in comparison with grav-

ity. In (Lois *et al.*, 2008) the mechanical response at the jamming transition has been studied and two second-order transitions are found in the attractive systems (Lois *et al.*, 2008): a connectivity percolation transition and a rigidity percolation transition, where a rigid backbone forms without floppy modes.

Numerical studies of adhesive granular systems have found a range of packing fractions as a function of particle sizes  $\phi \approx 0.1 - 0.6$  (Blum *et al.*, 2006; Head, 2007; Kadau and Herrmann, 2011; Martin and Bordia, 2008; Parteli *et al.*, 2014; Valverde *et al.*, 2004; Yang *et al.*, 2000). The effect of varying the force of adhesion has been systematically investigated in (Chen *et al.*, 2016; Liu *et al.*, 2017, 2015) using a DEM framework specifically developed for the ballistic deposition of adhesive Brownian soft spheres with sliding twisting and rolling friction (Marshall and Li, 2014). A dimensionless adhesion parameter  $Ad$ , defined as the ratio between interparticle adhesion work and particle inertia (Li and Marshall, 2007), can be used to quantify the combined effect of size and deposition velocity. In the case of  $Ad < 1$ , particle inertia dominates the adhesion and frictions exhibiting a broad range of densities and coordination numbers. At  $Ad \approx 1$  the isostatic value  $z = 4$  for infinitely rough spheres is observed, indicating that weak adhesion has a similar effect on the packing as strong friction. However, when  $Ad > 1$ , an adhesion-controlled regime is observed with a unique curve in the  $z$ - $\phi$  diagram. The lowest packing density achieved numerically is  $\phi = 0.154$  with  $z = 2.25$  for  $Ad \approx 48$ . The lowest density agrees well with the data from a random ballistic deposition experiment (Blum *et al.*, 2006) and other DEM simulations (Parteli *et al.*, 2014; Yang *et al.*, 2000).

An analytical representation of the adhesive equation of state can be derived within the framework of the mean-field Edwards volume function Eq. (53), where the CDF  $P_>$  is defined by Eq. (55). Assuming the same factorization of the  $n$ -point correlation function as in high dimensions leads to the approximation Eq. (90), which allows us to relate  $P_>$  with the structural properties of the packing expressed in the pair distribution function  $g_2$ . We then model  $g_2$  by extending the simple form considered so far for 3d hard-spheres in Eq. (91) in terms of four distinct contributions following the results of available simulations of hard-sphere packings and metastable hard-sphere glasses. We consider:

- (i) A delta-peak due to contacting particles (Donev *et al.*, 2005b; Song *et al.*, 2008; Torquato and Stillinger, 2006);
- (ii) A power-law peak as given by Eq. (46) over a range  $\epsilon$  due to near contacting particles (Donev *et al.*, 2005b; Wyart, 2012);
- (iii) A step function due to bulk particles (Song *et al.*, 2008; Torquato and Stillinger, 2006) mimicking a uniform density of bulk particles;
- (iv) A gap of width  $b$  separating bulk and (near) con-

tacting particles. This gap captures the effect of correlations due to adhesion and is assumed to depend on  $z$ :  $b = b(z)$ . In this way we model the increased porosity at a given  $z$  compared with adhesion-less packings. Overall, we obtain

$$g_2(\mathbf{r}, z) = \frac{z}{\rho\lambda} \delta(r - 2R) + \sigma(r - 2R)^{-\nu} \Theta(2R + \epsilon - r) + \Theta(r - (2R + b(z))). \quad (121)$$

For the power law term we assume  $\nu = 0.38$  from (Lerner *et al.*, 2013) and a width of  $\epsilon = 0.1R$ , which is approximately the range over which the peak decreases to the bulk value unity as observed in (Donev *et al.*, 2005b). The value  $\sigma$  is then fixed by continuity with the step function term in the absence of a gap.

Next, we have to determine the gap of width function  $b(z)$  which is the crucial assumption of the theory.  $b(z)$  needs to satisfy a set of constraints that we impose purely on physical grounds:

- (i)  $b(z)$  is a smooth monotonically decreasing function of  $z$ . Here, the physical picture is that for small  $z$  (corresponding to looser packings), the gap width is larger due to the increased porosity of the packing.
- (ii) At the isostatic limit  $z = 6$ , the gap disappears,  $b(6) = \epsilon$ , and we expect to recover the frictionless RCP value, since this value of  $z$  represents a maximally dense disordered packing of spheres. We obtain from Eq. (121) indeed the prediction for  $\phi_{\text{Edw}}$ , Eq. (82), by choosing an appropriate value of  $\lambda$  and accounting for low dimensional corrections due to the hard-core excluded volume of the reference sphere, such that  $\rho \rightarrow \bar{\rho} = 1/(\bar{W} - V_0)$ . This constraint thus fixes  $\rho$  and  $\lambda$ , as well as one of the parameters in  $b(z)$ .
- (iii) In addition, we conjecture the existence of an asymptotic *adhesive loose packing* (ALP) at  $z = 2$  and  $\phi = 1/2^3$  which yields  $b(2) = 1.47$  and fixes a second parameter in  $b(z)$ . This is motivated by the fact that  $\phi = 1/2^d$  is the lower bound density of saturated sphere packings of congruent spheres in  $d$  dimensions for all  $d$  (Torquato and Stillinger, 2006). A saturated packing of congruent spheres of unit diameter satisfies that each point in space lies within a unit distance from the center of some sphere. Moreover,  $z = 2$  is the lowest possible value for a physical packing: If  $z < 2$  there are more spheres with a single contact (i.e., dimers) than with three or more contacts, which identifies that the ALP point is only asymptotic.

Clearly,  $b(z)$  is a smoothly decreasing function, so that we can assume, e.g., the simple parametric form  $b(z) = c_1 + c_2 e^{-c_3 z}$ , such that one fitting parameter is left after the two constraints  $b(6) = \epsilon$  and  $b(2) = 1.47$

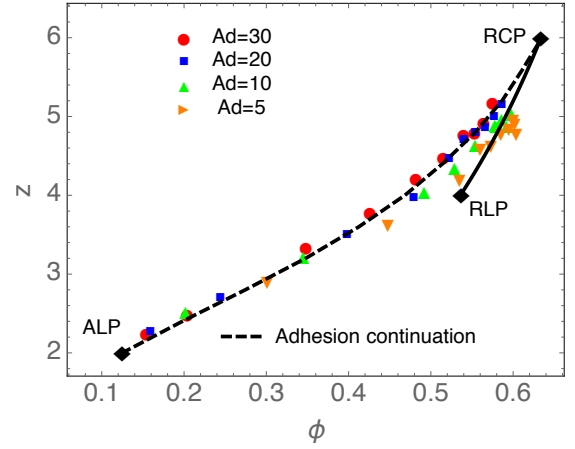


FIG. 16 (Colors online) Plot of high  $Ad$  simulation data in the  $z$ - $\phi$  plane (Liu *et al.*, 2015). The adhesive continuation with an exponential  $b(z)$  connects the RCP at  $\phi_{\text{Edw}}$  and  $z = 6$  with the conjectured adhesive loose packing point (ALP) at  $\phi = 2^{-3}$  and  $z = 2$ . The black solid line is the RLP line of Fig. 12(b). Adapted from (Liu *et al.*, 2015).

are imposed. Figure 16 highlights that the exponential decay of  $b(z)$  provides an excellent fit to the simulation data providing the equation of state  $\phi(z)$  for adhesive packings. Moreover, the resulting  $P(c, z)$  also agrees well with the empirically measured CDF over a large range of  $Ad$  values (Liu *et al.*, 2015). This means that including  $b(z)$  captures well the essential structural features of the packing. It is quite intriguing that such a simple modification of the non-adhesive theory, motivated on physical grounds, leads to such good agreement not only in the low density regime, but also for mid to high densities.

These results highlight that attraction in (spherical) particles leads to a lower density limit for percolation at the ALP with  $\phi_c = 1/2^3$ . The equivalent  $\phi_c$  in attractive colloids is observed empirically over a range of densities  $\phi_c \approx 0.1 - 0.2$  depending on the mechanism for the suppression of phase-separation (Zaccarelli, 2007), e.g., due to an interrupted liquid-gas phase separation (Lu *et al.*, 2008b; Trappe *et al.*, 2001). The situation is thus reminiscent of the adhesion-less and frictionless range of densities  $\phi \in [\phi_{\text{th}}, \phi_{\text{GCP}}]$  of the J-line (see Sec. V).

## G. Packing of non-spherical particles

The question of optimizing the density of packings made of particles of a particular shape is an outstanding scientific problem occupying scientists since the time of Apollonius of Perga (Andrade *et al.*, 2005; Herrmann *et al.*, 1990; Thomas, 1941) and Kepler (Kepler, 1611; Weaire and Aste, 2008), and still of great practical importance for all industries involved in granular processing. In addition, the complex structures that result from their assembly become increasingly important for the design of

new functional materials (Baule and Makse, 2014; Damasceno *et al.*, 2012; Glotzer and Solomon, 2007; Jaeger, 2015).

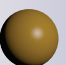





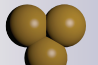





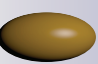
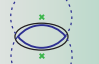





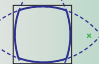


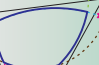

Object shape	Decomposition	Effective Voronoi interaction
<b>a</b>  Sphere	 One sphere	 Two points
<b>b</b>  Dimer	 Two spheres	 Four points
<b>c</b>  Trimer	 Three spheres	 Six points
<b>d</b>  Spherocylinder	 N spheres	 Two lines and four points
<b>e</b>  Ellipsoid	 Two spheres	 Two lines and four anti-points
<b>f</b>  Tetrahedron	 Four spheres	 Six lines, four points, four anti-points
<b>g</b>  Cube	 Six spheres	 Twelve lines, eight points, six anti-points
<b>h</b>  Irregular polyhedron	 Unequal spheres	 Points, lines, anti-points

FIG. 17 (Colors online) Table of different shapes and their VBs. (a–d) For shapes composed of spheres, the VB arises due to the effective interaction of the points at the centres of the spheres. Since spherocylinders are represented by a dense overlap of spheres, the effective interaction is that of two lines and four points. (e–h) For more complicated shapes that would in principle be modelled by a dense overlap of sphere with different radii, we propose approximations in terms of intersections of spheres leading to effective interactions between ‘anti-points’. For both classes of shapes, the VB follows an exact algorithm leading to analytical expressions (see Fig. 25). From (Baule *et al.*, 2013).

In the absence of theory, searches for the optimal

random packing of non-spherical shapes have focused on empirical studies on a case-by-case basis. Table V presents an overview of the maximal packing densities for a variety of shapes obtained in simulations, experiments and theory. Recent simulations have found the densest random packing fraction of, e.g., prolate ellipsoids at  $\phi \approx 0.735$  (Donev *et al.*, 2004); spherocylinders at  $\phi \approx 0.772$  (Zhao *et al.*, 2012) and 2d dimers at  $\phi \approx 0.885$  (Schreck *et al.*, 2010). The densest random tetrahedra packing has been found in simulations with  $\phi = 0.7858$  (Haji-Akbari *et al.*, 2009). More systematic investigations of the self-assembly of hard truncated polyhedra families has been done in (Chen *et al.*, 2014; Damasceno *et al.*, 2012). The organizing principles of ordered packings of Platonic and Archimedean solids and other convex and non-convex shapes have been investigated in (Torquato and Jiao, 2009, 2012). Interesting shapes have been considered also in a systematic way: superballs (Jiao *et al.*, 2010), puffy tetrahedra (Kallus and Elser, 2011), polygons (Wang *et al.*, 2015) and truncated vertices (Damasceno *et al.*, 2012; Gantapara *et al.*, 2013). A caveat of some empirical studies is the strong protocol dependence of the final close packed state even for the same shape: recent studies of spherocylinder packings, e.g., exhibit a large variance depending on the algorithm used (Abreu *et al.*, 2003; Bargiel, 2008; Jia *et al.*, 2007; Jiao and Torquato, 2011; Kyrylyuk *et al.*, 2011; Lu *et al.*, 2010; Williams and Philipse, 2003; Wouterse *et al.*, 2009; Zhao *et al.*, 2012). A generic theoretical insight is needed if one wants to search over more extended regions of parameter space of object shapes.

It is empirically clear that non-spherical shapes can generally achieve denser maximal packing densities than spheres. In fact, a conjecture attributed to Ulam (recorded in the book (Gardner, 2001)) in the context of regular packings, recently also formulated for random packings (Jiao and Torquato, 2011), states that the sphere is, indeed, the worst packing object among all convex shapes. In (Kallus, 2016) it has been shown for random packings that all sufficiently spherical shapes pack more densely than spheres. However, one should notice the local character of such a conjecture for random packings: Onsager already proved that elongated spaghetti-like thin rods pack randomly much worse than spheres (Onsager, 1949).

From a numerical point of view, a promising approach to find the best shape has been put forward by Jaeger and collaborators (Jaeger, 2015; Miskin and Jaeger, 2013, 2014; Roth and Jaeger, 2016) who used genetic algorithms (GA) to map the possible space of the constitutive particle shapes. They consider non-spherical composite particles formed by gluing spherical particles of different sizes rigidly connected into a polymer-like non-branched shape. A genetic algorithm starts with a given shape and perform ‘mutations’ to the constitutive particles until a desired property, for instance, maximal strength or max-



imal packing fraction is achieved. This reverse engineering approach can generate novel materials with desired properties but of limited shapes: within this framework, the limits to granular materials design are the limits to computation (Jaeger, 2015), since GA relies heavily on dynamically simulating (e.g., with MD or MC) the packings to be optimized. Thus, computational limitations are expected in more complicated shapes such as tetrahedra or irregular polyhedra, in general.

On the theoretical side, there are successful theories of high density liquids that have been extended to encompass non-spherical particles, such as mode-coupling theory (Götze, 2009) and density functional theory (Hansen-Goos and Mecke, 2009, 2010; Marechal and Löwen, 2013). However, they do not apply to the jamming regime. On the other hand, successful approaches to jamming based on replica theory so far only apply to spherical particles (Charbonneau *et al.*, 2017; Parisi and Zamponi, 2010) (see Sec. V). The difficulty to extend replica theory calculations from spheres to non-spherical particles stems from the fact that the system is not rotationally invariant, which adds more degrees of freedom to the description of the cage motion. Replica calculations also rely on liquid equations of state, which are typically not available in analytical form for non-spherical particles. These difficulties can be overcome in principle with numerics, but this is most likely cumbersome, and has not been accomplished so far. On the other hand, the Edwards approach can be generalized theoretically much more easily to non-spherical shapes.

The advantage of the mean-field Edwards approach is that it is based entirely on the geometry of the particles; its building block is directly the shape of the constitutive particle. Therefore, Edwards ensemble can be applied in a straightforward way to arbitrary shapes. Such a generalization, providing a comprehensive framework to describe packings of non-spherical particles, has recently been developed (Baule *et al.*, 2013). A drawback of employing a general theoretical approach rather than direct simulations using, e.g., artificial evolution (Jaeger, 2015), is that current theories are at the mean-field level and thus only approximate. However, both approaches can be complementing: A mean-field theory could identify a reduced region in the space of optimal parameters, which can then be tackled with more detail using more focused reverse engineering techniques.

As discussed in the previous sections, the central quantity to calculate is the average Voronoi volume  $\bar{W}$  as a function of  $z$ . In the case of frictionless spheres,  $z$  is fixed by isostaticity providing the prediction Eq. (82) for RCP. The situation is somewhat more complicated for frictionless non-spherical particles: Here, both  $z$  and  $\bar{W}$  depend independently on the particle shape. For simplicity, we assume rotationally symmetric particles in the following, where deviations from the sphere can be parametrized by a single parameter, e.g., the aspect ratio  $\alpha$  measuring

length over width. As a consequence, if we are interested in obtaining the function  $\phi(\alpha)$  at RCP, we need to combine the dependencies  $\bar{W}_\alpha(z)$  and  $z(\alpha)$ :

$$\phi(\alpha) = \frac{V_0}{\bar{W}_\alpha(z(\alpha))}. \quad (122)$$

We discuss next how to obtain  $\bar{W}_\alpha(z)$  by extending the framework of the coarse-grained Voronoi volume to non-spherical particles. A quantitative approach to describe  $z(\alpha)$  is discussed in Sec. IV.G.3, which requires a quantitative evaluation of the occurrence of degenerate configurations.

### 1. Coarse-grained Voronoi volume of non-spherical shapes

The key for the mean-field approach to the statistical mechanical ensemble based on the coarse-grained volume function is Eq. (52), which replaces the exact global minimization to obtain the Voronoi boundary  $l_i(\hat{\mathbf{c}})$  in the direction  $\hat{\mathbf{c}}$  by the pdf  $p(\mathbf{c}, z)$ . For a general particle-shape the cut-off  $c^*$  describes just the particle surface parametrized by  $\hat{\mathbf{c}}$ . Transforming Eq. (52) to the CDF  $P_>$  using  $p(\mathbf{c}, z) = -\frac{d}{dc}P_>(\mathbf{c}, z)$  leads to the volume integral (Baule *et al.*, 2013)

$$\bar{W}(z) = \int d\mathbf{c} P_>(\mathbf{c}, z), \quad (123)$$

where  $P_>$  is again interpreted as the probability that  $N - 1$  particles are outside a volume  $\Omega$  centered at  $\mathbf{c}$ , since otherwise they would contribute a shorter VB.  $\Omega$  is in principle defined as in Eq. (54), but is no longer a spherical volume due to the non-spherical interactions manifest in the parametrization of the VB. The VB now also depends on the relative orientation  $\hat{\mathbf{t}}$  of the two particles suggesting the definition:

$$\Omega(\mathbf{c}, \hat{\mathbf{t}}) = \int d\mathbf{r} \Theta(c - s(\mathbf{r}, \hat{\mathbf{t}}, \hat{\mathbf{c}})) \Theta(s(\mathbf{r}, \hat{\mathbf{t}}, \hat{\mathbf{c}})), \quad (124)$$

for a fixed relative orientation  $\hat{\mathbf{t}}$ .

So far, the description of  $\bar{W}$  is exact within the statistical mechanical approach. In order to solve the formalism, we introduce the following mean-field minimal model of the translational and orientational correlations in the packing (Baule *et al.*, 2013):

1. Following Onsager (Onsager, 1949), we treat particles of different orientations as belonging to different species. This is the key assumption to treat orientational correlations within a mean-field approach. Thus, the problem for non-spherical particles can be mapped to that of polydisperse spheres for which  $P_>$  factorizes into the contributions of the different radii (see Sec. IV.E).

Shape	$\phi_{\max}$ simulation	$\phi_{\max}$ experiment	$\phi_{\max}$ theory
disks (2d)	0.826 (Atkinson <i>et al.</i> , 2014)		0.85 (Jin <i>et al.</i> , 2014) 0.874 (Parisi and Zamponi, 2010) 0.834 (Tian <i>et al.</i> , 2015)
Sphere	0.645 (Skoge <i>et al.</i> , 2006)	0.64 (Bernal and Mason, 1960)	0.634 (Song <i>et al.</i> , 2008) 0.68 (Parisi and Zamponi, 2010)
M&M candy Dimer Ellipse (2d) Oblate ellipsoid Prolate ellipsoid Spherocylinder Lens-shaped particle	0.703 (Faure <i>et al.</i> , 2009) 0.895 (Delaney <i>et al.</i> , 2005) 0.707 (Donev <i>et al.</i> , 2004) 0.716 (Donev <i>et al.</i> , 2004) 0.722 (Zhao <i>et al.</i> , 2012)	0.665 (Donev <i>et al.</i> , 2004)	0.707 (Baule <i>et al.</i> , 2013)  0.731 (Baule <i>et al.</i> , 2013) 0.736 (Baule <i>et al.</i> , 2013)
Tetrahedron Cube Octahedron Dodecahedron Icosahedron	0.7858 (Haji-Akbari <i>et al.</i> , 2009) 0.697 (Jiao and Torquato, 2011) 0.716 (Jiao and Torquato, 2011) 0.707 (Jiao and Torquato, 2011)	0.76 (Jaoshvili <i>et al.</i> , 2010) 0.67 (Baker and Kudrolli, 2010) 0.64 (Baker and Kudrolli, 2010) 0.63 (Baker and Kudrolli, 2010) 0.59 (Baker and Kudrolli, 2010)	
General ellipsoid Superellipsoid Superball Trimer	0.735 (Donev <i>et al.</i> , 2004) 0.758 (Delaney <i>et al.</i> , 2010) 0.674 (Jiao <i>et al.</i> , 2010) 0.729 (Roth and Jaeger, 2016)	0.74 (Man <i>et al.</i> , 2005)	

TABLE V Overview of maximal packing fractions  $\phi_{\max}$  for a selection of regular shapes in disordered packings obtained with a variety of different packing protocols. Note that the  $\phi_{\max}$  value is achieved for the aspect ratio, where  $\phi$  is maximal, so every value is at a different aspect ratio.

- Translational correlations are treated as in the spherical case for high dimensions (see Sec. IV.C). Here, the Kirkwood superposition approximation leads to a factorization of the  $n$ -point correlation function into a product of pair-correlation functions, Eq. (89). Including also the factorization of orientations provides the form

$$P_{>}(\mathbf{c}, z) = \exp \left\{ -\rho \int d\hat{\mathbf{t}} \int_{\Omega(\mathbf{c}, \hat{\mathbf{t}})} d\mathbf{r} g_2(\mathbf{r}, \hat{\mathbf{t}}) \right\}. \quad (125)$$

- The pair correlation function is modelled by a delta function plus step function as for spheres, Eq. (91). This form captures the contacting particles and treats the remaining particles as an ideal gas-like background:

$$g_2(\mathbf{r}, \hat{\mathbf{t}}) = \frac{1}{4\pi} \left[ \frac{\sigma(z)}{\rho} \delta(r - r^*(\hat{\mathbf{r}}, \hat{\mathbf{t}})) + \Theta(r - r^*(\hat{\mathbf{r}}, \hat{\mathbf{t}})) \right]. \quad (126)$$

Here, the prefactor  $1/4\pi$  describes the density of orientations, which we assume isotropic. The contact radius  $r^*$  denotes the value of  $r$  in a direction  $\hat{\mathbf{r}}$  for which two particles are in contact without overlap. In the case of equal spheres the contact radius

is simply  $r^*(\hat{\mathbf{r}}, \hat{\mathbf{t}}) = 2R$ . For non-spherical objects,  $r^*$  depends on the object shape and the relative orientation.

Combining Eq. (126) with Eq. (125) recovers the product form of the CDF  $P_{>}$ :

$$P_{>}(\mathbf{c}, z) = \exp \left\{ -\rho \bar{V}^*(\mathbf{c}) - \sigma(z) \bar{S}^*(\mathbf{c}) \right\}, \quad (127)$$

where  $\bar{V}^*$  and  $\bar{S}^*$  are now orientationally averaged excluded volume and surface:  $\bar{V}^* = \langle \Omega - \Omega \cap V_{\text{ex}} \rangle_{\hat{\mathbf{t}}}$  and  $\bar{S}^* = \langle \partial V_{\text{ex}} \cap \Omega \rangle_{\hat{\mathbf{t}}}$  (compare with Eqs. (57,58)). The orientational average is defined as  $\langle \dots \rangle_{\hat{\mathbf{t}}} = \frac{1}{4\pi} \oint \dots d\hat{\mathbf{t}}$ . Substituting Eq. (127) into Eq. (123) leads to a self-consistent equation for  $\bar{W}$  due to the dependence of  $\rho$  on  $\bar{W}$ . In order to be consistent with the spherical limit, we use  $\rho \rightarrow \rho_f = 1/(\bar{W} - V_0)$  due to the low dimensional corrections discussed in Sec. IV.A.

In accordance with the treatment of the surface density term  $\sigma(z)$  for 3d spheres, we obtain  $\sigma(z)$  by simulating random local configurations of  $z$  contacting particles around a reference particle and determining the average available free surface. This surface is given by  $\bar{S}^*(\mathbf{c}_m)$ , where  $c_m$  is the minimal contributed VB among the  $z$  contacts in the direction  $\hat{\mathbf{c}}$ . Averaging over many realizations with a uniform distribution of orientations and averaging also over all directions  $\hat{\mathbf{c}}$  provides the

surface density in the form of a Monte-Carlo average  $\sigma(z) = \left\langle \left\langle \bar{S}^*(\mathbf{c}_m) \right\rangle \right\rangle_{\mathbf{e}}^{-1}$ . In this way we can only calculate  $\sigma(z)$  for integer values of  $z$ . For fractional  $z$  that are predicted from the evaluation of degenerate configurations in the next section, we use a linear interpolation to obtain  $\bar{W}(z)$ .

The theory developed so far captures the effect of particle shape on the average Voronoi volume as a function of a given  $z$ . The particle shape is taken into account in three quantities: (i)  $c^*(\hat{\mathbf{c}})$ , parametrizing the surface of the shape; (ii)  $s(\mathbf{r}, \hat{\mathbf{t}}, \hat{\mathbf{c}})$ , parametrizing the VB between two particles of relative position  $\mathbf{r}$  and orientation  $\hat{\mathbf{t}}$ ; and (iii) the contact radius  $r^*(\hat{\mathbf{r}}, \hat{\mathbf{t}})$ . In the spherical limit, all these quantities simplify considerably and the spherical theory is recovered, which is analytically solvable as discussed in Sec. IV.A. For non-spherical shapes, the VB Point (ii) above is in general not known in closed form. In the next section, we discuss a class of shapes for which the VB can be expressed in exact analytical form. For these shapes, the theory can be applied in a relatively straightforward way, solving  $\bar{V}^*$  and  $\bar{S}^*$  numerically and providing also  $\bar{W}(z)$  in numerical form. In Sec. IV.G.3 we then discuss the missing part in the theory so far, the dependence of  $z$  itself on the particle shape.

## 2. Parametrization of non-spherical shapes

In Sec. II.D.1 the precise definition of the VB between two particles has been given. We have seen that the VB between two equal spheres is identical to the VB between two points and is a flat plane perpendicular to the separation vector. Finding the VB for more complicated shapes is a challenging problem in computational geometry, which is typically only solved numerically (Boissonat *et al.*, 2006). Already for ellipsoids, one of the simplest non-spherical shape, there is no exact expression for the VB. We nevertheless approach this problem analytically by considering a decomposition of the shape into overlapping spheres (see Fig. 17a–d). Such a decomposition is trivial for dimers, trimers, and  $n$ -mers, where the VB arises effectively due to the interaction of four, six and  $2n$  points. It also applies exactly, e.g., to spherocylinders, which can be represented as dense overlaps of spheres. In this case, the VB arises due to the effective interaction of two lines and four points.

The Voronoi decomposition used for  $n$ -mers and spherocylinders can be generalized to arbitrary shapes by using a dense filling of spheres with unequal radii (Phillips *et al.*, 2012). However, even though this approach is algorithmically well defined, it may become practically tedious for dense unions of polydisperse spheres. An alternative approach that is analytically tractable has been proposed in (Baule *et al.*, 2013): Convex shapes are approximated by intersections of a finite number of

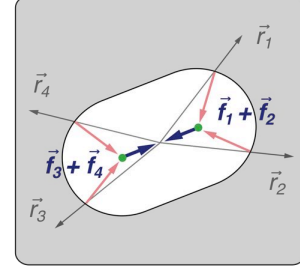


FIG. 18 (Colors online) Illustration of a degenerate configuration of a spherocylinder. Vectors  $\mathbf{r}_1, \dots, \mathbf{r}_4$  indicate contacts on the spherical caps. The normal vector projects the contact forces  $\mathbf{f}_1, \dots, \mathbf{f}_4$  onto the centres of the spherical caps. Due to the symmetry of the two centres, the respective force arms are equal and force balance automatically implies torque balance. The force and torque balance equations (2,3) are thus degenerate. From (Baule *et al.*, 2013).

spheres. An oblate ellipsoid, e.g., is approximated by a lens-shaped particle, which consists of the intersection of two spheres (Cinacchi and Torquato, 2015). Likewise, an intersection of four spheres can be considered an approximation to a tetrahedra, and six spheres that of a cube (see Fig. 17e–h). The main insight is that the effective Voronoi interaction of these shapes is governed by a symmetry: Points map to 'anti-points' (since the interactions between spheres is inverted). The VB of ellipsoid-like objects arises from the interaction between four anti-points and four points in two dimensions or lines in three dimensions, and thus falls into the same class as spherocylinders. The VB between two tetrahedra is then due to the interaction between the vertices (leading to four point interactions), the edges (leading to six line interactions), and the faces (leading to four anti-point interactions). For cubes the effective interaction is that of twelve lines, eight points and six anti-points. This approach can be generalized to arbitrary polyhedra.

With such a decomposition into overlapping and intersecting spheres, we can study a large space of particle shapes using Edwards ensemble. The resulting VBs can be parametrized analytically following an exact algorithm (Baule *et al.*, 2013) (see appendix C).

## 3. Dependence of coordination number on particle shape

As discussed in Sec. II.A the physical conditions of mechanical stability and assuming minimal correlations motivate the isostatic conjecture Eq. (35)  $z = 2d_f$  in the frictionless case. While isostaticity is well-satisfied for spheres, packings of non-spherical objects are in general hypoconstrained with  $z < 2d_f$ , where  $z(\alpha)$  increases smoothly from the spherical value for  $\alpha > 1$  (Baule *et al.*, 2013; Donev *et al.*, 2004, 2007; Wouterse *et al.*, 2009). The fact that these packings are still in a mechanically

stable state can be understood in terms of the occurrence of stable degenerate configurations, which have so far been shown to occur in packings of ellipses, ellipsoids, dimers, spherocylinders, and lens-shaped particles (Baule *et al.*, 2013; Chaikin *et al.*, 2006; Donev *et al.*, 2007). In the case of ellipses, one needs in general four contacts to fix (jam) the ellipse locally such that no displacement is possible (Alexander, 1998). However, it is possible to construct configurations, where only three contacts are sufficient, namely when the normal vectors from the points of contact meet at the same point and the curvature on at least one of the contacts is flat enough to prevent rotations (Chaikin *et al.*, 2006). Such a configuration is degenerate since force balance automatically implies torque balance such that the force and torque balance equations (2–3) are no longer linearly independent. Despite the fact that these configurations should have measure zero in the space of all possible configurations, they are believed to appear more frequently in simulation algorithms such as the LS algorithm (Donev *et al.*, 2007).

For spherocylinders, the degeneracy appears due to the spherical caps, which project the normal forces onto the end points of the central line of the cylindrical part. If all of the contacts are on the spherical caps, which will frequently occur for small aspect ratios, force balance will then always imply torque balance, since the force arms of the two points are identical (see Fig. 18). A similar argument applies to dimers and lens-shaped particles, and can possibly be extended to other smooth shapes. In the case of spherocylinders, a degeneracy also appears for very large aspect ratios, because then all contacts will predominantly be on the cylindrical part. As a consequence, the normal vectors are all coplanar and the number of linear independent force and torque balance equations is reduced by one predicting the contact number  $z \rightarrow 8$  as  $\alpha \rightarrow \infty$ , which is indeed observed in simulations (Wouterse *et al.*, 2009; Zhao *et al.*, 2012).

A quantitative method to estimate the probability of these degenerate configurations is based on the assumption that a particle is always found in an orientation such that the redundancy in the mechanical equilibrium conditions is maximal (Baule *et al.*, 2013). This condition allows us to associate the number of linearly independent equations involved in mechanical equilibrium with the set of contact directions. Averaging over the possible sets of contact directions then yields the average effective number of degrees of freedom  $\tilde{d}_f(\alpha)$ , from which the coordination number follows as  $z(\alpha) = 2\tilde{d}_f(\alpha)$  (Baule *et al.*, 2013). This approach recovers the continuous transition of  $z(\alpha)$  from the isostatic spherical value  $z = 6$  at  $\alpha = 1$ , to the isostatic value  $z = 10$ , for aspect ratios above  $\approx 1.5$  observed in ellipsoids of revolution, spherocylinders, dimers, and lens-shaped particles, Fig. 19a. The trend compares well to known data for ellipsoids (Donev *et al.*, 2004) and spherocylinders (Wouterse *et al.*, 2009;

Zhao *et al.*, 2012).

Combining these results on  $z(\alpha)$  with the results of Sec. IV.G.1 on the average Voronoi volume  $\bar{W}_\alpha$  leads to a close theoretical prediction for the packing density  $\phi(\alpha) = V_0/\bar{W}_\alpha(z(\alpha))$  which does not contain any adjustable parameters. Figure 19b presents the results for dimers, spherocylinders and lenses showing that the theory is an upper bound of the maximal densities measured in simulations. The theory predicts the maximum density of spherocylinders at  $\alpha = 1.3$  with a density  $\phi_{\max} = 0.731$  and that of dimers at  $\alpha = 1.3$  with  $\phi_{\max} = 0.707$ . For lens-shaped particles a density of  $\phi_{\max} = 0.736$  is obtained for  $\alpha = 0.8$ , representing the densest random packing of an axisymmetric shape known so far. The theoretical predictions of  $\phi(\alpha)$  compare quite well with the available numerical data for spherocylinders and dimers (Figs. 19c, d). The numerical results are obtained with a range of different packing algorithms and show a large variance in terms of the maximal packing densities obtained, for the same shape. The appearance of such a range of densities is understood in detail for the case of spheres, see the discussion in Sec. III.A.4. As for spheres, the single RCP value calculated within the Edwards ensemble for a given shape is interpreted as a maximum entropy value.

By plotting  $z$  against  $\phi$  parametrically as a function of  $\alpha$ , we can also include our results in the  $z$ – $\phi$  phase diagram, which is thus extended from spheres to non-spherical particles and discussed next. By plotting  $(\phi, z)$  the apparent cusp-like singularity at the spherical point  $\alpha = 1$  in  $z(\alpha)$  and  $\phi(\alpha)$  (Figs. 19a, b) disappears and the spherical RCP point becomes as any other point in the phase diagram.

## H. Towards an Edwards phase diagram for all jammed matter

The results from Secs. IV.B, IV.F, and IV.G.3 are combined in a phase diagram of jammed matter that can guide our understanding of how random arrangements of particles fill space as shown in Fig. 20. The representation in the  $z$ – $\phi$  plane is in a way the most natural choice, since both  $\phi$  and  $z$  are macroscopic observables that characterize the thermodynamic state of the packing. They can also be measured in simulations in a straightforward way. Although Fig. 20 is far from complete, we observe clear classifications of packings based on the *symmetry* and *surface properties* of the constituents. Horizontal phase boundaries are identified by the isostatic condition for frictionless particles, predicting  $z = 6$  for isotropic shapes and  $z = 10$  ( $z = 12$ ) for rotationally symmetric (fully asymmetric) shapes respectively. The frictionless RCP point at  $\phi_{\text{Edw}} = 0.634\dots$  and  $z = 6$  plays a prominent role in the phase diagram, despite that it contracts the J-line. It splits up (although in a continuous man-



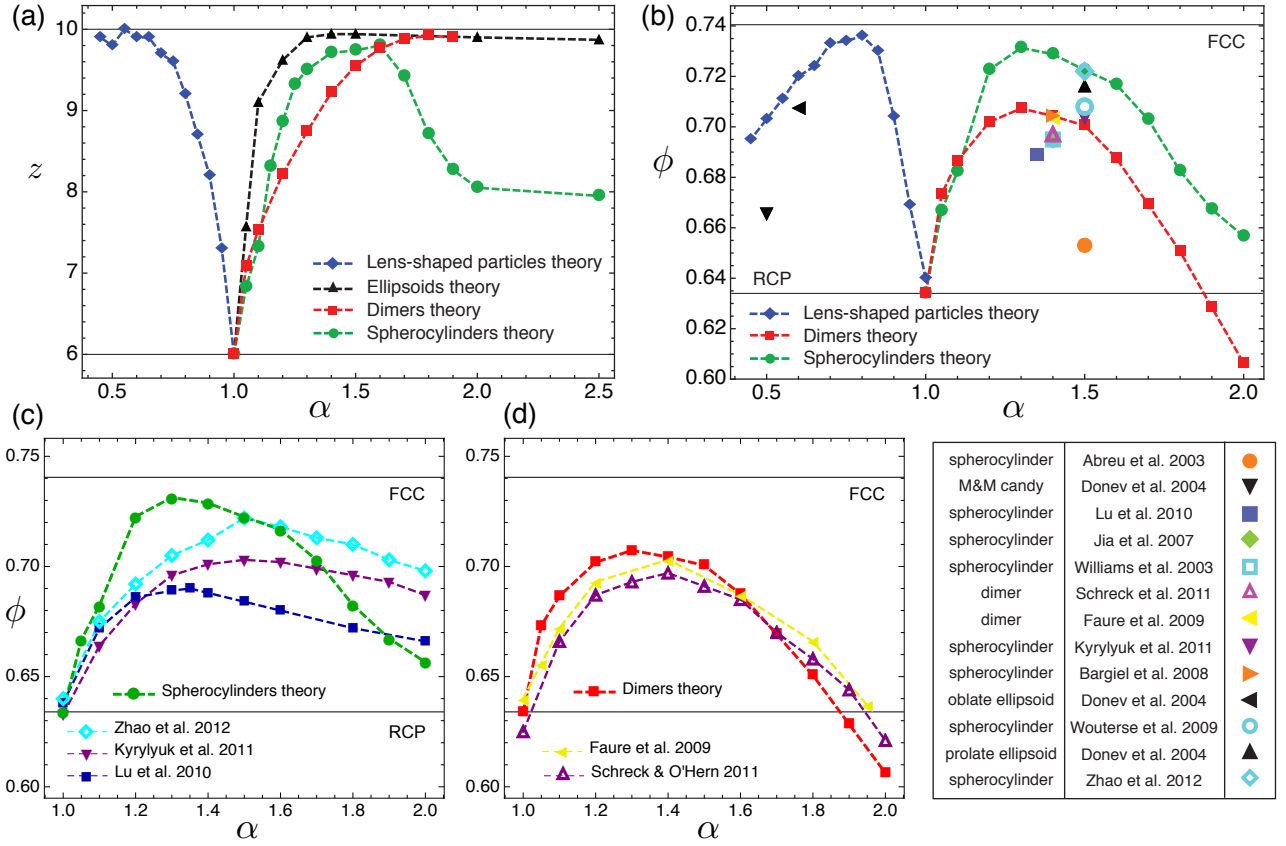


FIG. 19 (Colors online) Theoretical predictions for packings of non-spherical particles (Baule *et al.*, 2013). (a) The variation  $z(\alpha)$  obtained by evaluating the occurrence of degenerate configurations for dimers, spherocylinders, ellipsoids of revolution, and lens-shaped particles. A smooth increase is obtained in agreement with simulation data. For spherocylinders,  $z$  decreases to the value 8 as  $\alpha \rightarrow \infty$ . (b) Combining  $z(\alpha)$  with the results on  $\bar{W}_\alpha$  from the volume ensemble leads to theoretical predictions for  $\phi(\alpha)$  exhibiting a density peak for dimers, spherocylinders, and lens-shaped particles. Results on  $\phi_{\max}$  for the three shapes from simulations are indicated by symbols. The theory captures well both the location of the peak and the maximum density. (c) Detailed comparison of theory and simulations for spherocylinders (Kyrylyuk *et al.*, 2011; Lu *et al.*, 2010; Zhao *et al.*, 2012). The theoretical peak is slightly shifted to the left and more pronounced than in the empirical data. (d) Detailed comparison of theory and simulations for dimers (Faure *et al.*, 2009; Schreck and O’Hern, 2011) showing excellent agreement. Figs. (a,b) from (Baule *et al.*, 2013).

ner, except for ordering) the equation of state into four different branches governed by friction, shape, adhesion, and order, as follows:

*Frictional branch.* The infinite compactivity RLP branch connects the RCP point (0.634, 6) with the minimal RLP point at (0.536, 4). This branch is the upper limit of the triangle of mechanically stable disordered sphere packings depicted in the phase diagram for 3d monodisperse spheres in Fig. 12. The RLP branch is parametrized by varying the friction  $\mu$  and thus  $z$  in the equation of state (84).

*Non-spherical branch.* Surprisingly, we find that both dimer and spherocylinder packings appear as smooth continuations of spherical packings. The analytic form of this continuation from the spherical random branch can be derived (blue dashed line in Fig. 20) by solving the self-consistent equation (123) perturbatively for small

aspect ratios (Baule *et al.*, 2013).

A comparison of our theoretical results with empirical data for a large variety of shapes indicates that the analytic continuation provides an upper bound of density on the  $z$ - $\phi$  phase diagram for a fixed  $z$ . Maximally dense disordered packings appear to the left of this boundary, while the packings to the right of it are partially ordered. We observe that the maximally dense packings of dimers, spherocylinders, lens-shaped particles and tetrahedra all lie surprisingly close to the analytic continuation of RCP. Whether there is any deeper geometrical meaning to this remains an open question. Recent exact local expansions from the spherical RCP point to arbitrary shapes agree very well with our results and may shed further light on this question (Kallus, 2016). We also notice that the frictional and non-spherical branches are continuous at the spherical RCP point suggesting that a variation in fric-

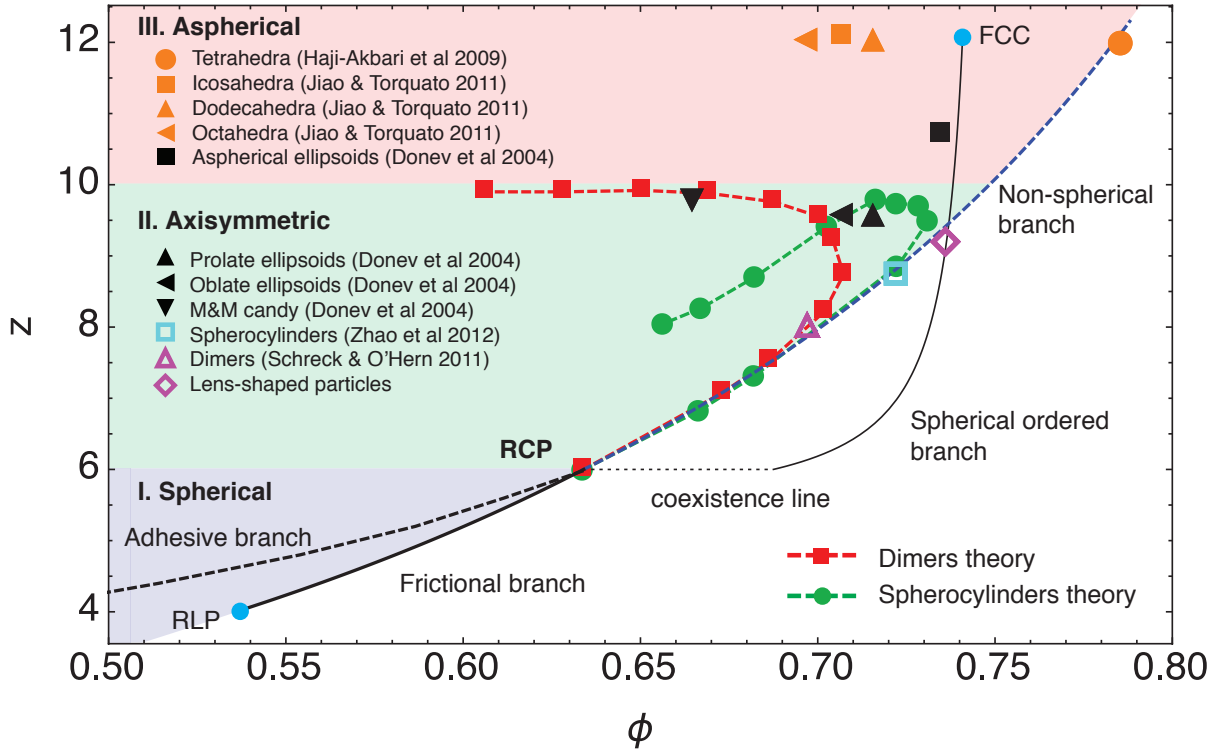


FIG. 20 (Colors online) Unifying phase diagram in the  $z$ - $\phi$  plane resulting from the Edwards volume ensemble theory. Theoretical results on the equations of state for spheres with and without adhesion and dimers/spherocylinders are plotted together with empirical results on maximal packing densities for non-spherical shapes from the literature (where  $z$  and  $\phi$  have been determined in the same simulation). Different phases are identified by the symmetry of the constituents. Different equations of state due to friction, adhesion, shape, and (partial) order all come together at the RCP point. Indicated are the frictional branch (Song *et al.*, 2008), spherical ordered branch (Jin and Makse, 2010), non-spherical branch (Baule *et al.*, 2013), and adhesive branch (Liu *et al.*, 2015). Adapted from (Baule and Makse, 2014).

tion might be analogous to varying shape in the phase diagram.

*Adhesive branch.* The non-spherical branch can also be continued into the adhesive branch of spheres, which splits off at RCP. The adhesive branch describes the universal high adhesion regime for  $Ad > 1$  reaching the adhesive loose packing (ALP) point at  $\phi = 1/2^3$  and  $z = 2$  (see Sec. IV.F).

*Spherical ordered branch.* As discussed in Sec. III.A.4, the RCP point has been associated with the freezing point of a first order phase transition between a fully disordered packing of spheres and the crystalline FCC phase (Jin and Makse, 2010; Radin, 2008). The signature of this disorder-order transition is a discontinuity in the entropy density of jammed configurations as a function of the compactivity. Experiments on hard sphere packings indeed confirm the first order transition scenario, observing the onset of crystallization at  $\phi_f \approx 0.64$  at the end of the frictional branch, as well as the coexistence line (Francois *et al.*, 2013; Hanifpour *et al.*, 2015, 2014). The spherical ordered branch provides another boundary, which separates tetrahedra from all other shapes: Tetrahedra are the only shape that pack in a disordered way

denser than spheres in a FCC crystal.

The picture that emerges from this phase diagram is that spherical packings can be generated on the frictional branch between the RLP and RCP limits by variation of the inter-particle friction and along the adhesion branch by varying interparticle attraction. Beyond RCP, these two lines can be continued smoothly by deforming the sphere into elongated shapes. The ordered branch does not connect smoothly to any of these branches, instead appears through a first order phase transition with a coexistence regime. It suggests that introducing order is a more drastic modification than modifying the particle interactions due to geometry or surface frictional properties. This distinction is similar to the one between discontinuous first and continuous higher-order phase transitions.

Overall, it seems that the central importance historically given to the spherical RCP point may not be justified. In the whole share of things, the spherical point appears as any other inconsequential point in a continuous variation of jammed states driven by friction, attraction and shape. It is as though each jammed state (ranging from spherical to dimers, trimers, polymers, spher-

cylinders, ellipsoids, tetrahedra and cubes, from frictionless to frictional and adhesive grains) carries the features of one great single organizing principle in which all the jammed states organize, too; so that everything links to everything else, moved by one organizing idea which is the universal physical principle in nature (Schopenhauer, 1974).

Such an organizing principle is captured by the phase diagram in Fig. 20 where the volume fraction as a function of  $\alpha$  for non-spherical particles appears as an analytical continuation of the equation of state for the spherical particles. It is as though the sphere system with friction can be made analogous to a non-spherical system without friction by following the continuation branch. Likewise, the RCP point bifurcates into other equations of state following the appearance of adhesion between particles as seen in Fig. 20. We may conjecture that all these packings with different interactions (from hard-spheres to attraction and friction) and different shapes (from spheres to ellipsoids, etc.) can be made part of an organizing principle embodied in the statistical mechanical laws.

## V. JAMMING SATISFACTION PROBLEM, JSP

We close our review by providing a novel understanding of the jamming criticality under the Edwards ensemble as the phase transition between the satisfiable and the unsatisfiable phases of the Jamming Satisfaction Problem. At the very end we suggest a unifying view of the Edwards ensemble of grains with the statistical mechanics of spin-glasses.

As we explained in Sec. II.A, a packing can be described as an ensemble of particles with given positions and orientations, satisfying a set of geometrical and mechanical constraints. As such, it is an instance of a constraint satisfaction problem: the Jamming Satisfaction Problem (JSP). Solving the JSP, in general, is a very complicated task, and one needs to resort to some approximations. The first main approximation that we applied across this review consisted in decoupling the geometrical problem of determining the contact network of the packing from the mechanical problem of finding the force distribution. Thus, in Sec. IV we developed the Edwards volume ensemble that considers in detail the volume ensemble, but does not directly consider the full force ensemble, which is only taken into account by the global isostatic constraint on the average coordination number establishing force balance.

Below, we consider another reduced JSP where one now fixes the geometry of the packing considering it as a random graph (thus, fixing the volume ensemble), and then considering the full force ensemble on these random graphs to find the force distribution (Bo *et al.*, 2014). An ensemble average over all possible random graphs consistent with prescribed (local) conditions of jamming

and excluded volume on the positions of neighbouring particles is performed to obtain the force distribution. Such a reduced JSP is therefore amenable to be solved for sparse networks by the cavity method from spin-glass theory (Mézard and Montanari, 2009; Mézard and Parisi, 2001), where one considers the geometric configuration of the particles in the packing as fixed, and then finds the force distribution (Bo *et al.*, 2014).

This force distribution is nothing but the uniform Edwards' measure  $\Theta_{\text{jam}}$  over all possible solutions of the JSP Eq. (10) where the hard-core constraint is relaxed, being automatically satisfied because we are considering the contact network fixed. To emphasize the dependence of  $\Theta_{\text{jam}}$  solely on the force configuration  $\{\mathbf{f}\}$  for a given realization of the contact network  $\{\mathbf{d}\}$ , we use the notation  $\Theta_{\text{jam}}(\{\mathbf{f}\}|\{\mathbf{d}\}) = P(\{\mathbf{f}\})$ , with the normalization or partition function  $\mathcal{Z}$  is the number of solutions of this JSP. The important point is that if  $\mathcal{Z} \geq 1$  then there exists a solution to the JSP, i.e., it is satisfiable (SAT). Conversely, if  $\mathcal{Z} < 1$  there are no solutions to the JSP, i.e., it is unsatisfiable (UNSAT) (Kirkpatrick and Selman, 1994).

The SAT/UNSAT threshold of the JSP is marked by the coordination number  $z_c^{\min}(\mu)$  that separates the region where solutions do exist (i.e. where  $\mathcal{Z} > 1$ ) from the region without solutions (where  $\mathcal{Z} < 1$ ), corresponding to an underdetermined/overdetermined set of equations, respectively (Bo *et al.*, 2014). In the limiting case of frictionless particles,  $z_c^{\min}(\mu)$  should be compared with the naive Maxwell counting isostatic condition:  $z_c^{\min}(\mu = 0) = 2d_f$ , although the JSP takes into account the full set of constraints, Eqs. (10), rather than only force balance as in Maxwell counting. The JSP thus extends this naive counting to the full set of constraints including friction  $\mu$ . A jammed isostatic assembly of particles lies exactly on the edge between these two phases, i.e., where a solution to the JSP first appears as one increases the average coordination number  $z(\mu)$ . Figure 23 shows the average coordination number  $z_c^{\min}(\mu)$  at the jamming transition as a function of the friction coefficient  $\mu$  in a 2d sphere packing, obtained by solving the JSP through the cavity method as explained next (Bo *et al.*, 2014). Results are consistent with existing numerical simulations (Kasahara and Nakanishi, 2004; Makse *et al.*, 2000; Papanikolaou *et al.*, 2013; Shen *et al.*, 2014; Shundyak *et al.*, 2007; Silbert, 2010; Silbert *et al.*, 2002a; Song *et al.*, 2008).

### A. Cavity approach to JSP

Solving the JSP amounts to compute the single force distributions  $P(\mathbf{f}_a^i)$  at the contacts  $a$ 's of the particle  $i$ 's. However, calculating these single force distributions  $P(\mathbf{f}_a^i)$  from the joint distribution  $P(\{\mathbf{f}\})$  Eq. (10) is still a very demanding computational task, which requires some

additional mean-field approximations to be solved.

There are two preferred mean-field theories (both of infinite dimensional nature): the first one is the infinite range model, which assumes that each particle is in contact with every other particle in the packing. The archetypical model is the Sherrington-Kirkpatrick (SK) model of fully connected spin-glasses (Sherrington and Kirkpatrick, 1975) which has been adapted to the hard-sphere case in (Parisi and Zamponi, 2010) (see Secs. III.A.4). As a result of this approximation scheme, the real finite dimensional contact network Fig. 21a is substituted by a fully-connected network of possible interactions, i.e., a complete graph as shown in Fig. 21b. The solution of such a model is possible since, in a complete graph, each interaction becomes very weak, rendering a fully connected model into a weakly connected system that can be solved exactly under the hierarchy of replica symmetry breaking schemes (Mézard and Montanari, 2009; Parisi and Zamponi, 2010). A simpler version than the SK model, yet showing all the phenomenology of jamming, is a model adapted from machine learning; the perceptron recently studied in (Franz and Parisi, 2016; Franz *et al.*, 2015).

A second mean-field theory of choice consists in approximating the contact network by a sparse random graph (Mézard and Parisi, 2001), which allows one to preserve an essential property of real finite dimensional packings: the finite coordination number  $z$ . The sparse random graph scheme assumes that the local contact network around each particle can be approximated by a tree-like structure, i.e. it neglects the strong local correlations of loops and force chains of a real packing Fig. 21a by a locally tree-like structure, Fig. 21c. Under this approximation the JSP can be solved by a method known as cavity method (Mézard and Montanari, 2009; Mézard and Parisi, 2001), which we explain next.

It should be noticed that, although the cavity approach is a mean field theory valid for infinite dimensions, a dimensional dependence appears in the non-overlap condition in the definition of the network ensemble, see (Bo *et al.*, 2014) for details. The crucial quantity to consider in the cavity method is not the single force distribution itself  $P(\mathbf{f}_a^i)$ , but a modified one, called the cavity force distribution and denoted by  $P_{i \rightarrow a}(\mathbf{f}_a^i)$ . Physically,  $P_{i \rightarrow a}(\mathbf{f}_a^i)$  is the probability distribution of the force  $\mathbf{f}_a^i$  at the contact  $a$  in a modified packing where the particle  $j$  touching the particle  $i$  at the contact  $a$  has been removed (from where the name cavity derives). The rationale to consider  $P_{i \rightarrow a}(\mathbf{f}_a^i)$  instead of the “true” force distribution  $P(\mathbf{f}_a^i)$  is that for the cavity distributions it is possible to derive a set of self-consistent equations if one neglects the correlation between  $P_{i \rightarrow a}(\mathbf{f}_a^i)$  and  $P_{j \rightarrow a}(\mathbf{f}_a^j)$  (hence the need of a tree-like network) (Bo *et al.*, 2014).

For example, the cavity equation for  $P_{i \rightarrow a}(\mathbf{f}_a^i)$  can be obtained by simply convoluting the cavity force distributions  $P_{k \rightarrow b}(\mathbf{f}_b^k)$  of the particles  $k \neq j$  neighbors of particle

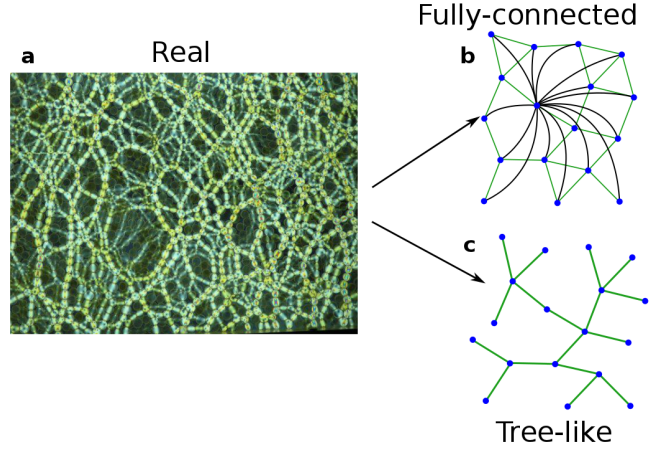


FIG. 21 (a) A real finite-dimensional packing is composed of strongly correlated force chains and geometrical loops at short scale (image reprinted with permission from the Behringer Group, Duke University). However, state-of-the-art theoretical approaches to describe this correlated structure rely upon mean-field infinite-dimensional approximate treatments of such a packing as a: (b) Fully-connected packing where every single particle interacts with any other particle in the packing; the real interaction network is approximated by a complete graph, i.e., each node is connected with all other nodes as shown for one of them. (c) Locally-tree like packing where the real network is approximated by a sparse random graph that locally looks like a tree structure with no loops, i.e., loops in the network are neglected, except at relatively large scales that diverge with system size, although very slowly as  $\ell \sim \ln N$ .

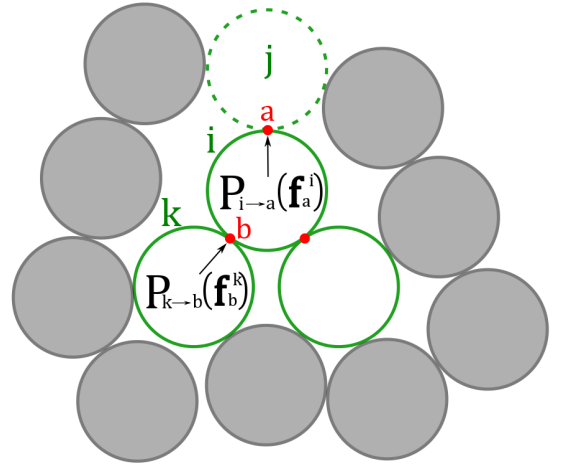


FIG. 22 Calculation of the cavity force distribution  $P_{i \rightarrow a}$ . First particle  $j$  (dashed contour) is virtually removed from the packing. Then  $P_{i \rightarrow a}$  for particle  $i$  is computed by convoluting the distributions  $P_{k \rightarrow b}$  of the neighboring particles  $k$  with the local mechanical constraint  $\chi_i$  enforcing force and torque balances.



$i$  with the local mechanical constraint  $\chi_i$ , as depicted in Fig. 22, and mathematically expressed as follows:

$$P_{i \rightarrow a}(\mathbf{f}_a^i) \propto \int \prod_{b \in \partial i \setminus a} d\mathbf{f}_b^k \chi_i \prod_{k \in \partial b \setminus i} P_{k \rightarrow b}(\mathbf{f}_b^k), \quad (128)$$

where the symbol  $\propto$  implies a normalization factor, and the mechanical constraint  $\chi_i$  on particle  $i$  is given by:

$$\begin{aligned} \chi_i(\{\mathbf{f}_a^i\}_{a \in \partial i}) &= \delta\left(\sum_{a \in \partial i} \mathbf{f}_a^i\right) \delta\left(\sum_{a \in \partial i} \mathbf{d}_a^i \times \mathbf{f}_a^i\right) \\ &\times \prod_{a \in \partial i} \theta(\mu f_{a,n}^i - |\mathbf{f}_{a,\tau}^i|) \theta(-\mathbf{d}_a^i \cdot \mathbf{f}_a^i). \end{aligned} \quad (129)$$

Notice that the contact directions  $\{\mathbf{d}_a^i\}$  are kept fixed: they represent the "quenched" disorder introduced by the underlying contact network, which is kept fixed.

Once the set of cavity equations (128) has been solved—e.g. by iteration under the Replica Symmetric (RS) assumption (Bo *et al.*, 2014)—one can reconstruct back the original force distribution at contact  $a$  by simply multiplying the cavity force distributions  $P_{i \rightarrow a}(\mathbf{f}_a^i)$  and  $P_{j \rightarrow a}(\mathbf{f}_a^j)$  coming from the two particles  $i$  and  $j$  in contact at  $a$ :

$$P(\mathbf{f}_a^i) \propto P_{i \rightarrow a}(\mathbf{f}_a^i) P_{j \rightarrow a}(\mathbf{f}_a^j). \quad (130)$$

The result shows an exponential decay at large forces and a non-zero value for  $P(f)$  at  $f = 0$ , i.e., it gives an exponent at the RS level

$$\theta_{\text{RS}} = 0 \quad (131)$$

for the small force scaling  $P(f) \sim f^\theta$ , Eq. (48). This last prediction is inconsistent with simulation results, which find a nonzero value of the exponent  $\theta$  in the interval  $0.2 \leq \theta \leq 0.5$ . It should be noted that Eq. (131) is obtained exactly at the thermodynamic limit, so no finite size effects are expected.

The discrepancy could be in principle due to the abundance of short loops in the real finite-dimensional contact network that are neglected by the locally tree-like contact network structure considered by the cavity method. However, it is known that the fraction of short force loops decreases with dimension at jamming—a results valid for any random network in infinite dimensions—yet, the non-zero weak force power-law exponent is obtained in the high dimensional calculations in the fully connected case (Charbonneau *et al.*, 2012). In this case, the complexity lost by the consideration of a uniform fully connected network is somehow overcome by the fractal complexity provided by the fullRSB solution, which in this case, gives rise to the concomitant non-zero small-force exponent. Whether a zero exponent result is the byproduct of the cavity calculation being done at the RS level or of the absence of loops in the structure is to be determined.

A similar situation appears in the replica approach to the problem: The original 1RSB calculation under the replica approach of the force distribution for hard sphere glasses done in (Parisi and Zamponi, 2010) led to a trivial scaling

$$\theta_{\text{1RSB}} = 0, \quad (132)$$

while the non-zero exponent was only obtained when the full RSB calculation was performed (Charbonneau *et al.*, 2014b)

$$\theta_{\text{fullRSB}} = 0.42... \quad (133)$$

It should be noticed, though, that 1RSB level calculations and above are substantially more difficult to perform with the cavity method than with replicas (e.g., no calculation exists above 1RSB with the cavity method for any model, although it has recently been conjectured how the cavity method could be used to describe the full RSB scenario (Parisi, 2017)).

Despite these discrepancies, the main result of the cavity approach is the detection of the SAT/UNSAT transition of the JSP for sphere packings with arbitrary friction coefficient, and a lower bound estimate of the critical coordination number  $z_c^{\min}(\mu)$  at the jamming transition as a function of the friction coefficient  $\mu$ , as shown in Fig. 23. Moreover, the cavity method seems a promising way to study JSPs for packings with particles of arbitrary shapes, which are difficult to perform with replicas.

## B. Edwards uniform measure hypothesis in the Edwards-Anderson spin-glass model

The main goal of this section is to investigate Edwards' conjecture of equiprobable jammed states in the spin-glass model first introduced by Edwards together with Anderson (Edwards and Anderson, 1975), thus, bringing together two of the most significance contributions of Edwards: spin-glasses (Edwards and Anderson, 1975) and granular matter (Edwards and Oakeshott, 1989). We leverage some rigorous results (Newman and Stein, 1999) to understand what is effectively right and what may go wrong with that hypothesis by precisely stating it in terms of metastable states in spin-glasses and jamming. We will see how this definition of metastable jammed states leads to the most precise test so far of the Edwards uniform measure hypothesis in the exactly solvable SK model (Sherrington and Kirkpatrick, 1975), which we propose to perform in Sec. V.C.

The Ising spin-glass on the  $d$ -dimensional cubic lattice  $Z^d$ , also known as the Edwards-Anderson model, is described by the following Hamiltonian (Edwards and Anderson, 1975):

$$\mathcal{H}(\vec{\sigma}) = - \sum_{\langle ij \rangle} J_{ij} \sigma_i \sigma_j, \quad (134)$$

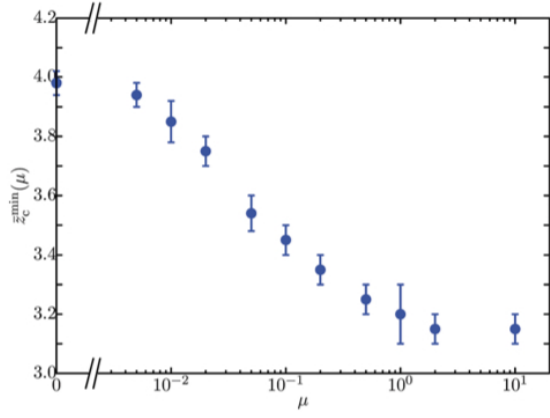


FIG. 23 Linear-log plot of average coordination number  $z_c^{\min}(\mu)$  at the jamming transition as a function of the friction coefficient  $\mu$  in 2-D sphere packing calculated with the cavity method. The curve  $z_c^{\min}(\mu)$  separates the SAT/UNSAT phases of jamming. For  $z > z_c^{\min}(\mu)$ , the force balance equations are satisfied while they are not when  $z < z_c^{\min}(\mu)$ . At the transition  $z_c^{\min}(\mu)$  for a given  $\mu$  a jammed critical state exists separating the SAT from the UNSAT phases.  $z_c^{\min}(\mu)$  shows a monotonic decrease with increasing  $\mu$  from the isostatic Maxwell estimation  $z_c^{\min}(\mu = 0) = 2D = 4$  to  $z_c^{\min}(\mu = \infty) \geq D + 1 = 3$ . Error bar indicates the range from the largest  $z_c^{\min}(\mu)$  having no solution to the smallest  $z_c^{\min}(\mu)$  having solution. Data points represents the mean of the range. From (Bo et al., 2014).

where  $i$  are the sites of  $Z^d$ , the spins  $\sigma_i = \pm 1$ , and the sum is over nearest neighbor spins. The couplings  $J_{ij}$  are independent identically distributed random variables, and we assume their common distribution to be continuous and to have a finite mean.

A distinguishing property of spin glasses, which pertains to many complex systems including granular media, is that they feature a “rugged energy (or free energy) landscape”. To be more clear, let us consider a zero-temperature dynamics, where at each time step a spin is randomly chosen and flips if it lowers the energy, otherwise it does not move, until no more spins will flip. At variance with a pure ferromagnet, in the spin glass this dynamics arrests very quickly, and also at a quite high-energy state, the reason being due to, precisely, the abundance of metastable states. The type of metastable states concerned in this specific case are 1-SF metastable states, discussed in Section II.B and Fig. 4a, since they are reached following a dynamics that flips one spin at a time: when the system arrives in one of these configurations, no single spin can lower the energy by flipping, but if two neighboring spins are allowed to flip simultaneously, then lower energy states are available. In other words, 1-SF states are stable against a single spin-flip, but not necessarily against two (or more) simultaneous spins-flip. An example of one-spin-flip metastable state is shown in Fig. 24 along with a possible two-spin-flip move (shown in the lowest panel) needed to escape the

1-SF metastable trap. As discussed in Table I these 1-SF metastable states are analogous to the locally jammed states introduced by (Torquato and Stillinger, 2001) and called 1-PD in the table.

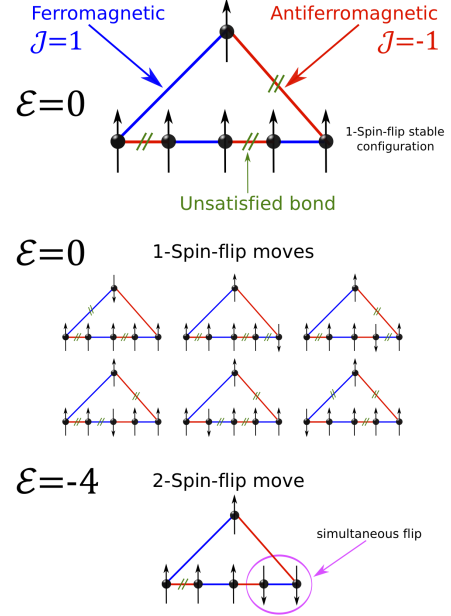


FIG. 24 Example of a 1-Spin flip stable configuration.

The concept of 1-SF metastable states can be easily extended to  $k$ -spin-flip ( $k$ -SF) metastable states, even without resorting to a specific dynamics, but using solely the Hamiltonian of the system Eq. (134) (Biroli and Monasson, 2000). We define a  $k$ -spin-flip metastable state as a (infinite volume) configuration whose energy cannot be lowered by flipping any connected subset of  $1, 2, \dots, k$  spins. In particular, the ground states of the system correspond to configurations whose energy cannot be lowered by flipping any finite number of spins, i.e., they are found in the limit  $k \rightarrow \infty$ , hence the ground state of the spin-glass is the  $\infty$ -SF state, Fig. 4a.

The  $k$ -SF metastable states are analogous to the  $k$ -PD metastable collective jamming states defined in Table I that generalize the concept of collective jamming in (Torquato and Stillinger, 2001). The corresponding ground state of jamming is then the  $\infty$ -PD state. We, thus, end up with a nice analogy between spin-glasses and jamming which we can leverage to harness the nature of metastable jammed states in terms of exact results for spin-glass metastable states obtained by (Newman and Stein, 1999).

It is important to see that the  $k$ -PD or  $k$ -SF states are hierarchically organized one inside another as seen in Fig. 4a. For instance, 2-PD (2-SF) metastable states form a subset of the 1-PD (1-SF) metastable states, since states which are 2-SF-stable are automatically 1-SF-stable, but

the converse is not necessarily true. Also, the energies of 2-SF metastable states may cross, in principle, the energies of 1-SF metastable states, Fig. 4a. This hierarchy defines the  $k$ -SF-core metastable states and the  $k$ -SF-shell: the 1-SF-shell consists of 1-SF metastable states which are not in 2-SF-core. In general, the  $k$ -SF-shell consists of  $k$ -SF metastable states which are not in the  $k+1$ -SF-core. The  $\infty$ -SF core is then the ground state.

Now we may ask: how do we visit the  $k$ -SF metastable states for  $k > 1$ ? To answer this question we need to introduce more precisely the concept of *dynamics*.

A  $k$ -spin-flips dynamics is defined in such a way that rigid flips of all lattice animals (finite connected subset of  $Z^d$ ) up to  $k$  spins can occur. For example, in the case  $k = 2$  both single-spin flips and rigid flips of all nearest neighbor pairs of spins are allowed (see the bottom panel in Fig. 24 as an example of a 2-SF move). At each step of the dynamics a lattice animal of size  $\ell \leq k$  is chosen at random with probability  $p_\ell$  and it flips if the resulting configuration has lower energy, otherwise it does not flip. We denote by  $\omega_k$  a given realization of this  $k$ -SF dynamics (Newman and Stein, 1999) and the ending metastable configuration of such a path as  $\vec{\sigma}_k^\infty$ .

Having defined the  $k$ -SF dynamics, we can now state an important rigorous result obtained by Newman and Stein (Newman and Stein, 1999): *every end state  $\vec{\sigma}_k^\infty$  of a dynamics  $\omega_k$  has the same energy density  $e_k$  (energy per site), which thus depends only on the choice of the  $k$ -SF dynamics. Therefore, once a given  $k$ -SF dynamics is chosen, almost all realizations  $\omega_k$  of this dynamics will end in configurations  $\vec{\sigma}_k^\infty$  having the same energy density. Furthermore, if we focus only on the states of energy  $e_k$  reachable by the dynamics we chose (which may not be all the available states with that energy), can we say something about the way they are sampled by the dynamics? The answer is yes, in that all these final states not only have the same energy, but they are *equiprobable*, i.e., they are reachable with the same probability as rigorously proved by (Newman and Stein, 1999). Due to the fact that the states reachable by the dynamics may not represent all the available states with that energy, then, this rigorous proof represent a weak proof of the Edwards uniform measure. The strong proof would imply that all states available at energy  $e_k$  are indeed accessed by the dynamics. We can explain graphically this point with the aid of Fig. 4a. Consider a given energy  $\epsilon_k$  and the corresponding set of  $k$ -SF/PD metastable states with energy  $\epsilon_k$ , i.e. the ones with complexity  $\Sigma_{kSF}(\epsilon_k)$ . The whole set of *available*  $k$ -SF/PD states with energy  $\epsilon_k$  forms the  $k$ -SF-core. Thus, the strong proof of the Edwards uniform measure would imply all the states in the  $k$ -SF-core to be *accessible* by the  $k$ -SF-dynamics.*

We thus arrive to the following important conclusions:

1. For a given choice of the dynamics, we can never visit all the available  $k$ -SF/PD metastable states,

because they span a continuous range of energies (or volume fractions) and, evidently, it does not make much sense to ask if we visit those states with equal probability, without further specifying their energy (or volume fraction).

2. If a given  $k$ -SF/PD dynamics visits all the metastable states in the  $k$ -SF/PD-core, then these states are also visited with the same probability.

In light of the conclusion 1. we may reformulate Edwards hypothesis for a particular  $k$ -PD state rather than for all the states (all  $k$ -PD states) together, saying that “when  $N$  grains occupy a volume  $V$ , they do so in such a way that all the  $k$ -PD metastable states corresponding to that volume  $V$  are equally weighted”.

From conclusion 2. we arrive to the real meaningful question and related Edwards’ conjecture, which is: *does a given dynamics, which terminates always in configurations having the same energy (or volume fraction), sample uniformly ALL the available metastable states at that given energy, i.e., the whole  $k$ SF/PD-core?*

As discussed in Sec. III.B there exist certain protocols that do not sample packing states with a uniform probability, therefore, Edwards hypothesis may not be provable correct for all possible protocols. Likewise, simulations of jammed states, for instance using LS algorithms (Lubachevsky and Stillinger, 1990), may not be able to provide an answer to this question for systems large enough to be of definitive value. Thus, in the next section we propose an exact calculation to test Edwards ergodic assumption in the exactly solvable Sherrington-Kirkpatrick model (Sherrington and Kirkpatrick, 1975), which is a mean-field model of a spin glass where the metastable states can be mathematically and precisely defined and allows for a rigorous test of Edwards hypothesis.

The Edwards hypothesis in a more general sense applies to granular matter and spin glasses and hard sphere glasses as well. Thus we explore this analogy in the next section to test Edwards ergodic hypothesis in more detail.

### C. Opening Pandora’s box: Test of Edwards uniform measure in the Sherrington-Kirkpatrick spin-glass model

As explained across this review, four recent (and not so recent) remarkable results have been achieved that support the validity of the uniform measure hypothesis for jammed states as proposed by Edwards:

1. The state-of-the-art simulations done in (Martini et al., 2017) allowing a direct computation of basin volumes of distinct jammed states, which confirm the validity of Edwards ergodicity at the jamming transition (Section III.B and Fig. 10).

2. The exact solution of the jammed ground state in infinite-dimensional fully-connected hard-sphere model done in (Charbonneau *et al.*, 2014b) using full replica symmetry breaking. The  $\infty$ -PD ground states stable under  $k$ -PD displacements with  $k \rightarrow \infty$  and  $N \rightarrow \infty$  and finite  $\alpha = k/N$  define the J-line ranging from  $\alpha = 0$  to  $\alpha = 1$  (see Fig. 4a), and are obtained using the Edwards uniform measure.
3. The analytical study in (Sharma *et al.*, 2016) of zero-temperature metastable minima in classical Heisenberg spin glass in a random magnetic field. Such a study confirms that the energy reached dynamically is in agreement with a computation of metastable states using Edwards equiprobability, see Eq. (12) in (Sharma *et al.*, 2016).
4. The rigorous results of Newman and Stein (Newman and Stein, 1999) probing a weaker formulation of Edwards uniform measure: the final states that a zero-temperature dynamics in spin-glass model arrive at a given energy are solely determined by the dynamical protocol and are accessed with equal probability for a given energy. The important fact is that for every protocol there are certain states with a given energy that are achievable and those states are equally probable. Although, the final states visited by the protocol may not be all the available states with that energy, hence the weak Edwards formulation.

Armed with these four results, we now propose to perform a fifth exact calculation to integrate them and provide another (most probably penultimate, perhaps final) test to the long-standing saga on the validity of the Edwards uniform measure (Fig. 4b). The test consists to validate the Edwards measure in the metastable states as done in (Sharma *et al.*, 2016), following the use of the Edwards assumption to calculate the ground state of the hard sphere model in (Charbonneau *et al.*, 2014b) and using the exact results of (Newman and Stein, 1999). This test can be done for the 1-SF metastable state in the exactly solvable Sherrington-Kirkpatrick (SK) spin-glass model (Sherrington and Kirkpatrick, 1975), which is the canonical mean field model of spin glasses. The interest in considering this particular model stems from the fact that it allows one to calculate analytically the metastable states using Edwards uniform measure. The results of this calculation then can be compared with the corresponding quantities measured in dynamical simulations of the SK model. Comparing exact measurements in the Edwards ensemble with dynamics provides the ideal testing ground to examine the applicability of Edwards predictions.

### 1. Penultimate test of Edwards in the SK model

The SK model is the infinite dimensional limit of the Edwards-Anderson model, whose Hamiltonian is akin to the one given in Eq. (134), but the sum runs over all  $N(N-1)/2$  pairs of distinct spins, becoming a solvable mean-field model:

$$\mathcal{H}_{\text{SK}}(\vec{\sigma}) = -\frac{1}{\sqrt{N}} \sum_{i,j=1}^N J_{ij} \sigma_i \sigma_j. \quad (135)$$

A key quantity which can be calculated exactly in the SK model is the ‘complexity’  $\Sigma(\epsilon)$  as a function of the energy density,  $\epsilon$ , as schematically shown in Fig. 4a (we only consider the system at zero temperature) (Bray and Moore, 1980). Physically, the complexity  $\Sigma(\epsilon)$  is defined as the logarithmic scaled number of metastable states  $\mathcal{N}_N(\epsilon)$  of a given energy density  $\epsilon$ :

$$\Sigma(\epsilon) = \lim_{N \rightarrow \infty} \frac{\log \mathcal{N}_N(\epsilon)}{N}, \quad (136)$$

where  $N$  is the size of the system (i.e. the number of spins). The word ‘scaled’ indicates that  $\Sigma(\epsilon)$  is the logarithm of  $\mathcal{N}_N(\epsilon)$  scaled by  $N$ .

We propose to solve the SK model for the 1-SF metastable states to obtain analytically their number  $\mathcal{N}_N(\epsilon)$ . From the ‘dynamic’ point of view, we consider a 1-SF dynamics at zero temperature, starting from a random initial configuration, sampled, for example, from a symmetric Bernoulli distribution. We can then apply the general results discussed above. Specifically, the 1-SF dynamics will arrest always in states (i.e. configurations) having the same energy (Newman and Stein, 1999), say  $\epsilon$ , and the number of such states, which we denote by  $\Gamma_N(\epsilon)$ , is exponentially large in the system size  $N$ . On the other side, from the ‘static’ point of view, we can calculate analytically the total number of available 1-SF metastable states of energy  $\epsilon$  under the Edwards uniform measure from Eq. (136), which is given precisely by  $\mathcal{N}_N(\epsilon) \sim e^{N\Sigma(\epsilon)}$  (Bray and Moore, 1980).

The Edwards ergodic hypothesis is: does the dynamically generated  $\Gamma_N(\epsilon)$  equal the static uniform averaged  $\mathcal{N}_N(\epsilon)$ :

$$\Gamma_N(\epsilon) \stackrel{\text{Edw}}{=} \mathcal{N}_N(\epsilon) ? \quad (137)$$

And, if so, does the dynamics pick up all the  $\mathcal{N}_N(\epsilon)$  states with the same probability?

If Edwards hypothesis is correct, then the answer to both these questions is affirmative. Actually, the first condition, i.e.  $\Gamma_N(\epsilon) = \mathcal{N}_N(\epsilon)$ , is also sufficient for the second to be true according to the exact results of Newman and Stein, point 4 above (Newman and Stein, 1999). However, measuring  $\Gamma_N(\epsilon)$  from the dynamics is not an



easy task, and hence we have to resort to another convenient quantity. A suitable, and easily measurable, observable to test Edwards hypothesis is the distribution of local fields  $P(h)$ . The local field  $h_i$  acting on spin  $i$  is defined as  $h_i = \frac{1}{\sqrt{N}} \sum_{j \neq i} J_{ij} \sigma_j$ , and, in a 1-SF stable configuration, all these local fields satisfy the condition  $h_i \sigma_i > 0$  for any  $i$  [see (Bray and Moore, 1980; Roberts, 1981) and Eq. (12) in (Sharma *et al.*, 2016)].

Thus, we arrive at a mathematically tractable definition of metastable 1-SF state in the SK model, which can be incorporated into the partition function of the SK model. This has been done in (Roberts, 1981) by considering the 1-SF condition  $h_i \sigma_i > 0$  by adding the constraint  $\Theta(\sum_{j \neq i} \sigma_i J_{ij} \sigma_j)$  in the partition function. Thus, the exact mean-field solution for  $P(h)$  for this 1-SF metastable state under the Edwards uniform measure can be obtained. We notice *en passant* that the work (Roberts, 1981) predates by a decade the Edwards formulation. Indeed, the validity of Edwards uniform measure has been debated in the spin glass community (Mézard and Parisi, 2003) earlier than in the granular community.

The number of 1-SF metastable states is then obtained from:

$$\mathcal{N}_N(\epsilon) = \sum_{\sigma} \delta \left( \epsilon + \frac{1}{\sqrt{N}} \sum_{i,j=1}^N J_{ij} \sigma_i \sigma_j \right) \prod_{i=1}^N \Theta \left[ \sigma_i \sum_{j \neq i} J_{ij} \sigma_j \right]. \quad (138)$$

Such a prediction can be then compared with the states dynamically obtained under a 1-SF dynamics from the SK model by using, for instance, a single-spin-flip Glauber dynamics as done in (Eastham *et al.*, 2006). Thus, a precise analytical test of Edwards ergodicity can be achieved in the SK model for metastable states. To perform similar test in a realistic model of granular matter would require a mathematical definition of 1-PD locally metastable states for jammed hard spheres analogous to 1-SF in the SK model, which eventually might be incorporated into the Edwards partition function of hard-spheres to test Edwards hypothesis in such a jammed model. Such an approach has already proven to be fruitful. In (Müller and Wyart, 2015), corresponding properties of the SK model and jammed hard spheres based on marginal stability have been derived by exploiting the analogy between a spin flip and the opening or closing of a particle contact.

Specifically, the test consists to compare the form of  $P(h)$  measured at the ending configurations of the 1-SF dynamics with the one predicted by Edwards uniform measure, in particular for small values of the local fields  $h \sim 0$ , which assumes the scaling form in analogy with the force distribution, Eq. (48):

$$P(h) \sim h^\alpha, \quad \text{for } h \rightarrow 0, \quad (139)$$

We note that a lower bound on the exponent  $\alpha$  can be already derived by imposing the stability of 1-SF

metastable states with respect to single spin-flips. The argument goes as follows: consider two spins  $\sigma_i$  and  $\sigma_j$ , along with their local fields  $h_i$  and  $h_j$  and their coupling  $J_{ij}$ . The energy cost to flip one spin, say  $\sigma_i$ , is given by  $\Delta E = 2|h_i| - 2J_{ij}\sigma_i\sigma_j$ . The non trivial case is realized when the bond  $J_{ij}$  is satisfied, i.e. when  $J_{ij}\sigma_i\sigma_j > 0$ , so that we have  $\Delta E = 2|h_i| - 2|J_{ij}|$ . Since this condition must be satisfied even by the smallest possible field  $h_i \sim N^{-1/(1+\alpha)}$ , and since  $|J_{ij}| \sim N^{-1/2}$ , then the stability condition  $\Delta E > 0$  of the 1-SF metastable state gives  $\alpha \geq 1$ . Therefore, the distribution  $P(h)$  must vanish at small fields like  $h^\alpha$  with an exponent  $\alpha$  not smaller than one. A direct dynamical measurement of  $P(h)$  in the final configurations of a 1-SF dynamics shows that  $P(h)$  indeed vanishes linearly for  $h \rightarrow 0$  (Eastham *et al.*, 2006):

$$P(h) \sim h, \quad \text{dynamics}, \quad (140)$$

i.e. the lower bound  $\alpha \geq 1$  is actually saturated.

On the other side, what is the form of  $P(h)$  calculated by using Edwards hypothesis on the equiprobability of all the available 1-SF metastable states of energy  $\epsilon$  from Eq. (138)?

The exact calculation of  $P(h)$  for the 1-SF metastable states using Edwards ensemble can be carried out. In fact, at the present,  $P(h)$  has been already obtained using the Edwards partition function Eq. (138) but only at the replica symmetry (RS) level in (Eastham *et al.*, 2006; Roberts, 1981). This calculation gives for  $h \rightarrow 0$ ,  $P(0) \propto \text{const} > 0$  in contradiction with the dynamical result Eq. (140). This result has led the authors of (Eastham *et al.*, 2006) to claim the failure of the Edwards hypothesis in the Sherrington-Kirkpatrick spin glass.

However, there is an inconsistency in the RS calculation of  $P(h)$  performed in (Eastham *et al.*, 2006; Roberts, 1981) in the fact that the RS calculation is exact only above a certain energy density  $\epsilon_c \sim -0.672...$  (Bray and Moore, 1980) (to the left of the full RSB transition at  $\alpha = 0$  in Fig. 4a), and ceases to be valid below that energy. But the energy  $\epsilon$  of the states selected by the 1-SF dynamics leading to Eq. (140) (and any protocol we are aware of) lies below the critical energy  $\epsilon_c$  ( $\epsilon < \epsilon_c$ ), where the RS calculation of  $P(h)$  is not correct. As a consequence, also the RS value of the intercept  $P(0)$  obtained in (Eastham *et al.*, 2006) is wrong. Therefore, the correct calculation to predict  $P(h)$  for energies  $\epsilon < \epsilon_c$  to obtain the exponent  $\alpha$  in Eq. (139) to be compared to the dynamical result  $\alpha = 1$  needs to be done by taking into account the effect of full RSB, as in the low temperature phase of the SK model to the right of the full RSB transition in Fig. 4a. This calculation has not been carried out yet (mainly because of its algebraic complexity) and could represent a strong theoretical test of the Edwards uniform measure at the mean-field level for 1-SF metastable states.

It should be noted that the analog of  $P(h)$  is the distribution of inter-particle forces  $P(f)$  in the hard-sphere model, Eq. (48). Now, in the hard-spheres model, a RS calculation of  $P(f)$  gives  $P(0) > 0$  (Bo *et al.*, 2014), i.e., a finite intercept at zero force, and even the 1-RSB solution (i.e. the solution accounting for just the first level in the hierarchical breaking of replica symmetry) gives  $P(0) > 0$  as well (Parisi and Zamponi, 2010), as discussed in Eq. (132). Only at the full-RSB level one finds the correct behavior (Charbonneau *et al.*, 2014b):  $P(f) \sim f^\theta$  with  $\theta = 0.42$ , Eq. (133), and  $P(0) = 0$ .

In light of these results, we expect that the full RSB calculation of  $P(h)$  for 1-SF in the SK model will be needed as well to obtain the correct scaling. This calculation is based on similar calculations done by Bray and Moore in (Eastham *et al.*, 2006) that goes back to old controversies regarding equiprobability of metastable states in the spin-glass field that started with (Roberts, 1981), see Fig. 7 in (Mézard and Parisi, 2003). We recognize that the behavior of  $P(f)$  is not a direct measure of the equiprobability. However,  $P(f)$  is the most accessible calculation that can be done to test the predictions of Edwards theory.

## VI. CONCLUSIONS AND OUTLOOK

More than 25 years after Edwards original hypothesis on the entropy of granular matter, it becomes increasingly evident that the consequences of Edwards simple statement are far reaching. For one, it allows us to understand the properties of jammed granular matter — one of the paradigms of athermal matter states — by analogy with thermal equilibrium systems. The first-order transition of jammed spheres identified within Edwards' thermodynamics (Jin and Makse, 2010) is reminiscent of the entropy induced phase transition of equilibrium hard spheres, which is found at  $\phi = 0.494$  and  $\phi = 0.545$ , respectively. Despite this analogy, the physical origins of these two transitions are fundamentally different: the equilibrium phase transition is a consequence of the maximization of the conventional entropy, while the transition at RCP of jammed spheres is driven by the competition between volume minimization and maximization of the entropy of jammed configurations, Eq. (8).

Such an analogy can probably be extended to other disorder-order phase transition observed in equilibrium systems. Anisotropic elongated particles, e.g., exhibit transitions between isotropic and nematic phases: For large  $\alpha$ , Onsager's theory of equilibrium hard rods predicts a first order isotropic-nematic transition with freezing point at the rescaled density  $\phi\alpha = 3.29$  and melting point at  $\phi\alpha = 4.19$  (Onsager, 1949). By analogy with the case of jammed spheres, one might wonder whether packings of non-spherical particles exhibit similar transitions that could be characterized in the  $z$ - $\phi$  phase di-

agram. Packings of hard thin rods indeed satisfy a scaling law, where the RCP has been experimentally identified at  $\phi\alpha \approx 5.4$  (Philippe, 1996). Dynamically, transitions to orientationally ordered states can be induced in rod systems by shaking (Yadav *et al.*, 2013), but the entropic characterization of such transitions remains an open problem.

For colloidal suspensions of more complex shapes like polyhedra, both liquid crystalline as well as plastic crystalline and even quasicrystalline phases have been found (Agarwal and Escobedo, 2011; Damasceno *et al.*, 2012; Haji-Akbari *et al.*, 2009; Marechal and Löwen, 2013). Entropic concepts based on shape are only starting to be explored even for equilibrium systems (van Anders *et al.*, 2014; Cohen *et al.*, 2016; Escobedo, 2014). In the jammed regime, the behavior of packing density as a function of shape has been shown to be exceedingly complex (Chen *et al.*, 2014). Edwards granular entropy might be the key to understand such empirical data on a more fundamental level.

Our approach based on the self-consistent equation (123) can be applied to a large variety of both convex and non-convex shapes. The key is to parametrize the Voronoi boundary between two such shapes, which allows for the calculation of the Voronoi excluded volume and surface. In fact, analytical expressions for the Voronoi boundary can be derived following an exact algorithm for arbitrary shapes by decomposing the shape into overlapping and intersecting spheres (see Figs. 17 and 25). Therefore, a systematic search for maximally dense packings in the space of given object shapes can be performed using our framework. Extensions to mixtures and polydisperse packings can also be formulated. This might elucidate in particular the validity of Ulam's conjecture that the sphere is the worst packing object in 3d (Gardner, 2001), which has also been formulated in a random version (Jiao and Torquato, 2011) locally around the sphere shape (Kallus, 2016).

Thus, the Edwards' approach could help generally to elucidate how macroscopic properties of granular matter arise from the anisotropy of the constituents — one of the central questions in present day materials science (Glotzer and Solomon, 2007). A better understanding of this problem will facilitate, e.g., the engineering of new functional materials with particular mechanical responses by tuning the shape of the building blocks (Athanasiadis *et al.*, 2014; Jaeger, 2015) or to new ways to construct space filling tilings (Andrade *et al.*, 2005; Herrmann *et al.*, 1990). Edwards statistical mechanics might be the key to tackle these problems guided by theory rather than direct simulations.

We postulate that a unifying theoretical framework can predict not only the structural properties (volume fraction and coordination number), but also mechanical properties (vibrational density of states and yield stress) and dissipative properties (damping) as a function of the

shape and interaction properties (e.g., friction) of the constitutive particles. If such an approach is possible, then one could envision to span the large parameter space of the problem from a theoretical point of view to obtain predictions of optimal packings with desired properties. The penalty for approaching the problem theoretically rather than by a direct numerical generation of the packings as with reverse-engineering evolutionary algorithms (Miskin and Jaeger, 2013) is that results are obtained theoretically at the mean-field level. Thus, predictions of the resulting optimal shapes can only be approximate.

On the other hand, it might be possible to develop a theory versatile enough to encompass a large portion of the parameter space which cannot be easily accessed by the direct simulation of packing protocols in reverse engineering. Such a theory might explore particles made by rigidly gluing spheres in arbitrary shapes, and also other generic shapes such as (a) union of spheres of arbitrary radius, (b) intersection of spheres of arbitrary radius leading to tetrahedral-like particles and in general (c) any irregular polyhedra, Fig. 17. Another advantage is the ability to possibly span over more than one relevant property of granular materials, not only density but also yield stress and dissipation. Furthermore, such an approach would include interparticle friction, a property that was not considered before, yet, it is of crucial importance in granular packings.

Additional insight can be provided by analytically solvable models that take into account realistic excluded volume effects due to non-spherical shapes. The recent solution of the ‘Paris car parking problem’, e.g., reveals the existence of two shape universality classes that are manifest in different exponents in the asymptotic approach to jamming (Baule, 2017).

On the more fundamental side of things, the controversy on the validity of Edwards’ statistical mechanics has been caused by different interpretations of Edwards’ laconic statement (Edwards, 1994): “We assume that when  $N$  grains occupy a volume  $V$  they do so in such a way that all configurations are equally weighted. We assume this; it is the analog of the ergodic hypothesis of conventional thermal physics.”

As regards the veracity of this statement, it is not rigorously established not disproved yet. We have reviewed the recent encouraging results of (Charbonneau *et al.*, 2014b; Martiniani *et al.*, 2017; Newman and Stein, 1999; Sharma *et al.*, 2016) and have proposed a calculation for the 1-SF states in the SK model. Besides, one must not be fooled by believing that a statistical mechanics description of granular media is a least well-founded branch of theoretical physics, if only one remembers that almost every branch of theoretical physics is lacking ‘rigorous proofs’, although this is not considered as an inappropriate foundation for such branches. The main issue with Edwards’ statement, and the reason why it will be likely hard to reach an end to the diatribe, is that the state-

ment, as it stands, is incomplete.

From a broad standpoint, the problem is whether it is possible to describe the properties of the asymptotic states of the dynamics by using only static features of the system. In Edwards’ statement there is no reference at all to which are those asymptotic dynamic states. To solve this issue, we have proposed a rigorous definition of jammed states as those configurations satisfying the geometrical hard-core and mechanical force and torque balances constraints. Then we have further classified those jammed states on the basis of their stability properties under  $k$ -Particle-Displacements, inspired by an analogous characterization of (energetically) metastable states in spin glasses through the concept of  $k$ -Spin-Flips. With this definition of the asymptotic dynamic states, we redefined (in italics) Edwards’ ensemble by the following proposition:

“We assume that when  $N$  grains occupy a volume  $V$  they do so in such a way that all stable jammed configurations *in a given  $k$ -PD jamming category (i.e. at given volume fraction)* are equally weighted. We assume this; it is the analogue of the ergodic hypothesis of conventional thermal physics (and also out-of-equilibrium spin glasses and hard-sphere glasses).”

This statement also clarifies the role of the protocol, i.e. of the dynamics, in the Edwards’ ensemble. A “legal” protocol is the one for which the asymptotic dynamic states are in a given  $k$ -PD-core. This is, again, motivated by a spin-glass analogy. In this case an example of correct protocol is, for instance, a single-spin-flip Glauber dynamics, for which the asymptotic dynamic states are in the 1-SF-core and all have the same energy. In the granular framework this is equivalent to say that the asymptotic jammed states of a legal protocol are only the  $k$ -PD metastable states (with a fixed  $k$ , for instance the 1-PD), and they (presumably) have the same volume. Then the question of whether these states are statistically equivalent (i.e. equiprobable) remains still open, and we have suggested a model (SK) where an end-to-end comparison between the results of dynamics and a static computation can be performed, in principle, in an exact analytical way.

An “illegal” protocol is one that mixes different  $k$ -PD metastable states, i.e., whose asymptotic dynamic states have different values of  $k$ , and hence different stability properties. Nothing can be claimed for such illegal protocols. In the case of legal protocols, it has been rigorously proved in spin glasses that statistical equivalence of the asymptotic dynamic states of the given protocol holds true, i.e., the  $k$ -SF visited by a given dynamics are indeed equiprobable (Newman and Stein, 1999). Whether this statement is also rigorous for jammed states is an open question, but the correctness in spin glasses points towards an affirmative answer. The stronger claim that

the asymptotic dynamic states are also the totality of  $k$ -PD ( $k$ -SF) metastable states with given volume fraction (energy density) is not analytically proved or disproved for any model we are aware of.

Conversely, in the strong tapping regime, the statistical equivalence of the asymptotic dynamic states cannot be claimed. Notwithstanding, this does not preclude the use of Edwards' ensemble as a very principled approximation supposedly more justified than other mean-field approaches. *A fortiori*, the great advantage of Edwards' approach is that it leads to concrete quantitative predictions for realistic packing scenarios. As we discuss in detail in Sec. IV, the volume ensemble in the Voronoi convention allows us to treat packings of frictional and frictionless particles, adhesive and non-adhesive, granular and colloidal sizes, mono-disperse and poly-disperse, in 2d, 3d and beyond, as well as spherical and non-spherical shapes within a unified framework. Such a comprehensive treatment is currently out of reach for any other approach that can treat glassy and/or jammed systems analytically, such as mode-coupling theory (Götze, 2009) or replica theory (Charbonneau *et al.*, 2014b; Parisi and Zamponi, 2010). Moreover, the analytical efforts needed to extend these theories to incorporate, for instance, friction or anisotropies may be unsurmountable. The verdict on Edwards' Alexandrian solution to this Gordian Knot, as on every physical theory, should be returned, ultimately, on the goodness of its predictions when compared with experimental data and practical applications.

## ACKNOWLEDGMENTS

AB acknowledges funding under EPSRC grant EP/L020955/1. FM and HAM acknowledge funding from NSF (Grant No. DMR-1308235) and DOE Geosciences Division (Grant No. DE-FG02-03ER15458). We are grateful to the following scientists whom, over the years, have shaped our vision of the granular problem: J. S. Andrade Jr., L. Bo, T. Boutreux, J. Brujić, S. F. Edwards, P.-G. de Gennes, N. Gland, S. Havlin, J. T. Jenkins, Y. Jin, D. L. Johnson, J. Kurchan, S. Li, G. Parisi, R. Mari, L. La Ragnone, M. Shattuck, C. Song, H. E. Stanley, M. S. Tomassone, J. J. Valenza, K. Wang, and P. Wang. We are grateful for comments on the review by: R. Blumenfeld, J.-P. Bouchaud, B. Chakraborty, P. Charbonneau, S. Franz, G. Gradenigo, S. Martiniani, M. Moore, C. O'Hern, G. Parisi, M. Saadatfar, M. Shattuck, M. Sperl, M. Wyart, A. Zaccone, and F. Zamponi. We also thank B. Behringer, S. Martiniani and S. Nagel for the permission to use their images.

## Appendix A: Bounds on the average coordination number

A packing is geometrically rigid if it can not be deformed under any translation or rotation of the particles without deforming the particles or breaking any of the contacts (Alexander, 1998). In  $d$  dimensions, there are  $d$  force balance equations Eq. (2) and  $d(d-1)/2$  torque balance equations Eq. (3). The number of equations can in general be associated with the configurational degrees of freedom (dofs), so that per particle we have in total  $d_f = d(d+1)/2$  configurational dofs.

Geometrical rigidity requires that all  $Nd_f$  degrees of freedom in the packing are constrained by contacts (assuming periodic boundary conditions). For frictional particles there are  $d$  force components at contact and since all contacts are shared by two particles we thus require  $Ndz/2 \geq Nd_f$  or

$$z \geq 2d_f/d = d + 1. \quad (\text{A1})$$

For frictionless particles there is only a single force component at each contact due to Eq. (4): The normal unit vector is fixed by  $\mathbf{d}_a^i$ . The equivalent rigidity condition is thus  $Nz/2 \geq Nd_f$  or

$$z \geq 2d_f. \quad (\text{A2})$$

For frictionless spheres the normal unit vector is parallel to  $\mathbf{d}_a^i$  so that Eqs. (3) are always trivially satisfied. In this case  $d_f = d$ , which corresponds to the translational dofs since rotations are irrelevant.

If Eqs. (A1,A2) are not satisfied there exist zero energy modes (so called floppy modes) that can deform the packing without any energy cost. If the equalities hold, i.e.,  $z = d + 1$  for frictional particles and  $z = 2d_f$  for frictionless particles,

On the other hand, we can obtain an upper bound on  $z$  by imposing that a generic disordered packing will have the minimal number of contacts. If any two particles precisely touch at a single point without deformation, we find that a single contact fixes one component of the vector connecting the two center of masses. Overall, there are then  $Nz/2$  constraints on the configurational dofs from touching contacts. From the constraint  $Nz/2 \leq Nd_f$  we obtain

$$z \leq 2d_f \quad (\text{A3})$$

for both frictional and frictionless particles. Note that for particles interacting with a soft potential the touching condition can only be satisfied at zero pressure. Likewise, realistic hard particles usually suffer slight deformations when jammed, complicating the analysis (Donev *et al.*, 2007; Roux, 2000)

## Appendix B: Density of states $g(z)$

The density of states  $g(z)$  can be calculated using analogies with a quantum mechanical system in three



steps:

(i) First, we consider that the packing of hard spheres is jammed in a  $\infty$ -PD configuration where there can be no collective motion of any contacting subset of particles leading to unjamming when including the normal and tangential forces between the particles. As discussed in the introduction, this jammed state is the ground state and corresponds to the collectively jammed category proposed in (Torquato and Stillinger, 2001). While the degrees of freedom are continuous, the fact that the packing is collectively jammed implies that the jammed configurations in the volume space are not continuous. Otherwise there would be a continuous transformation in the position space that would unjam the system contradicting the fact that the packing is collectively jammed. Thus, we consider that the configuration space of jammed matter is discrete, since we cannot change one configuration to another in a continuous way. A similar consideration of discreteness has been studied in (Torquato and Stillinger, 2001).

(ii) Second, we refer to the dimension per particle of the configuration space as  $\mathcal{D}$  and consider that the distance between two jammed configurations is not broadly distributed (meaning that the average distance is well-defined). We call the typical (average) distance between configurations in the configuration space as  $h_z$ , and therefore the number of configurations per particle is proportional to  $(h_z)^{-\mathcal{D}}$ . The constant  $h_z$  plays the role of Planck's constant in quantum mechanics which sets the discreteness of the phase space via the uncertainty principle.

(iii) Third, we add  $z$  constraints per particle due to the fact that the particle is jammed by  $z$  contacts. Thus, there are  $Nz$  position constraints ( $|r_{ij}| = 2R$ ) for a jammed state of hard spheres as compared to the unjammed “gas” state. Therefore, the number of degrees of freedom is reduced to  $\mathcal{D} - z$ , and the number of configurations is then  $1/(h_z)^{\mathcal{D}-z}$  leading to

$$g(z) = (h_z)^{z-\mathcal{D}}. \quad (\text{B1})$$

Note that the factor  $(h_z)^{-\mathcal{D}}$  will drop out when performing ensemble averages. Physically, we expect  $h_z \ll 1$ . The exact value of  $h_z$  can be determined by a fitting of the theoretical values to the simulation data, but it is not important as long as we take the limit at the end:  $h_z \rightarrow 0$ .

### Appendix C: Algorithm to calculate Voronoi boundaries analytically

Every segment of the VB arises due to the Voronoi interaction between a particular sphere on each of the two particles, reducing the problem to identifying the correct spheres that interact (see Fig. 25). The spheres that interact are determined by separation lines given as the

VBs between the spheres in the filling. For dimers, there is one separation line for each object, tessellating space into four areas, in which only one interaction is correct (Fig. 25a). The dense overlap of spheres in spherocylinders leads to a line as effective Voronoi interaction at the centre of the cylindrical part. This line interaction has to be separated from the point interactions due to the centres of the spherical caps as indicated. Overall, the two separation lines for each object lead to a tessellation of space into nine different areas, where only one of the possible line-line, line-point, point-line, and point-point interactions is possible (Fig. 25b).

The spherical decomposition of ellipsoid-like lens-shaped particles is analogous to dimers, only that now the opposite sphere centres interact (“anti-points”). In addition, the positive curvature at the intersection point leads to an additional line interaction, which is a circle in 3d (a point in 2d) and indicated here by two points. The separation lines are then given by radial vectors through the intersection point/line. The Voronoi interaction between two ellipsoids is thus given by two pairs of two anti-points and a line, which is the same class of interactions as spherocylinders. The different point and line interactions are separated analogously to spherocylinders, as shown in Fig. 25c.

## REFERENCES

- Abreu, C., F. Tavares, and M. Castier (2003), *Powder Technol.* **134**, 167.
- Agarwal, U., and F. A. Escobedo (2011), *Nature Mater.* **10**, 230.
- Alexander, S. (1998), *Phys. Rep.* **296**, 65.
- Alonso-Marroquín, F., and H. J. Herrmann (2004), *Phys. Rev. Lett.* **92**, 054301.
- van Anders, G., D. Klotsa, N. K. Ahmed, M. Engel, and S. C. Glotzer (2014), *Proc. Nat. Acad. Sci.* **111**, E4812.
- Andrade, J. S., H. J. Herrmann, R. F. S. Andrade, and L. R. da Silva (2005), *Phys. Rev. Lett.* **94**, 018702.
- Anikeenko, A. V., and N. N. Medvedev (2007), *Phys. Rev. Lett.* **98**, 235504.
- Anikeenko, A. V., N. N. Medvedev, and T. Aste (2008), *Phys. Rev. E* **77**, 031101.
- Aristoff, D., and C. Radin (2009), *J. Stat. Phys.* **135**, 1.
- Asenjo, D., F. Paillusson, and D. Frenkel (2014), *Phys. Rev. Lett.* **112**, 098002.
- Aste, T. (2005), *J. Phys. Cond. Mat.* **17**, S2361.
- Aste, T. (2006), *Phys. Rev. Lett.* **96**, 018002.
- Aste, T., and A. Coniglio (2004), *Europhys. Lett.* **67**, 165.
- Aste, T., and T. Di Matteo (2008a), *Phys. Rev. E* **77**, 021309.
- Aste, T., and T. Di Matteo (2008b), *Eur. Phys. J. B* **64**, 511.
- Aste, T., T. Di Matteo, M. Saadatfar, T. J. Senden, M. Schröter, and H. L. Swinney (2007), *Europhys. Lett.* **79**, 24003.
- Aste, T., M. Saadatfar, A. Sakellariou, and T. Senden (2004), “Investigating the geometrical structure of disordered sphere packings,” in *Proceedings of the International Conference New Materials and Complexity*, Vol. 339, pp. 16 – 23.

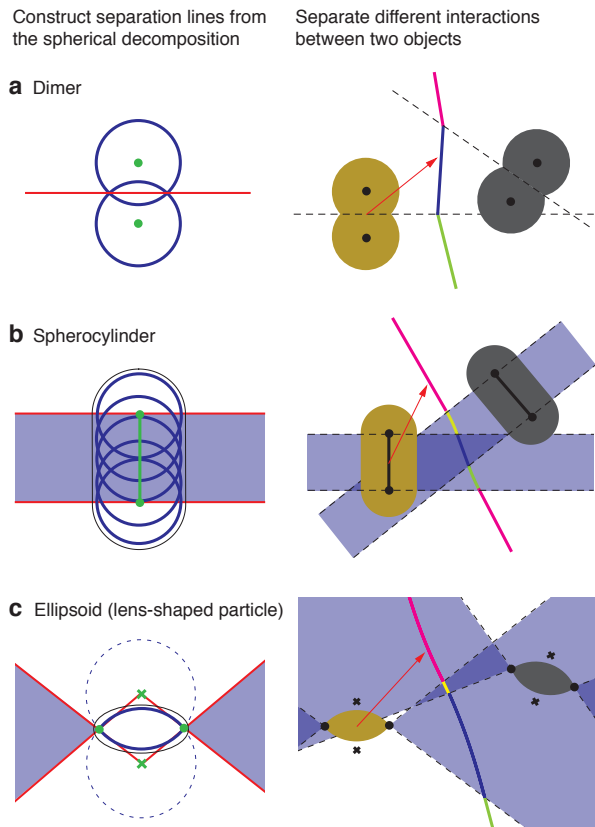


FIG. 25 (Colors online) Exact algorithm to obtain analytical expressions for the VB from the construction of separation lines (Baule *et al.*, 2013). (a) For dimers, the two separation lines identify the correct surface out of four possible ones. The pink part of the VB, e.g., is the VB between the two upper spheres. (b) For spherocylinders, the line-line, line-point, point-line, and point-point interactions lead to nine different surfaces that are separated by four lines. The yellow part of the VB, e.g., is due to the upper point on spherocylinder 1 and the line of 2. Regions of line interactions are indicated by blue shades. (c) For lens-shaped particles the separation lines are given by radial vectors through the intersection line of the sphere segments (shown as points in 2d). The different point and line interactions are separated analogously to spherocylinders, as shown. From (Baule *et al.*, 2013).

Aste, T., M. Saadatfar, and T. Senden (2005), *Phys. Rev. E* **71**, 061302.  
Aste, T., M. Saadatfar, and T. J. Senden (2006), *J. Stat. Mech.*, P07010.  
Athanassiadis, A. G., M. Z. Miskin, P. Kaplan, N. Rodenberg, S. H. Lee, J. Merritt, E. Brown, J. Amend, H. Lipson, and H. M. Jaeger (2014), *Soft Matter* **10**, 48.  
Atkinson, S., F. H. Stillinger, and S. Torquato (2014), *Proc. Nat. Acad. Sci.* **111**, 18436.  
Aurenhammer, F. (1991), *ACM Computing Surveys* **23**, 345.  
Bagi, K. (1997), “Analysis of micro-variables through entropy principles,” in *Powders and Grains 97*, edited by R. P. Behringer and J. T. Jenkins, pp. 251–254.  
Bagi, K. (2003), *Granular Matter* **5**, 45.  
Baker, J., and A. Kudrolli (2010), *Phys. Rev. E* **82**, 061304.

Ball, R., and R. Blumenfeld (2002), *Phys. Rev. Lett.* **88**, 115505.  
Baranau, V., S.-C. Zhao, M. Scheel, U. Tallarek, and M. Schröter (2016), *Soft Matter* **12**, 3991.  
Bargiel, M. (2008), *Computational Science–ICCS2008* **5102**, 126.  
Barrat, A., J. Kurchan, V. Loreto, and M. Sellitto (2000), *Phys. Rev. Lett.* **85**, 5034.  
Baule, A. (2017), *Phys. Rev. Lett.* **119**, 028003.  
Baule, A., and H. A. Makse (2014), *Soft Matter* **10**, 4423.  
Baule, A., R. Mari, L. Bo, L. Portal, and H. A. Makse (2013), *Nature Commun.* **4**, 2194.  
Becker, V., and K. Kassner (2015), *Phys. Rev. E* **92**, 052201.  
Becker, V., and K. Kassner (2017), *Phys. Rev. Lett.* **119**, 039801.  
Bellon, L., and S. Ciliberto (2002), *Physica D* **168–169**, 325.  
Berg, J., S. Franz, and M. Sellitto (2002), *Eur. Phys. J. B* **26**, 349.  
Bernal, J. D. (1960), *Nature* **185**, 68.  
Bernal, J. D. (1964), *Proc. Roy. Soc. London Ser. A* **280**, 299.  
Bernal, J. D., and J. Mason (1960), *Nature* **188**, 910.  
Berryman, J. G. (1983), *Phys. Rev. A* **27**, 1053.  
Berthier, L., J.-L. Barrat, and J. Kurchan (2000), *Phys. Rev. E* **61**, 5464.  
Bi, D., S. Henkes, K. E. Daniels, and B. Chakraborty (2015), *Annual Review of Condensed Matter Physics* **6**, 63.  
Biazzo, I., F. Caltagirone, G. Parisi, and F. Zamponi (2009), *Phys. Rev. Lett.* **102**, 195701.  
Biroli, G., and R. Monasson (2000), *EPL (Europhysics Letters)* **50** (2), 155.  
Blum, J., R. Schröpfer, B. J. R. Davidsson, and J. M. Trigo-Rodríguez (2006), *The Astrophysical Journal* **652**, 1768.  
Blumenfeld, R., S. Amitai, J. F. Jordan, and R. Hihinashvili (2016), *Phys. Rev. Lett.* **116**, 148001.  
Blumenfeld, R., and S. Edwards (2003), *Phys. Rev. Lett.* **90**, 10.1103/PhysRevLett.90.114303.  
Blumenfeld, R., and S. Edwards (2006), *Eur. Phys. J. E* **19**, 23.  
Blumenfeld, R., and S. F. Edwards (2009), *J. Phys. Chem. B* **113**, 3981.  
Blumenfeld, R., J. F. Jordan, and S. F. Edwards (2012), *Phys. Rev. Lett.* **109**, 238001.  
Bo, L., R. Mari, C. Song, and H. A. Makse (2014), *Soft Matter* **10**, 7379.  
Bohannon, J. (2017), *Science* **355** (6324), 470.  
Boissonat, J. D., C. Wormser, and M. Yvinec (2006), in *Effective Computational Geometry for Curves and Surfaces*, Mathematics and Visualization, edited by J. D. Boissonnat and M. Teillaud (Springer) p. 67.  
Borzsanyi, T., and R. Stannarius (2013), *Soft Matter* **9**, 7401.  
Bouchaud, J.-P. (2002), “Granular media: Some ideas from statistical physics,” in *Slow Relaxations and Nonequilibrium Dynamics in Condensed Matter*, Les Houches Lecture Notes, Vol. 77, edited by J.-L. Barrat, M. Feigelman, J. Kurchan, and J. Dalibard, Chap. 4 (Springer-Verlag) pp. 131–197.  
Bovet, A., F. Morone, and H. A. Makse (2016), ArXiv e-prints [arXiv:1610.01587](https://arxiv.org/abs/1610.01587).  
Bowles, R. K., and S. S. Ashwin (2011), *Phys. Rev. E* **83**, 031302.  
Bray, A. J., and M. A. Moore (1980), *Journal of Physics C: Solid State Physics* **13** (19), L469.  
Brey, J., A. Prados, and B. Sanchez-Rey (2000), *Physica A*

- 275**, 310 .
- Briscoe, C., C. Song, P. Wang, and H. A. Makse (2008), *Phys. Rev. Lett.* **101**, 188001.
- Briscoe, C., C. Song, P. Wang, and H. A. Makse (2010), *Physica A* **389**, 3978.
- Brouwers, H. J. H. (2006), *Phys. Rev. E* **74**, 031309.
- Brujić, J., S. Edwards, D. Grinev, I. Hopkinson, D. Brujić, and H. Makse (2003a), *Farad. Disc.* **123**, 207.
- Brujić, J., S. Edwards, I. Hopkinson, and H. Makse (2003b), *Physica A* **327**, 201.
- Brujić, J., C. Song, P. Wang, C. Briscoe, G. Marty, and H. A. Makse (2007), *Phys. Rev. Lett.* **98**, 248001.
- Brujić, J., P. Wang, C. Song, D. L. Johnson, O. Sindt, and H. A. Makse (2005), *Phys. Rev. Lett.* **95**, 128001.
- Caglioti, E., V. Loreto, H. Herrmann, and M. Nicodemi (1997), *Phys. Rev. Lett.* **79**, 1575.
- Cates, M., J. Wittmer, J. Bouchaud, and P. Claudin (1998), *Phys. Rev. Lett.* **81**, 1841.
- Cates, M. E., and V. N. Manoharan (2015), *Soft Matter* **11**, 6538.
- Chaikin, P. M., A. Donev, W. Man, F. H. Stillinger, and S. Torquato (2006), *Ind. Eng. Chem. Res.* **45**, 6960.
- Chakraborty, B. (2010), *Soft Matter* **6**, 2884.
- Chakravarty, A., S. Edwards, D. Grinev, M. Mann, T. Phillipson, and A. Walton (2003), in *Proceedings of the Workshop on the Quasi-static Deformations of Particulate Materials*.
- Charbonneau, P., E. I. Corwin, G. Parisi, A. Poncet, and F. Zamponi (2015a), ArXiv e-prints [arXiv:1512.09100](https://arxiv.org/abs/1512.09100) [cond-mat.dis-nn].
- Charbonneau, P., E. I. Corwin, G. Parisi, and F. Zamponi (2012), *Phys. Rev. Lett.* **109**, 205501.
- Charbonneau, P., E. I. Corwin, G. Parisi, and F. Zamponi (2015b), *Phys. Rev. Lett.* **114**, 125504.
- Charbonneau, P., J. Kurchan, G. Parisi, P. Urbani, and F. Zamponi (2014a), *J. Stat. Mech.* **2014**, P10009.
- Charbonneau, P., J. Kurchan, G. Parisi, P. Urbani, and F. Zamponi (2014b), *Nature Commun.* **5**, 3725.
- Charbonneau, P., J. Kurchan, G. Parisi, P. Urbani, and F. Zamponi (2017), *Annual Review of Condensed Matter Physics* **8** (1), 265.
- Chaudhuri, P., L. Berthier, and S. Sastry (2010), *Phys. Rev. Lett.* **104**, 165701.
- Chen, E. R., D. Klotz, M. Engel, P. F. Damasceno, and S. C. Glotzer (2014), *Phys. Rev. X* **4**, 011024.
- Chen, S., S. Li, W. Liu, and H. A. Makse (2016), *Soft Matter* **12**, 1836.
- Ciamarra, M. P. (2007), *Phys. Rev. Lett.* **99**, 089401.
- Ciamarra, M. P., and A. Coniglio (2008), *Phys. Rev. Lett.* **101**, 10.1103/PhysRevLett.101.128001.
- Ciamarra, M. P., A. Coniglio, and A. de Candia (2010), *Soft Matter* **6**, 2975.
- Ciamarra, M. P., A. Coniglio, and M. Nicodemi (2006), *Phys. Rev. Lett.* **97**, 158001.
- Cinacchi, G., and S. Torquato (2015), *The Journal of Chemical Physics* **143**, 224506.
- Clarke, A. S., and H. Jónsson (1993), *Phys. Rev. E* **47**, 3975.
- Clarke, A. S., and J. D. Wiley (1987), *Phys. Rev. B* **35**, 7350.
- Clusel, M., E. I. Corwin, A. O. N. Siemens, and J. Brujić (2009), *Nature* **460**, 611.
- Cohen, A. P., S. Dorosz, A. B. Schofield, T. Schilling, and E. Sloutskin (2016), *Phys. Rev. Lett.* **116**, 098001.
- Coniglio, A., A. de Candia, A. Fierro, M. Nicodemi, and M. Tarzia (2004), *Physica A* **344**, 431.
- Coniglio, A., A. Fierro, and M. Nicodemi (2002), *Eur. Phys. J. E* **9**, 219.
- Coniglio, A., and H. Herrmann (1996), *Physica A* **225**, 1 .
- Coniglio, A., and M. Nicodemi (2000), *J. Phys. Cond. Mat.* **12**, 6601.
- Coniglio, A., and M. Nicodemi (2001), *Physica A* **296**, 451.
- Conway, J., and N. J. A. Sloane (1999), *Sphere packings, Lattices and Groups*, 3rd ed., A series of comprehensive mathematics, Vol. 290 (Springer, New York).
- Corwin, E., H. Jaeger, and S. Nagel (2005), *Nature* **435**, 1075.
- Corwin, E. I., M. Clusel, A. O. N. Siemens, and J. Brujić (2010), *Soft Matter* **6**, 2949.
- Cremona, L. (1890), *Graphical statics: two treatises on the graphical calculus and reciprocal figures in graphical statics* (Clarendon Press).
- Crisanti, A., and L. Leuzzi (2006), *Phys. Rev. B* **73**, 014412.
- Crisanti, A., and F. Ritort (2003), *J. Phys. A* **36**, R181.
- Cugliandolo, L. F. (2011), *J. Phys. A* **44**, 483001.
- Cugliandolo, L. F., J. Kurchan, and L. Peliti (1997), *Phys. Rev. E* **55**, 3898.
- Damasceno, P. F., M. Engel, and S. C. Glotzer (2012), *Science* **337**, 453.
- Danisch, M., Y. Jin, and H. A. Makse (2010), *Phys. Rev. E* **81**, 051303.
- Dauchot, O. (2007), “Glassy behaviours in athermal systems, the case of granular media: A tentative review,” in *Ageing and the Glass Transition*, Lecture Notes in Physics, Vol. 716, edited by M. Henkel, M. Pleimling, and R. Sanctuary (Springer) pp. 161–206.
- Dean, D., and A. Lefevre (2003), *Phys. Rev. Lett.* **90**, 10.1103/PhysRevLett.90.198301.
- Dean, D. S., and A. Lefèvre (2001), *Phys. Rev. Lett.* **86**, 5639.
- DeGiuli, E., A. Laversanne-Finot, G. During, E. Lerner, and M. Wyart (2014a), *Soft Matter* **10**, 5628.
- DeGiuli, E., E. Lerner, C. Brito, and M. Wyart (2014b), *Proc. Nat. Acad. Sci.* **111**, 17054.
- DeGiuli, E., E. Lerner, and M. Wyart (2015), *The Journal of Chemical Physics* **142** (16), 164503.
- Delaney, G. W., T. Di Matteo, and T. Aste (2010), *Soft Matter* **6**, 2992.
- Delaney, G. W., D. Weaire, S. Hutzler, and S. Murphy (2005), *Philos. Mag. Lett.* **85**, 89.
- Desmond, K. W., and E. R. Weeks (2014), *Phys. Rev. E* **90**, 022204.
- Dieterich, E., J. Camunas-Soler, M. Ribezzi-Crivellari, U. Seifert, and F. Ritort (2015), *Nature Phys.* **11**, 971.
- Digby, P. J. (1981), *Journal of Applied Mechanics* **48**, 803.
- Donev, A., I. Cisse, D. Sachs, E. Variano, F. Stillinger, R. Connelly, S. Torquato, and P. Chaikin (2004), *Science* **303**, 990.
- Donev, A., R. Connelly, F. H. Stillinger, and S. Torquato (2007), *Phys. Rev. E* **75**, 051304.
- Donev, A., F. H. Stillinger, and S. Torquato (2005a), *Phys. Rev. Lett.* **95**, 090604.
- Donev, A., S. Torquato, and F. Stillinger (2005b), *Phys. Rev. E* **71**, 011105.
- Drocco, J. A., M. B. Hastings, C. J. O. Reichhardt, and C. Reichhardt (2005), *Phys. Rev. Lett.* **95**, 088001.
- During, G., E. Lerner, and M. Wyart (2013), *Soft Matter* **9**, 146.
- Eastham, P. R., R. A. Blythe, A. J. Bray, and M. A. Moore (2006), *Phys. Rev. B* **74**, 020406.
- Edwards, S., and D. Grinev (1999a), *Phys. Rev. Lett.* **82**,

- 5397.
- Edwards, S., and D. Grinev (2001), *Chem. Eng. Sci.* **56**, 5451.
- Edwards, S., and R. Oakeshott (1989), *Physica A* **157**, 1080.
- Edwards, S. F. (1991), “The aging of glass forming liquids,” in *Disorder in Condensed Matter Physics*, edited by J. Blackman and J. Taguena (Oxford University Press, Oxford) pp. 147–154.
- Edwards, S. F. (1994), “The role of entropy in the specification of a powder,” in *Granular matter: an interdisciplinary approach*, edited by A. Mehta (Springer, New York) pp. 121–140.
- Edwards, S. F. (2008), *J. Phys. A* **41**, 324019.
- Edwards, S. F., and P. W. Anderson (1975), *Journal of Physics F: Metal Physics* **5** (5), 965.
- Edwards, S. F., J. Brujić, and H. A. Makse (2004), “A basis for the statistical mechanics of granular systems,” in *Unifying Concepts in Granular Media and Glasses*, edited by A. Coniglio, A. Fierro, H. Herrmann, and M. Nicodemi (Elsevier Science BV) pp. 9–23.
- Edwards, S. F., and D. V. Grinev (1999b), *Chaos* **9**, 551.
- van Eerd, A. R. T., W. G. Ellenbroek, M. van Hecke, J. H. Snoeijer, and T. J. H. Vlugt (2007), *Phys. Rev. E* **75**, 060302.
- Ellenbroek, W. G., M. van Hecke, and W. van Saarloos (2009), *Phys. Rev. E* **80**, 061307.
- Ellenbroek, W. G., E. Somfai, M. van Hecke, and W. van Saarloos (2006), *Phys. Rev. Lett.* **97**, 258001.
- Erikson, J. M., N. W. Mueggenburg, H. M. Jaeger, and S. R. Nagel (2002), *Phys. Rev. E* **66**, 040301.
- Escobedo, F. A. (2014), *Soft Matter* **10**, 8388.
- Farrell, G. R., K. M. Martini, and N. Menon (2010), *Soft Matter* **6**, 2925.
- Faure, S., A. Lefebvre-Lepot, and B. Semin (2009), “Dynamic numerical investigation of random packing for spherical and nonconvex particles,” in *ESAIM: Proceedings*, Vol. 28, edited by M. Ismail, B. Maury, and J.-F. Gerbeau, pp. 13–32.
- Ferenc, J.-S., and Z. Neda (2007), *Physica A: Statistical Mechanics and its Applications* **385** (2), 518.
- Fierro, A., M. Nicodemi, and A. Coniglio (2002a), *Europhys. Lett.* **59**, 642.
- Fierro, A., M. Nicodemi, and A. Coniglio (2002b), *Phys. Rev. E* **66**, 061301.
- Fierro, A., M. Nicodemi, and A. Coniglio (2003), *J. Phys. Cond. Mat.* **15**, S1095.
- Finney, J. L. (1970), *Proc. Roy. Soc. London A* **319**, 479.
- Francois, N., M. Saadatfar, R. Cruikshank, and A. Sheppard (2013), *Phys. Rev. Lett.* **111**, 148001.
- Franz, S., and G. Parisi (2016), *J. Phys. A of Physics A: Mathematical and Theoretical* **49**, 145001.
- Franz, S., G. Parisi, P. Urbani, and F. Zamponi (2015), *Proc. Nat. Acad. Sci.* **112**, 14539.
- Frenkel, D. (2014), *Molecular Physics* **112** (17), 2325, <http://dx.doi.org/10.1080/00268976.2014.904051>.
- Frenkel, G., R. Blumenfeld, Z. Grof, and P. R. King (2008), *Phys. Rev. E* **77**, 10.1103/PhysRevE.77.041304.
- Gago, P. A., D. Maza, and L. A. Pugnaloni (2016), *Papers in Physics* **8**, 080001.
- Gantapara, A. P., J. de Graaf, R. van Roij, and M. Dijkstra (2013), *Phys. Rev. Lett.* **111**, 015501.
- Gao, G.-J., J. Blawdziewicz, and C. S. O’Hern (2006), *Phys. Rev. E* **74**, 061304.
- Gao, G.-J., J. Blawdziewicz, C. S. O’Hern, and M. Shattuck (2009), *Phys. Rev. E* **80**, 061304.
- Gardner, M. (2001), *The Colossal Book of Mathematics: Classic Puzzles, Paradoxes, and Problems* (Norton).
- Gendelman, O., Y. G. Pollack, I. Procaccia, S. Sengupta, and J. Zylberg (2016), *Phys. Rev. Lett.* **116**, 078001.
- Glotzer, S. C., and M. J. Solomon (2007), *Nature Mater.* **6**, 557.
- Goddard, J. (2004), *Int. J. Solids Struct.* **41**, 5851.
- Goldbart, P. M., N. Goldenfeld, and D. Sherrington (2005), *Stealing the gold: A celebration of the pioneering physics of Sam Edwards*.
- Götze, W. (2009), *Complex Dynamics of Glass-Forming Liquids: A Mode-Coupling Theory* (Oxford University Press).
- Gradenigo, G., E. E. Ferrero, E. Bertin, and J.-L. Barrat (2015), *Phys. Rev. Lett.* **115**, 140601.
- Haji-Akbari, A., M. Engel, A. S. Keys, X. Zheng, R. G. Petschek, P. Palfy-Muhoray, and S. C. Glotzer (2009), *Nature* **462**, 773.
- Hales, T. C. (2005), *Ann. Math.* **162**, 1065.
- Hanifpour, M., N. Francois, V. Robins, A. Kingston, S. M. Vaez Allaei, and M. Saadatfar (2015), *Phys. Rev. E* **91**, 062202.
- Hanifpour, M., N. Francois, S. M. Vaez Allaei, T. Senden, and M. Saadatfar (2014), *Phys. Rev. Lett.* **113**, 148001.
- Hansen-Goos, H., and K. Mecke (2009), *Phys. Rev. Lett.* **102**, 018302.
- Hansen-Goos, H., and K. Mecke (2010), *Journal of Physics: Condensed Matter* **22** (36), 364107.
- Head, D. A. (2007), *Eur. Phys. J. E* **22** (2), 151.
- van Hecke, M. (2010), *J. Phys. Cond. Mat.* **22**, 033101.
- Henkes, S., and B. Chakraborty (2005), *Phys. Rev. Lett.* **95**, 198002.
- Henkes, S., and B. Chakraborty (2009), *Phys. Rev. E* **79**, 061301.
- Henkes, S., M. van Hecke, and W. van Saarloos (2010), *Europhys. Lett.* **90**, 14003.
- Henkes, S., C. S. O’Hern, and B. Chakraborty (2007), *Phys. Rev. Lett.* **99**, 038002.
- Hermes, M., and M. Dijkstra (2010), *EPL* **89**, 38005.
- Herrmann, H. J. (1993), *Physica A* **191**, 263.
- Herrmann, H. J., G. Mantica, and D. Bessis (1990), *Phys. Rev. Lett.* **65**, 3223.
- Hiwatari, Y., T. Saito, and A. Ueda (1984), *J. Chem. Phys.* **81**, 6044.
- Hopkins, A. B., F. H. Stillinger, and S. Torquato (2013), *Phys. Rev. E* **88**, 022205.
- Hsu, C.-J., D. L. Johnson, R. A. Ingale, J. J. Valenza, N. Gland, and H. A. Makse (2009), *Phys. Rev. Lett.* **102**, 058001.
- Hu, Y., D. L. Johnson, J. J. Valenza, F. Santibanez, and H. A. Makse (2014a), *Phys. Rev. E* **89**.
- Hu, Y., H. A. Makse, J. J. Valenza, and D. L. Johnson (2014b), *Geophysics* **79**, L41.
- Huang, K. (1987), *Statistical Mechanics* (Wiley).
- Ikeda, A., and L. Berthier (2015), *Phys. Rev. E* **92**, 012309.
- Ikeda, A., L. Berthier, and G. Parisi (2017), *Phys. Rev. E* **95**, 052125.
- Ikeda, A., L. Berthier, and P. Sollich (2012), *Phys. Rev. Lett.* **109**, 018301.
- Ikeda, A., and K. Miyazaki (2010), *Phys. Rev. Lett.* **104**, 255704.
- Irastorza, R. M., C. M. Carlevaro, and L. A. Pugnaloni (2013), *Journal of Statistical Mechanics: Theory and Experiment* **2013** (12), P12012.



- Jaeger, H. M. (2015), *Soft Matter* **11**, 12.
- Jaeger, H. M., S. R. Nagel, and R. P. Behringer (1996), *Rev. Mod. Phys.* **68**, 1259.
- Jaoshvili, A., A. Esakia, M. Porrati, and P. M. Chaikin (2010), *Phys. Rev. Lett.* **104**, 185501.
- Jaynes, E. T. (1957a), *Phys. Rev.* **106**, 620.
- Jaynes, E. T. (1957b), *Phys. Rev.* **108**, 171.
- Jenkins, J., D. Johnson, L. L. Ragione, and H. Makse (2005), *J. Mech. Phys. Solids* **53**, 197.
- Jia, X., G. M., R. A. Williams, and D. Rhodes (2007), *Powder Technol.* **174**, 10.
- Jiao, Y., F. H. Stillinger, and S. Torquato (2010), *Phys. Rev. E* **81**, 041304.
- Jiao, Y., and S. Torquato (2011), *Phys. Rev. E* **84**, 041309.
- Jin, Y., P. Charbonneau, S. Meyer, C. Song, and F. Zamponi (2010), *Phys. Rev. E* **82**.
- Jin, Y., and H. A. Makse (2010), *Physica A* **389**, 5362.
- Jin, Y., J. G. Puckett, and H. A. Makse (2014), *Phys. Rev. E* **89**, 052207.
- Johnson, D. L., Y. Hu, and H. Makse (2015), *Phys. Rev. E* **91**, 062208.
- Johnson, K. L. (1985), *Contact Mechanics* (Cambridge University Press).
- Jorjadze, I., L.-L. Pontani, K. A. Newhall, and J. Brujić (2011), *Proc. Nat. Acad. Sci.* **108**, 4286.
- Kadanoff, L. P. (1999), *Rev. Mod. Phys.* **71**, 435.
- Kadau, D., and H. J. Herrmann (2011), *Phys. Rev. E* **83**, 031301.
- Kallus, Y. (2016), *Soft Matter* **12**, 4123.
- Kallus, Y., and V. Elser (2011), *Phys. Rev. E* **83**, 036703.
- Kamien, R. D., and A. J. Liu (2007), *Phys. Rev. Lett.* **99**, 155501.
- Kapfer, S. C., W. Mickel, K. Mecke, and G. E. Schröder-Turk (2012), *Phys. Rev. E* **85**, 030301.
- Kasahara, A., and H. Nakanishi (2004), *Phys. Rev. E* **70**, 051309.
- Kepler, J. (1611), *Strena seu de nive sexangula (The six-cornered snowflake)* (<http://www.thelatinlibrary.com/kepler/strena.html>).
- Kirkpatrick, S., and B. Selman (1994), *Science* **264**, 1297.
- Kirkpatrick, T. R., and P. G. Wolynes (1987), *Phys. Rev. A* **35**, 3072.
- Kirkwood, J. G. (1935), *J. Chem. Phys.* **3**, 300.
- Klumov, B. A., Y. Jin, and H. A. Makse (2014), *The J. Phys. Chem. B* **118**, 10761.
- Klumov, B. A., S. A. Khrapak, and G. E. Morfill (2011), *Phys. Rev. B* **83**, 184105.
- Knight, J. B., C. G. Fandrich, C. N. Lau, H. M. Jaeger, and S. R. Nagel (1995), *Phys. Rev. E* **51**, 3957.
- Krapivsky, P. L., and E. BenNaim (1994), *The Journal of Chemical Physics* **100**, 6778.
- Kruyt, N., and L. Rothenburg (2002), *Int. J. Solids. Struct.* **39**, 571.
- Krzakala, F., and J. Kurchan (2007), *Phys. Rev. E* **76**, 021122.
- Kumar, S., S. K. Kurtz, J. R. Banavar, and M. G. Sharma (1992), *Journal of Statistical Physics* **67** (3), 523.
- Kurchan, J. (2000), *Journal of Physics: Condensed Matter* **12**, 6611.
- Kurchan, J. (2001), “Rheology and how to stop aging,” in *Jamming and Rheology: Constrained Dynamics on Microscopic and Macroscopic Scales*, edited by A. Liu and S. R. Nagel (Taylor & Francis, London).
- Kurchan, J., T. Maimbourg, and F. Zamponi (2016), *Journal of Statistical Mechanics: Theory and Experiment* **2016** (3), 033210.
- Kyeeyune-Nyombi, E., F. Morone, W. Liu, S. Li, M. L. Gilchrist, and H. A. Makse (2018), *Physica A* **490**, 1387.
- Kyrylyuk, A. V., M. A. van de Haar, L. Rossi, A. Wouterse, and A. P. Philipse (2011), *Soft Matter* **7**, 1671.
- Landau, L. D., and E. M. Lifshitz (1980), *Statistical Physics* (Butterworth-Heinemann).
- Landau, L. D., L. P. Pitaevskii, A. M. Kosevich, and E. M. Lifshitz (1986), *Theory of Elasticity* (Butterworth-Heinemann).
- de Lange Kristiansen, K., A. Wouterse, and A. Philipse (2005), *Physica A: Statistical Mechanics and its Applications* **358** (2–4), 249.
- de Larrard, F. (1999), “Concrete mixture proportioning: A scientific approach,” (CRC Press).
- Lazar, E. A., J. K. Mason, R. D. MacPherson, and D. J. Srolovitz (2013), *Phys. Rev. E* **88**, 063309.
- Lechenault, F., F. da Cruz, O. Dauchot, and E. Bertin (2006), *J. Stat. Mech.*, P07009.
- Lefevre, A. (2002), *J. Phys. A* **35**, 9037.
- Lefèvre, A., and D. S. Dean (2002), *Phys. Rev. B* **65**, 220403.
- Lerner, E., E. DeGiuli, G. During, and M. Wyart (2014), *Soft Matter* **10**, 5085.
- Lerner, E., G. Düring, and E. Bouchbinder (2016), *Phys. Rev. Lett.* **117**, 035501.
- Lerner, E., G. During, and M. Wyart (2013), *Soft Matter* **9**, 8252.
- Leuzzi, L. (2009), *J. Non-Crystall. Solids* **355**, 686.
- Li, S.-Q., and J. Marshall (2007), *J. Aeros. Sci.* **38**, 1031.
- Lieou, C. K. C., and J. S. Langer (2012), *Phys. Rev. E* **85**, 061308.
- Lin, J., I. Jorjadze, L.-L. Pontani, M. Wyart, and J. Brujić (2016), *Phys. Rev. Lett.* **117**, 208001.
- Liu, A. J., and S. R. Nagel (2010), *Annu. Rev. Cond. Matt. Phys.* **1**, 347.
- Liu, C. h., S. R. Nagel, D. A. Schecter, S. N. Coppersmith, S. Majumdar, O. Narayan, and T. A. Witten (1995), *Science* **269**, 513.
- Liu, W., Y. Jin, S. Chen, H. A. Makse, and S. Li (2017), *Soft Matter* **13**, 421.
- Liu, W., S. Li, A. Baule, and H. A. Makse (2015), *Soft Matter* **11**, 6492.
- Loi, D., S. Mossa, and L. F. Cugliandolo (2008), *Phys. Rev. E* **77**, 051111.
- Lois, G., J. Blawdziewicz, and C. S. O’Hern (2008), *Phys. Rev. Lett.* **100**, 028001.
- Løvøll, G., K. J. Måløy, and E. G. Flekkøy (1999), *Phys. Rev. E* **60**, 5872.
- Lu, K., E. E. Brodsky, and H. P. Kavehpour (2008a), *Nature Phys.* **4**, 404.
- Lu, P., S. Li, J. Zhao, and L. Meng (2010), *Science China* **53**, 2284.
- Lu, P. J., E. Zaccarelli, F. Ciulla, A. B. Schofield, F. Sciortino, and D. A. Weitz (2008b), *Nature* **453**, 499.
- Lubachevsky, B. D., and F. H. Stillinger (1990), *J. Stat. Phys.* **60**, 561.
- Luchnikov, V. A., N. N. Medvedev, L. Oger, and J.-P. Troadec (1999), *Phys. Rev. E* **59**, 7205.
- Magnanimo, V., L. L. Ragione, J. T. Jenkins, P. Wang, and H. A. Makse (2008), *EPL* **81**, 34006.
- Mailman, M., and B. Chakraborty (2011), *J. Stat. Mech.* **2011**, L07002.
- Mailman, M., and B. Chakraborty (2012), *J. Stat. Mech.*

- 2012, P05001.
- Maimbourg, T., J. Kurchan, and F. Zamponi (2016), *Phys. Rev. Lett.* **116**, 015902.
- Majmudar, T. S., and R. P. Behringer (2005), *Nature* **435**, 1079.
- Majmudar, T. S., M. Sperl, S. Luding, and R. P. Behringer (2007), *Phys. Rev. Lett.* **98**, 10.1103/PhysRevLett.98.058001.
- Makse, H., and J. Kurchan (2002), *Nature* **415**, 614.
- Makse, H. A., J. Brujić, and S. F. Edwards (2005), “Statistical mechanics of jammed matter,” in *The Physics of Granular Media*, edited by H. Hinrichsen and D. E. Wolf (Wiley-VCH).
- Makse, H. A., N. Gland, D. L. Johnson, and L. Schwartz (2004), *Phys. Rev. E* **70**, 061302.
- Makse, H. A., N. Gland, D. L. Johnson, and L. M. Schwartz (1999), *Phys. Rev. Lett.* **83**, 5070.
- Makse, H. A., D. L. Johnson, and L. M. Schwartz (2000), *Phys. Rev. Lett.* **84**, 4160.
- Man, W., A. Donev, F. H. Stillinger, M. T. Sullivan, W. B. Russel, D. Heeger, S. Inati, S. Torquato, and P. M. Chaikin (2005), *Phys. Rev. Lett.* **94**, 198001.
- Mangeat, M., and F. Zamponi (2016), *Phys. Rev. E* **93**, 012609.
- Marconi, U. M. B., A. Puglisi, L. Rondoni, and A. Vulpiani (2008), *Phys. Rep.* **461**, 111.
- Marechal, M., and H. Löwen (2013), *Phys. Rev. Lett.* **110**, 137801.
- Mari, R., F. Krzakala, and J. Kurchan (2009), *Phys. Rev. Lett.* **103**, 025701.
- Marshall, J. S., and S. Li (2014), *Adhesive Particle Flow* (Cambridge University Press).
- Martin, C. L., and R. K. Bordia (2008), *Phys. Rev. E* **77**, 031307.
- Martiniani, S., K. J. Schrenk, K. Ramola, B. Chakraborty, and D. Frenkel (2017), *Nat Phys* **13** (9), 848.
- Martiniani, S., K. J. Schrenk, J. D. Stevenson, D. J. Wales, and D. Frenkel (2016a), *Phys. Rev. E* **94**, 031301.
- Martiniani, S., K. J. Schrenk, J. D. Stevenson, D. J. Wales, and D. Frenkel (2016b), *Phys. Rev. E* **94**, 031301.
- Martiniani, S., K. J. Schrenk, J. D. Stevenson, D. J. Wales, and D. Frenkel (2016c), *Phys. Rev. E* **93**, 012906.
- Matsushima, T., and R. Blumenfeld (2014), *Phys. Rev. Lett.* **112**, 098003.
- Maxwell, J. C. (1864), *Philosophical Magazine* **26**, 250.
- Maxwell, J. C. (1870), *Transactions of the Royal Society of Edinburgh* **26**, 1.
- McNamara, S., and H. Herrmann (2004), *Phys. Rev. E* **70**, 061303.
- McNamara, S., P. Richard, S. K. de Richter, G. Le Caer, and R. Delannay (2009a), *Phys. Rev. E* **80**, 031301.
- McNamara, S., P. Richard, S. K. de Richter, G. Le Caer, and R. Delannay (2009b), “Overlapping histogram method for testing edward’s statistical mechanics of powders,” in *Powders and Grains 2009*, AIP Conference Proceedings, Vol. 1145, edited by M. Nakagawa and S. Luding (AIP) pp. 465–468.
- Medvedev, N., and Y. Naberukhin (1987), *J. Non-Crystall. Solids* **94**, 402.
- van Meel, J. A., B. Charbonneau, A. Fortini, and P. Charbonneau (2009a), *Phys. Rev. E* **80**, 061110.
- van Meel, J. A., D. Frenkel, and P. Charbonneau (2009b), *Phys. Rev. E* **79**, 030201.
- Mehta, A., and S. Edwards (1990), *Physica A* **168**, 714.
- Metzger, P. (2004), *Phys. Rev. E* **70**, 051303.
- Metzger, P., and C. Donahue (2005), *Phys. Rev. Lett.* **94**, 148001.
- Meyer, S., C. Song, Y. Jin, K. Wang, and H. A. Makse (2010), *Physica A* **389**, 5137.
- Mézard, M., and A. Montanari (2009), *Information, Physics, and Computation* (Oxford University Press).
- Mézard, M., and G. Parisi (2001), *Eur. Phys. J. B* **20**, 217.
- Mézard, M., and G. Parisi (2003), *Journal of Statistical Physics* **111** (1), 1.
- Mindlin, R. D. (1949), *Journal of Applied Mechanics (ASME)* **71**, 259.
- Miskin, M. Z., and H. M. Jaeger (2013), *Nature Mater.* **12**, 326.
- Miskin, M. Z., and H. M. Jaeger (2014), *Soft Matter* **10**, 3708.
- Mizuno, H., H. Shiba, and A. Ikeda (2017), ArXiv e-prints [arXiv:1703.10004](https://arxiv.org/abs/1703.10004) [cond-mat.soft].
- Monasson, R. (1995), *Phys. Rev. Lett.* **75**, 2847.
- Moukarzel, C. F. (1998), *Phys. Rev. Lett.* **81**, 1634.
- Mounfield, C., and S. Edwards (1994), *Physica A* **210**, 279.
- Mueth, D. M., H. M. Jaeger, and S. R. Nagel (1998), *Phys. Rev. E* **57**, 3164.
- Müller, M., and M. Wyart (2015), *Annual Review of Condensed Matter Physics* **6** (1), 177.
- Neudecker, M., S. Ulrich, S. Herminghaus, and M. Schröter (2013), *Phys. Rev. Lett.* **111**, 028001.
- Newhall, K. A., I. Jorjadze, E. Vanden-Eijnden, and J. Brujić (2011), *Soft Matter* **7**, 11518.
- Newman, C. M., and D. L. Stein (1999), *Phys. Rev. E* **60**, 5244.
- Ngan, A. (2004), *Physica A* **339**, 207.
- Ngan, A. H. W. (2003), *Phys. Rev. E* **68**, 011301.
- Ni, R., M. A. C. Stuart, and M. Dijkstra (2013), *Nature Communications* **4**, 2704.
- Nicodemi, M. (1999), *Phys. Rev. Lett.* **82**, 3734.
- Nicodemi, M., A. Coniglio, A. de Candia, A. Fierro, M. Ciarrarra, and M. Tarzia (2004), “Statistical mechanics of jamming and segregation in granular media,” in *Unifying Concepts in Granular Media and Glasses*, edited by A. Coniglio, A. Fierro, H. Herrmann, and M. Nicodemi (Elsevier) pp. 47–61.
- Nicodemi, M., A. Coniglio, and H. Herrmann (1997a), *Physica A* **240**, 405.
- Nicodemi, M., A. Coniglio, and H. J. Herrmann (1997b), *J. Phys. A* **30**, L379.
- Nicodemi, M., A. Coniglio, and H. J. Herrmann (1997c), *Phys. Rev. E* **55**, 3962.
- Nicodemi, M., A. Coniglio, and H. J. Herrmann (1999), *Phys. Rev. E* **59**, 6830.
- Norris, A. N., and D. L. Johnson (1997), *J. App. Mech.* **64**, 39.
- Nowak, E., J. Knight, E. Ben-Naim, H. Jaeger, and S. Nagel (1998), *Phys. Rev. E* **57**, 1971.
- Nowak, E., J. Knight, M. Povinelli, H. Jaeger, and S. Nagel (1997), *Powd. Tech.* **94**, 79.
- O’Hern, C., A. Liu, and S. Nagel (2004), *Phys. Rev. Lett.* **93**, 165702.
- O’Hern, C., L. Silbert, A. Liu, and S. Nagel (2003), *Phys. Rev. E* **68**, 011306.
- O’Hern, C. S., S. A. Langer, A. J. Liu, and S. R. Nagel (2001), *Phys. Rev. Lett.* **86**, 111.
- O’Hern, C. S., S. A. Langer, A. J. Liu, and S. R. Nagel (2002), *Phys. Rev. Lett.* **88**, 075507.

- Okabe, A., B. Boots, K. Sugihara, and S. Nok Chiu (2000), *Spatial Tessellations: Concepts and Applications of Voronoi Diagrams* (Wiley-Blackwell).
- Olsson, P., and S. Teitel (2007), *Phys. Rev. Lett.* **99**, 178001.
- Ono, I., C. O'Hern, D. Durian, S. Langer, A. Liu, and S. Nagel (2002), *Phys. Rev. Lett.* **89**, 095703.
- Onoda, G. Y., and E. G. Liniger (1990), *Phys. Rev. Lett.* **64**, 2727.
- Onsager, L. (1949), *Ann. N. Y. Acad. Sci.* **51**, 627.
- Oquendo, W. F., J. D. Muñoz, and F. Radjai (2016), *EPL (Europhysics Letters)* **114** (1), 14004.
- Oron, G., and H. Herrmann (1999), *Physica A* **265**, 455.
- Oron, G., and H. J. Herrmann (1998), *Phys. Rev. E* **58**, 2079.
- Ozawa, M., L. Berthier, and D. Coslovich (2017), *ArXiv e-prints* [arXiv:1705.10156](https://arxiv.org/abs/1705.10156) [cond-mat.stat-mech].
- Ozawa, M., T. Kuroiwa, A. Ikeda, and K. Miyazaki (2012), *Phys. Rev. Lett.* **109**, 205701.
- Paillusson, F. (2015), *Phys. Rev. E* **91**, 012204.
- Paillusson, F., and D. Frenkel (2012), *Phys. Rev. Lett.* **109**, 208001.
- Palásti, I. (1960), *Publ. Math. Res. Inst. Hung. Acad. Sci.* **5**, 353.
- Panaiteescu, A., and A. Kudrolli (2014), *Phys. Rev. E* **90**, 032203.
- Papanikolaou, S., C. S. O'Hern, and M. D. Shattuck (2013), *Phys. Rev. Lett.* **110**, 198002.
- Parisi, G. (1988), *Statistical Field Theory* (Addison-Wesley).
- Parisi, G. (2017), *Journal of Statistical Physics* **167** (3), 515.
- Parisi, G., and F. Zamponi (2005), *J. Chem. Phys.* **123**, 144501.
- Parisi, G., and F. Zamponi (2010), *Rev. Mod. Phys.* **82**, 789.
- Parteli, E. J. R., J. Schmidt, C. Blumel, K.-E. Wirth, W. Peukert, and T. Poschel (2014), *Sci. Rep.* **4**.
- Pathria, R. K., and P. D. Beale (2011), *Statistical Mechanics* (Elsevier).
- Philippe, P., and D. Bideau (2002), *Europhys. Lett.* **60**, 677.
- Philipse, A. (1996), *Langmuir* **12**, 1127.
- Phillips, C. L., J. A. Anderson, G. Huber, and S. C. Glotzer (2012), *Phys. Rev. Lett.* **108**, 198304.
- Portal, L., M. Danisch, A. Baule, R. Mari, and H. A. Makse (2013), *J. Stat. Mech.*, P11009.
- Potiguar, F., and H. Makse (2006), *Eur. Phys. J. E* **19**, 171.
- Pouliquen, O., M. Nicolas, and P. D. Weidman (1997), *Phys. Rev. Lett.* **79**, 3640.
- Prados, A., J. Brey, and B. Sanchez-Rey (2000), *Physica A* **284**, 277.
- Prados, A., and J. J. Brey (2002), *Phys. Rev. E* **66**, 041308.
- Puckett, J. G., and K. E. Daniels (2013), *Phys. Rev. Lett.* **110**, 058001.
- Puckett, J. G., F. Lechenault, and K. E. Daniels (2011), *Phys. Rev. E* **83**, 041301.
- Pugnaloni, L. A., I. Sanchez, P. A. Gago, J. Damas, I. Zuriguel, and D. Maza (2010), *Phys. Rev. E* **82**, 10.1103/PhysRevE.82.050301.
- Qiong, C., and H. Mei-Ying (2014), *Chin. Phys. B* **23**, 074501.
- Radeke, C., K. Bagi, B. Paláncz, and D. Stoyan (2004), *Granular Matter* **6**, 17.
- Radin, C. (2008), *J. Stat. Phys.* **131**, 567.
- Radjai, F., M. Jean, J.-J. Moreau, and S. Roux (1996), *Phys. Rev. Lett.* **77**, 274.
- Radjai, F., and V. Richefeu (2009), *Mech. Mater.* **41**, 715.
- Rainone, C., and P. Urbani (2016), *Journal of Statistical Mechanics: Theory and Experiment* **2016** (5), 053302.
- Rényi, A. (1958), *Publ. Math. Res. Inst. Hung. Acad. Sci.* **3**, 109.
- Ribiere, P., P. Richard, P. Philippe, D. Bideau, and R. Delannay (2007), *Eur. Phys. J. E* **22**, 249.
- Richard, P., M. Nicodemi, R. Delannay, P. Ribiere, and D. Bideau (2005), *Nature Mater.* **4**, 121.
- Richard, P., P. Philippe, F. Barbe, S. Bourles, X. Thibault, and D. Bideau (2003), *Phys. Rev. E* **68**, 020301.
- Roberts, S. A. (1981), *Journal of Physics C: Solid State Physics* **14** (21), 3015.
- Roth, L. K., and H. M. Jaeger (2016), *Soft Matter* **12**, 1107.
- Rothenburg, L., and N. P. Kruyt (2009), *J. Mech. Phys. Solids* **57**, 634.
- Roux, J.-N. (2000), *Phys. Rev. E* **61**, 6802.
- Saadatfar, M., A. P. Sheppard, T. J. Senden, and A. J. Kabla (2012), *Journal of the Mechanics and Physics of Solids* **60** (1), 55.
- Santiso, E., and E. A. Müller (2002), *Molecular Physics* **100** (15), 2461.
- Satake, M. (1993), *Mech. Mater.* **16**, 65.
- Schaller, F. M., S. C. Kapfer, M. E. Evans, M. J. F. Hoffmann, T. Aste, M. Saadatfar, K. Mecke, G. W. Delaney, and G. E. Schröder-Turk (2013), *Philos. Mag.* **93**, 3993.
- Schaller, F. M., S. C. Kapfer, J. E. Hilton, P. W. Cleary, K. Mecke, C. D. Michele, T. Schilling, M. Saadatfar, M. Schröter, G. W. Delaney, and G. E. Schröder-Turk (2015a), *EPL* **111**, 24002.
- Schaller, F. M., M. Neudecker, M. Saadatfar, G. W. Delaney, G. E. Schröder-Turk, and M. Schröter (2015b), *Phys. Rev. Lett.* **114**, 158001.
- Schopenhauer, A. (1974), "Transcendent speculation on the apparent deliberateness in the fate of the individual," in *Parerga and Paralipomena: Short Philosophical Essays*, Vol. I (Oxford University Press) pp. 199–225.
- Schreck, C. F., M. Mailman, B. Chakraborty, and C. S. O'Hern (2012), *Phys. Rev. E* **85**, 061305.
- Schreck, C. F., and C. S. O'Hern (2011), .
- Schreck, C. F., N. Xu, and C. S. O'Hern (2010), *Soft Matter* **6**, 2960.
- Schröder-Turk, G. E., W. Mickel, M. Schröter, G. W. Delaney, M. Saadatfar, T. J. Senden, K. Mecke, and T. Aste (2010), *EPL* **90**, 34001.
- Schröter, M., D. Goldman, and H. Swinney (2005), *Phys. Rev. E* **71**, 030301.
- Schwarz, J. M., A. J. Liu, and L. Q. Chayes (2006), *EPL* **73**, 560.
- Scott, G. D. (1960), *Nature* **188**, 908.
- Scott, G. D. (1962), *Nature* **194**, 956.
- Sharma, A., J. Yeo, and M. A. Moore (2016), *Phys. Rev. E* **94**, 052143.
- Shen, T., S. Papanikolaou, C. S. O'Hern, and M. D. Shattuck (2014), *Phys. Rev. Lett.* **113**, 128302.
- Sherrington, D., and S. Kirkpatrick (1975), *Phys. Rev. Lett.* **35**, 1792.
- Shundyak, K., M. van Hecke, and W. van Saarloos (2007), *Phys. Rev. E* **75**, 010301.
- Silbert, L., A. Liu, and S. Nagel (2005), *Phys. Rev. Lett.* **95**, 098301.
- Silbert, L. E. (2010), *Soft Matter* **6**, 2918.
- Silbert, L. E., D. Ertas, G. S. Grest, T. C. Halsey, and D. Levine (2002a), *Phys. Rev. E* **65**, 031304.
- Silbert, L. E., G. S. Grest, and J. W. Landry (2002b), *Phys. Rev. E* **66**, 061303.
- Silbert, L. E., A. J. Liu, and S. R. Nagel (2006), *Phys. Rev.*

- E **73**, 041304.
- Silbert, L. E., A. J. Liu, and S. R. Nagel (2009), *Phys. Rev. E* **79**, 021308.
- Skoge, M., A. Donev, F. H. Stillinger, and S. Torquato (2006), *Phys. Rev. E* **74**, 041127.
- Slobinsky, D., and L. Pagnaloni (2015a), *Papers in Physics* **7** (0).
- Slobinsky, D., and L. A. Pagnaloni (2015b), *Journal of Statistical Mechanics: Theory and Experiment* **2015** (2), P02005.
- Smith, K. C., T. S. Fisher, and M. Alam (2011), *Phys. Rev. E* **84**, 030301.
- Snoeijer, J., T. Vlugt, W. Ellenbroek, M. van Hecke, and J. van Leeuwen (2004), *Phys. Rev. E* **70**, 061306.
- Sohn, H. Y., and C. Moreland (1968), *Canad. J. Chem. Eng.* **46**, 162.
- Somfai, E., M. van Hecke, W. G. Ellenbroek, K. Shundyak, and W. van Saarloos (2007), *Phys. Rev. E* **75**, 020301.
- Song, C., P. Wang, Y. Jin, and H. A. Makse (2010), *Physica A* **389**, 4497.
- Song, C., P. Wang, and H. Makse (2005), *Proc. Nat. Acad. Sci.* **102**, 2299.
- Song, C., P. Wang, and H. A. Makse (2008), *Nature* **453**, 629.
- Steinhardt, P. J., D. R. Nelson, and M. Ronchetti (1983), *Phys. Rev. B* **28**, 784.
- Swendsen, R. H. (2006), *American Journal of Physics* **74** (3), 187.
- Tarjus, G., and P. Viot (2004), *Phys. Rev. E* **69**, 011307.
- Thomas, I. (1941), “Greek mathematical works, volume ii: Aristarchus to pappus,” (Harvard University Press).
- Thue, A. (1892), *Forand. Skand. Natur.* **14**, 352.
- Tian, J., Y. Xu, Y. Jiao, and S. Torquato (2015), *Sci. Rep.* **5**, 16722 EP.
- Tighe, B. P., A. R. T. van Eerd, and T. J. H. Vlugt (2008), *Phys. Rev. Lett.* **100**, 238001.
- Tighe, B. P., J. H. Snoeijer, T. J. H. Vlugt, and M. van Hecke (2010), *Soft Matter* **6**, 2908.
- Tighe, B. P., and T. J. H. Vlugt (2010), *J. Stat. Mech.*, P01015.
- Tighe, B. P., and T. J. H. Vlugt (2011), *J. Stat. Mech.*, P04002.
- Tkachenko, A. V., and T. A. Witten (2000), *Phys. Rev. E* **62**, 2510.
- Toninelli, C., G. Biroli, and D. S. Fisher (2006), *Phys. Rev. Lett.* **96**, 035702.
- Tonks, L. (1936), *Phys. Rev.* **50**, 955.
- Torquato, S., and Y. Jiao (2009), *Nature* **460**, 876.
- Torquato, S., and Y. Jiao (2010), *Phys. Rev. E* **82**, 061302.
- Torquato, S., and Y. Jiao (2012), *Phys. Rev. E* **86**, 011102.
- Torquato, S., and F. Stillinger (2010), *Rev. Mod. Phys.* **82**, 2633.
- Torquato, S., and F. H. Stillinger (2001), *J. Phys. Chem. B* **105**, 11849.
- Torquato, S., and F. H. Stillinger (2003), *Phys. Rev. E* **68**, 041113.
- Torquato, S., and F. H. Stillinger (2006), *Phys. Rev. E* **73**, 031106.
- Torquato, S., T. M. Truskett, and P. G. Debenedetti (2000), *Phys. Rev. Lett.* **84**, 2064.
- Trappe, V., V. Prasad, L. Cipelletti, P. N. Segre, and D. A. Weitz (2001), *Nature* **411**, 772.
- Unger, T., J. Kertesz, and D. Wolf (2005), *Phys. Rev. Lett.* **94**, 178001.
- Valverde, J. M., M. A. S. Quintanilla, and A. Castellanos (2004), *Phys. Rev. Lett.* **92**, 258303.
- Walton, K. (1987), *J. Mech. Phys. Solids* **35**, 213.
- Wang, C., K. Dong, and A. Yu (2015), *Phys. Rev. E* **92**, 062203.
- Wang, K., C. Song, P. Wang, and H. A. Makse (2010a), *EPL* **91**, 68001.
- Wang, K., C. Song, P. Wang, and H. A. Makse (2012), *Phys. Rev. E* **86**, 10.1103/PhysRevE.86.011305.
- Wang, P., C. Song, C. Briscoe, and H. A. Makse (2008), *Phys. Rev. E* **77**, 10.1103/PhysRevE.77.061309.
- Wang, P., C. Song, C. Briscoe, K. Wang, and H. A. Makse (2010b), *Physica A* **389**, 3972.
- Wang, P., C. Song, Y. Jin, and H. A. Makse (2011), *Physica A* **390**, 427.
- Wang, P., C. Song, Y. Jin, K. Wang, and H. A. Makse (2010c), *J. Stat. Mech.* 10.1088/1742-5468/2010/12/P12005.
- Wang, P., C. Song, and H. A. Makse (2006), *Nature Phys.* **2**, 526.
- Warner, M. (2017), *Biographical Memoirs of Fellows of the Royal Society* 10.1098/rsbm.2016.0028.
- Weaire, D., and T. Aste (2008), *The pursuit of perfect packing* (CRC Press).
- Williams, S. R., and A. P. Philipse (2003), *Phys. Rev. E* **67**, 051301.
- Wouterse, A., S. Luding, and A. P. Philipse (2009), *Granular Matter* **11**, 169.
- Wu, Y., P. Olsson, and S. Teitel (2015), *Phys. Rev. E* **92**, 052206.
- Wyart, M. (2005), *Annales de Physique* **30**, 1.
- Wyart, M. (2010), *EPL* **89**, 64001.
- Wyart, M. (2012), *Phys. Rev. Lett.* **109**, 125502.
- Wyart, M., S. Nagel, and T. Witten (2005a), *EPL* **72**, 486.
- Wyart, M., L. Silbert, S. Nagel, and T. Witten (2005b), *Phys. Rev. E* **72**, 051306.
- Xu, N., J. Blawdziewicz, and C. O’Hern (2005), *Phys. Rev. E* **71**, 061306.
- Xu, N., D. Frenkel, and A. J. Liu (2011), *Phys. Rev. Lett.* **106**, 245502.
- Yadav, V., J.-Y. Chastaing, and A. Kudrolli (2013), *Phys. Rev. E* **88**, 052203.
- Yang, R., R. Zou, and A. Yu (2000), *Phys. Rev. E* **62**, 3900.
- Zaccarelli, E. (2007), *J. Phys. Cond. Mat.* **19**, 323101.
- Zaccone, A., and E. Scossa-Romano (2011), *Phys. Rev. B* **83**, 184205.
- Zhang, H., and H. Makse (2005), *Phys. Rev. E* **72**, 011301.
- Zhao, J., S. Li, R. Zou, and A. Yu (2012), *Soft Matter* **8**, 1003.
- Zhao, S.-C., and M. Schröter (2014), *Soft Matter* **10**, 4208.
- Zhou, J., S. Long, Q. Wang, and A. D. Dinsmore (2006), *Science* **312**, 1631.